

FEASIBILITY ANALYSIS OF USING NEUCUBE 3D
SNN ENVIRONMENT FOR SPATIO-TEMPORAL EEG
DATA CLASSIFICATION RELATED TO
PERCEPTION OF ART

Yulia Turkova

A THESIS SUBMITTED TO
THE AUCKLAND UNIVERSITY OF TECHNOLOGY
IN FULFILLMENT OF THE REQUIREMENTS
FOR THE DEGREE OF
MASTER OF PHILOSOPHY (MPHIL)
2014

PRIMARY SUPERVISOR: PROF. NIKOLA KASABOV
SECONDARY SUPERVISOR: DR. STEFAN SCHLIEBS

KNOWLEDGE ENGINEERING & DISCOVERY RESEARCH INSTITUTE
FACULTY OF DESIGN AND CREATIVE TECHNOLOGIES
AUCKLAND UNIVERSITY OF TECHNOLOGY
AUCKLAND, NEW ZEALAND

“I hereby declare that this submission is my own work and that, to the best of my knowledge and belief, it contains no material previously published or written by another person (except where explicitly defined in the acknowledgements), nor material which to a substantial extent has been submitted for the award of any other degree or diploma of a university or other institution of higher learning. “

Yulia Turkova

Acknowledgments

I have the pleasure to acknowledge all the people who have inspired, supported, and educated me over the past years. First and foremost, I am very grateful to my primary supervisor Prof. Nikola Kasabov for his support and inspiration. I wish to express my sincere appreciation to my secondary supervisor Dr. Stefan Schliebs for his constant encouragement. I am especially grateful to Joyce D’Mello, the heart of KEDRI, for her guidance and support. I would also like to thank the past and present members and alumni of KEDRI at the Auckland University of Technology who kindly helped me with collection of data. Also I would like to thank my family for their invaluable support and patience.

Contents

Abstract	11
Chapter 1: Motivation and objectives of the study	13
1.1 Significance of brain study for the contemporary world and its modern challenges.	13
1.2 Definition of human brain perception	15
1.3 Reasoning for the original stimuli used in the experiments	16
Chapter 2: Literature review of methods of measuring of brain signals	20
2.1 Introduction to the Human Brain	20
2.2 Methods for the measurements of brain signals	23
2.3 Advantages of EEG method.....	24
2.4 EEG data review	28
2.5 Methods of classification of EEG data.....	32
2.6 Summary	41
Chapter 3: Introduction to SNN.....	42
3.1 What is ASNN?.....	42
3.2 SNN models	44
3.3 Reservoir NN frameworks	49
3.4 Summary	51
Chapter 4: The NeuCube based methodology of the study	53
4.1 The NeuCube objectives and challenges.....	53
4.2 The NeuCube Main Principles and Framework for STBD	55
4.3 The NeuCube module architecture	57
Chapter 5: Experimental case study of EEG STBD classification in the NeuCube model with audio stimuli	64

5.1 Audio perception review	64
5.2 EEG NeuCube model and mapping structure	67
5.3 EEG brain perception data and experiment description	70
5.4 Visualization of EEG recorded data.....	76
5.5 Conclusion	82
Chapter 6: Experimental case study of EEG STBD classification in the NeuCube model with video stimuli	83
6.1 Visual perception review.....	83
6.2 EEG brain perception data and experiment description	84
6.3 Visualization of EEG recorded data.....	90
6.4 Summary	92
Chapter 7: Experimental case study of EEG STBD classification in the NeuCube model with mixed audio/video stimuli	93
7.1 EEG brain perception data and experiment description	93
7.2 EEG data samples' length experiment	98
7.3 Special case of EEG STBD classification in the NeuCube model with mixed audio/video “contradictory pairs” stimuli	101
7.4 Visualization of EEG recorded data.....	104
7.5 Summary	105
Chapter 8: Conclusion and future work.....	107
References.....	110
Appendix A:	118

List of figures

1.3.1 Screenshots of the video stimuli	17
2.1.1 Human brain structure.....	21
2.1.2 Spatio-temporal signaling paths in the brain.....	21
2.1.3 Localization of the brain functions	22
2.1.4 (Left) Simulation of a cm ² -scale cortical EEG source representing an area of locally synchronized cortical surface-negative field activity, and (right) its broad projection to the scalp.	22
2.3.1 EEG system.....	26
2.3.2 Electrode locations and names specified by the International 10–20 system.	26
2.3.3 The EPOC Emotiv neuroheadset	27
2.3.4 High-Density Mobile & Wireless EEG systems MINDO-32 and -64.....	28
2.4.1 Action potentials transferring between neurons through synapse.....	29
2.4.2 Common oscillatory modes in EEG.....	29
2.4.3 Mixture of signals	31
2.5.1 Linear Regression.....	33
2.5.2 The logistic function	34
2.5.3 Only hyperplane H3 separates classes with the maximum margin.....	35
2.5.4 Multilayer perceptron.....	36
2.5.5 Probabilistic parameters of a hidden Markov model, x – states, y - possible observations, a - state transition probabilities, b - output probabilities	37
2.5.6 Fifteen seconds of EEG data at 9 (of 100) scalp channels (top panel) with activities of 9 (of 100) independent components (ICs, bottom panel). While nearby electrodes (upper panel) record highly similar mixtures of brain and non-brain activities, ICA component activities (lower panel) are temporally distinct.	38
2.5.7 EEGLAB BCI tool.	40
2.5.8 Still images of SIFT 3D visualization / brainmovie	41
3.1.1: Schematics of a biological neuron illustrating signal propagation and synapsis.	43

3.2.1 Hodgkin-Huxley type models represent the biophysical characteristic of cell membranes. The lipid bilayer is represented as a capacitance (C_m). Voltage-gated and leak ion channels are represented by nonlinear (g_n) and linear (g_L) conductance, respectively. The electrochemical gradients driving the flow of ions are represented by batteries (E), and ion pumps and exchangers are represented by current sources (I_p). Adapted from Hodgkin and Huxley [65].	45
3.2.2. Schematic diagram of the integrate-and-fire model. The basic circuit is the module inside the dashed circle on the right-hand side. A current $I(t)$ charges the RC circuit. The voltage $u(t)$ across the capacitance (points) is compared to a threshold θ . If $u(t) = \theta$ at time $t_i(f)$ an output pulse $\delta(t - t_i(f))$ is generated. Left part: A presynaptic spike $\delta(t - t_j(f))$ is low-pass filtered at the synapse and generates an input current pulse $i(t - t_j(f))$.	46
4.2.1 A schematic diagram of a general NeuCube architecture, consisting of: input encoding module; NeuCube module; output function module; gene regulatory networks (GRN) module (optional)	56
4.3.1 Population rank order coding of input information	58
4.3.2 AER of continuous value time series input data into spike trains, the idealized pixel encoding and reconstruction of video data.	58
4.3.3 AER of continuous value time series, the idealized pixel reconstruction of video data	59
4.3.4. Actual one EEG channel signal (top); the spike representation of the above figure obtained using BSA (middle); and the bottom –the actual one EEG channel signal (red) plus superimposed with representation of the reconstructed EEG signal from the BSA encoded spikes (dashed).	59
4.3.5 Visualization of connectivity and spiking activity of a SNNr: (a) spiking activity—active neurons are represented in red color and large size; (b) connectivity before training – small world connections – positive connections are represented in blue and negative—in red; (c) connectivity after training	60
4.3.6. The structure of the LIFM	61
4.3.7. Functionality of the LIFM	61
4.3.8 Rank-order learning neuron	62
5.1.1 (a) Brodmann areas 41 & 42 of the human brain; (b) The Primary Auditory Cortex is highlighted in magenta, and has been known to interact with all areas highlighted on this neural map.	65
5.1.2. Areas of brain activation for reading and listening comprehension	66
5.2.1 Positioning of 64 EEG channels on a human head (a); EEG channels representation in a 3D space (b)	68

5.2.2 The Talairach template development and mapping	68
5.2.3 The whole framework for classification of STBD	69
5.2.4 The NeuCube.	70
5.3.1 Emotiv software GUI screenshot	71
5.4.1 NeuCube Exp 4-3 visualization of connectivity and spiking activity after training of a SNNr; positive connections are represented in blue and negative—in red;	76
5.4.2 The visualization of simple network of <i>Experiment 4-1</i> for classification of three subjects 1, 2, and 3 with stimuli length of 1 sec.	77
5.4.3 The visualization of more complex Experiment 14 which classified the stimuli M1, M2, N and based on the mixed samples of perception of all three subjects 1, 2, 3 in each class with stimuli length of 1sec.	77
5.4.4 2D EEG scalp maps of dataset EEG epochs; subject 1, stimulus M1.....	78
5.4.5 2D EEG scalp maps of dataset EEG epochs; subject 1, stimulus N	79
5.4.6 3D visualization of subject 1, music stimulus M2	79
5.4.7 2D and 3D plotting of sensor T7 and sensor T8 which are corresponding roughly with Brodmann areas 41 and 42 /auditory cortex areas; recorded with Music stimuli...	80
5.4.8 2D and 3D plotting of sensor T7 and sensor T8 which are corresponding roughly with Brodmann areas 41 and 42 /auditory cortex areas; recorded with N Noise stimuli	81
5.4.9 Spike state of NeuCube on training (up) and testing (bottom) samples	81
6.1.1. The visual dorsal stream (green) and ventral stream (purple) are shown. Much of the human cerebral cortex is involved in vision.....	84
6.2.1. (a) Natural snowflake crystal; (b) Tibetan mandala Chakrasamvara;.....	85
6.2.2. (a) abstract art of V. Kandinsky; (b) surrealism art work of S. Dali.....	85
6.3.1 2D EEG scalp maps of dataset EEG epochs; subject 1, P2 Patterned video stimulus	90
6.3.2 2D EEG scalp maps of dataset EEG epochs; subject 1, A Abstract video stimulus	90
6.3.3 2D plotting of sensor O1 and sensor O2 that are corresponding roughly with visual dorsal and ventral stream areas; recorded with A/Abstract video stimuli	91
6.3.4 2D plotting of sensor O1 and sensor O2 that are corresponding roughly with visual dorsal and ventral stream areas; recorded with P2/Patterned video stimuli.....	91
6.3.5 NeuCube visualizations of Experiment 2-1 (left) and Experiment 2-2 (right) EEG data classification of subjects with video stimuli.....	91

7.4.1 BrainMovie3DVisualization of EEG data with mixed audio/video 1/MP2 patterned stimuli; SIFT Matlab/EEGLAB plugin	104
7.4.2. The NeuCube network after training of complicated experiments 8 and 17	105

List of abbreviations

AER:	Address Event Representation
AI:	Artificial Intelligence
ANN:	Artificial Neural Network
BPDC:	Backpropagation-Decorrelation
BCI:	Brain Computer Interface
CT:	Computed Tomography
deSNN:	Dynamic Evolving Spiking Neural Network
deSNNr:	Dynamic Evolving Spiking Neural Network Reservoir
ECOS:	Evolving Connectionist Systems
EEG:	Electroencephalography
epSNN:	Evolving Probabilistic Spiking Neural Network
epSNNa-s:	epSNNr Architecture for Spectro-Temporal Data
epSNNa-v:	epSNNr Architecture for Spatio-Temporal Data
epSNNr:	Evolving Probabilistic Spiking Neural Network Reservoir
eSNN:	Evolving Spiking Neural Network
GRN:	Gene Regulatory Network
ICA:	Independent Component Analysis
LIF:	Leaky Integrate-and-Fire Neuron
LSM:	Liquid State Machine
MRI:	Magnetic resonance imaging
NR:	Noisy Reset Neuron Model
NT:	Noisy Threshold Neuron Model
PCA:	Principal component analysis
ROSC:	Rank Order Spike Coding
RNN:	Recurrent Neural Network

RC:	Reservoir Computing
SDSP:	Spike-Driven Synaptic Plasticity
SNN:	Spiking Neural Network
SOM:	Self-Organizing Map
SPAN:	Spike Pattern Association Neuron
SSTD:	Spatio- and Spectro-Temporal Data STBD
STBD:	Spatio-Temporal Brain Data
STDP:	Spike-timing dependent plasticity
STPR:	Spatio-Temporal Pattern Recognition

Abstract

This thesis is a feasibility study of using a Spiking Neural Network (SNN) architecture named NeuCube for the classification of electroencephalography (EEG) data related to the perception of art. We have performed classification of human brain perception EEG data obtained via a set of experiments on originally created audio, video, and audio & video mixed stimuli. The analysis of results confirms that the proposed method is feasible for further analysis and experimentation, and for the study of art perception and creativity.

Massive amounts of complex Spatio-Temporal Brain Data (STBD) have been accumulated recently. As it is critical in many disciplines to rely on proper analysis, understanding and utilization of complex spatio-temporal brain data, such as that from an EEG, this is a great challenge which this study seeks to contribute to. In this study, for classification purposes, a new evolving Spiking Neural Network (SNN) architecture called NeuCube will be used. NeuCube is the latest neuroscience software tool developed at KEDRI, AUT, for spatio- and spectro -temporal pattern recognition of brain data, for the creation of concrete models to map, learn and understand STBD. A NeuCube model is based on a 3D evolving SNN that is an approximate map of structural and functional areas of interest of the brain related to the modeling of STBD. An evaluation of feasibility of NeuCube for classification of Spatio-Temporal EEG brain perception data is performed in this study.

An authentication methodology is proposed and illustrated on several small-scale examples of classification of EEG human brain perception data collected on audio and visual stimuli pairs. A methodology for person identification is proposed that uses a certain audio and/or video stimulus as a “security key” for the authentication process. The stimuli pairs used for experiments in this study were created the following way; an

audio pair is highly structural classical music versus disordered / chaotic noise, a visual pair is a set of opposing structural repetitive archetypical video patterns from an abstract modern art video, and also mixed audio/video pairs are used. The term of “brainprints” is offered by the analogy with fingerprints and prospectively having the ability to supply similar functionality but with an even higher level of security.

In addition the following hypotheses on the nature of human creativity are proposed in this study: human creativity might be defined as naturally inherited human ability and necessity to decipher, digest and transfer the universe global programme (human-independent) into patterned structures, expressed in some unique distinctive way. Therefore the concept of a genius might be defined as human ability to decipher and translate “global universe postulates” into human-readable patterns, performed the best possible way for the majority of a certain population.

Chapter 1

Motivation and objectives of the study

1.1 Significance of brain study for the contemporary world and its modern challenges

The brain is the most mysterious and little-understood organ in the entire human body. It monitors and controls everything that happens inside our bodies and it's the source of our thoughts, emotions and our memories. Therefore, it's responsible for every conscious and subconscious effort or activity we make. It's our supercomputer and we must know how it works.

Studying a human brain taken separately is similar to studying a cell isolated from its' surroundings in a body: the picture is too small and the knowledge is too limited for full

understanding. In modern individual-oriented society we seem to have forgotten the critical fact of mutual dependency of all human beings; an individual isn't capable of surviving alone but needs to live in a community. The belonging to a community network, the necessity of receiving, processing and transmitting information is vital to a human. To understand ourselves, as to who we are, we have to explore and study the human network and research its rules and principles. This global networking research is extremely complex and arguably infeasible due to the level of abstraction a single researcher should possess.

The amount of various data, which should be collected and analyzed, is enormous and the time frame for experimentation would exceed an average human lifetime. But the network that is always with us and ready to be explored, is the human brain network. When a developing fetus is only four weeks old, brain cells form at a rate of a quarter-million per minute [3]. The latest study [2] shows that the average human brain has on average 86.1 ± 8.1 billion (86.1×10^{11}) neurons. The number of connections for a neuron can range from 1000 to 200000 [1]. Eventually, billions of neurons will interact and form trillions of connections. This tremendous human brain network might be just a fractal “neuron” of the global network and may be governed by the same rules. Many questions might be answered in a variety of science fields from neuroscience and microbiology to macro sociology with an increased understanding and modelling of the human brain network.

Human brain networking processes may be used as a reference network model in analyzing and better understanding of functioning of a human society network on each level starting from a family, or a «nuclear» network through community level network. This knowledge might then be generalized for studying of processes underlying formation of nationalities and nations networks. Following the fractal theory idea we may assume that deeper research into human brain networking would finally bring us to

the root question of human self-identification and will fill us with new knowledge and deep understanding of our own being.

1.2 Definition of a human brain perception

Coming back to the Earth and to the current study, the key factor in the study of human abilities to receive, process and transmit information is a phenomenon of human brain perception. This phenomenon will be the major object of this study.

We have to mention that a study of perception shouldn't be taken in isolation. Instead it is interesting for us and should be considered as a part of a complex problem of the definition of a notion of intelligence. This is widely considered as the main feature characterizing and defining a human or if being more precise, a homo sapience.

Perception is defined in literature as the organization, identification, and interpretation of sensory information in order to represent and understand the environment [4], as the ability to learn or understand things or to deal with new or difficult situations [7]. Perception is not the passive receipt of nervous system signals, but is shaped by learning, memory, expectation, and attention [5] [6]. Intelligence is defined as a very general mental capability that involves the ability to reason, plan, solve problems, think abstractly, comprehend complex ideas, learn quickly and learn from experience [8].

The key points in the above mentioned definitions is the notion of learning; so ability to learn is considered as the core characteristic of intelligence. To understand the main principles of human intelligence, we have to discover the mystery of human ability to learn, and the research of human brain perception is the essential part of that.

The whole field of science that we call artificial intelligence (AI) was founded more than half a century ago, on the claim that a central property of humans, intelligence, can be precisely described and therefore can be simulated by a machine [9].

This arguable statement has been criticized vigorously since then, but now AI has become an essential part of the technology industry and helps solve many of the most difficult problems in computer science [10][11][12]. Still the central goals of AI research include reasoning, knowledge, planning, learning, communication, perception and the ability to move and manipulate objects [10]. Contemporary technologies allow us to make another qualitative step on this way. Here we may detail the objectives of this study. The main purpose is using the newest neuroscience software tool to explore experimentally the brain data of human perception. Primarily (and as the first step) the classification of the experimentally obtained brain perception data will be targeted.

In the later stages of the proposed research and if the stage of qualitative collection of experimental data is successful, further steps of more detailed comparative research are to be undertaken.

1.3 Reasoning for the original stimuli used in the experiments

Attempts to describe the phenomenon of human intelligence has brought us to the concept of learning which is, in turn, revealing the problem of transmitting or passing from one generation to the future generations the information blocks which were carefully collected and saved. Our point of interest in this area is to understand the role of art in this enigmatic process.

The specific audio and video stimuli for experiments were prepared to represent specific aspects of human art and in particular to represent the hypothesis of the patterned nature of human inspiration and creativity and the hypothesis of information coding nature of human creativity, fig.1.3.1.



Fig.1.3.1 Screenshots of the video stimuli, (a) Natural snowflake, (b) Tibetan mandala

Human art objects might be considered as products of non-verbal, and moreover, as pre-verbal coding systems with core objectives of transferring highly important information between generations and across generations. The transferred information is not part of any linguistic system. The origin of that information lays deeper, it is pre-linguistic and is supposed to be available for absorption by any human community, despite their specific language and religion beliefs. The information is encoded as repetitive archetypical symbols (see the appendix A), which persistently exists in almost every known culture starting from very deep historical layers. Paradoxically, the same symbols have appeared recently with the current era of technological development which we suppose, had not been reached by our predecessors and ancestors. An unanswered question is how they could generate the patterns, which later on were reproducing and repeating through the centuries, the hidden meaning of which we

probably have just started to understand? The full understanding of the origin of this information is only possible via complete understanding, deciphering and interpretation of key postulates encoded inside of the repetitive archetypical symbols of human art.

Considering art objects from this perspective, we may find a new meaning in such categories of art as colour (a certain frequency waves), sound (again a certain frequency sound waves), rhythm (time dependence of both mentioned above categories), shape, and such philosophical notion as harmony that bond together all the categories. Harmony might be defined then as a coded structure, derivative product of the universe programme running on the principles given as “global variables” with “read only” or “strictly limited” human access. Human creativity might be defined as the ability to decipher, digest and transfer the mentioned above running global programme product in his or her unique manner. When we are talking about a human ability to receive, process or “digest”, and transfer the universe information in some distinctive way, we mean that a final art object consists of two compulsory parts: the one is an information “nucleus” or the core content message, and another part is an additional surplus delta which is a unique “deciphering” manner of a certain human. A theory of a surplus element of an art object was declared first by the famous avant-garde artist and philosopher K. Malewitsch [13]. The more universal and digestible this deciphering implementation, the closer he and his works match the definition of a genius.

To reflect the declared hypothesis, three sets of audio and video stimuli were composed. The first visual stimulus consisted of ancient human art patterns (repetitive patterns of ancient Tibetan mandalas [14], one of them is shown in fig.1.3.1(b)). The second stimulus employed the natural objects that were perpetually used as inspiration art models and as decoration patterns by humans (pictures of snow crystals or snowflakes made by professor Kenneth G. Libbrecht at CALTECH, California [15] for the Physics of Crystal Growth and Pattern Formation in Ice project; snowflake is a highly structural

repetitive pattern reproduced in a range of ancient symbols, fig.1.3.1 (a)). The third stimulus was composed of works of modern abstract art (works of S. Dali, A. Warhol and V. Kandinsky [16], fig.6.2.2 (a) (b)).

Audio components were associated accordingly with the video components: for the first and the second audio stimuli we used two ingeniously structural pieces of classical music of 16th century: music works by Johann Sebastian Bach the Ich ruf⁷ zu dir, Herr Jesu Christ (BWV 639) and the Wachet auf, ruft uns die Stimme (BWV 140).

The third stimulus was composed from pure unstructured industrial noise.

Chapter 2

Literature review of methods of measuring of brain signals

2.1 Introduction to the Human Brain

The fundamental principles of the human brain structure and functions are briefly highlighted in this section.

The human brain is divided into two hemispheres, right and left, each of those consists of four lobes: the frontal, temporal, parietal, and occipital fig.2.1.1 [17].

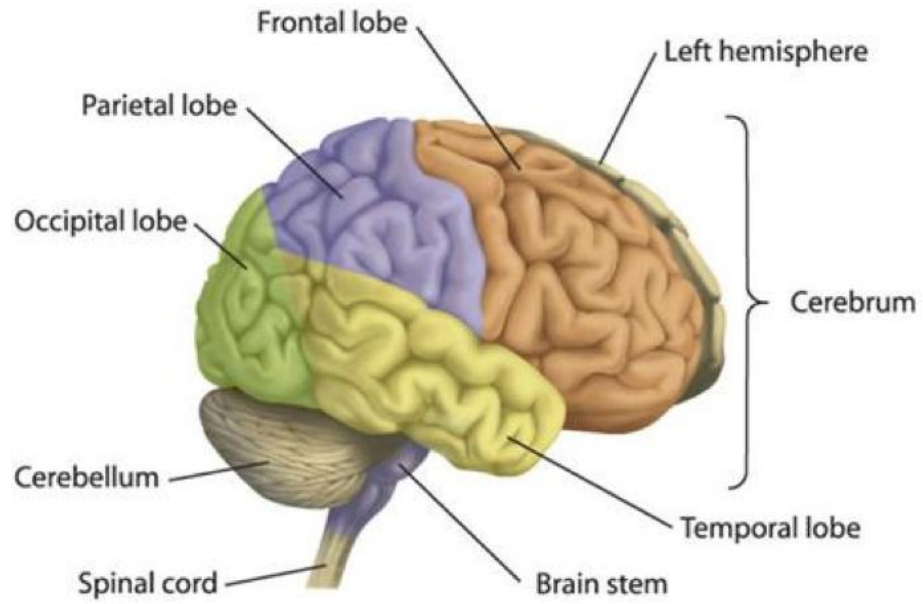


Fig.2.1.1. Human brain structure.

The human brain has different functional areas that are spatially distributed in a constrained 3D space. When the brain processes information obtained through visual, auditory, olfactory, somatosensory, emotional or combined stimuli complex spatiotemporal paths are activated and patterns are formed across the whole brain, e.g. fig.2.1.2 [18].

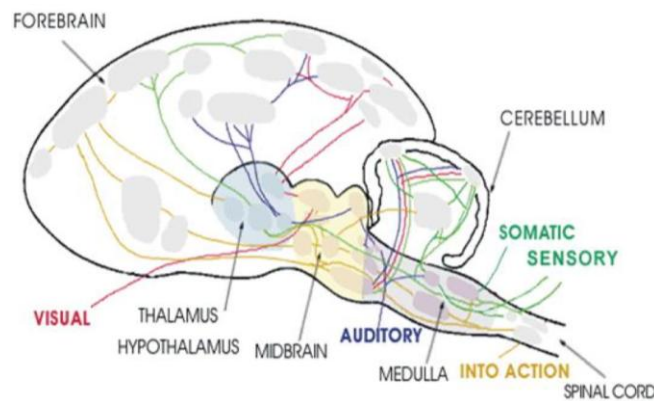


Fig. 2.1.2 Spatio-temporal signaling paths in the brain.

The cognitive functions occur mainly in the cerebral cortex, which is a thin outer layer of the human brain with breadth of 2-4 mm. With the assistance of brain imaging technologies the brain functions are precisely localized, fig. 2.1.3 [17]

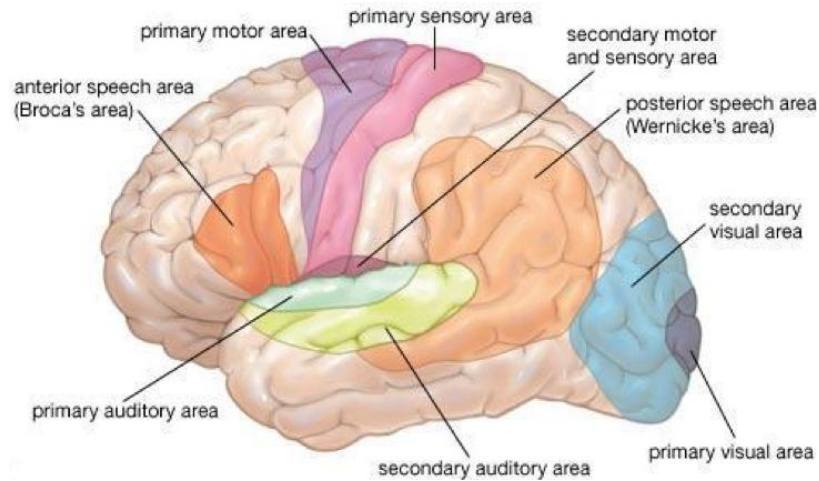


Fig. 2.1.3. Localization of the brain functions.

When brain signals and brain activities are measured, the most common types of data collected are Spatio- and Spectro-Temporal data (SSTD). The processing of information by the brain involves many brain areas. The open source EEGLAB experiments and simulations illustrate the involvements of several large brain areas, and the sensor-space mixing problem fig.2.1.4 [19].

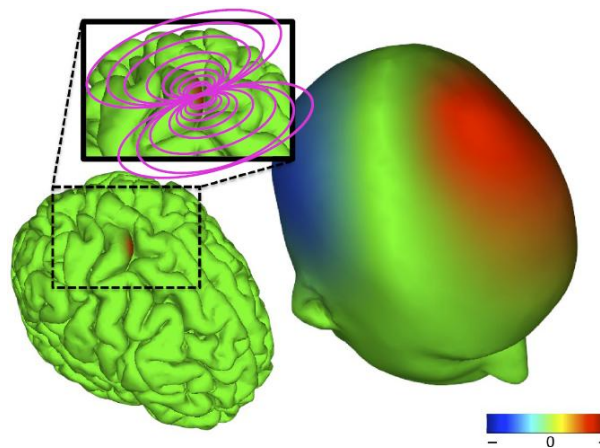


Fig. 2.1.4 (Left) Simulation of a cm²-scale cortical EEG source representing an area of locally synchronized cortical surface-negative field activity, and (right) its broad projection to the scalp.

The brain activity patterns can be acquired by recording the electrical, metabolic or magnetic measurements of the neurons, forming what is called brain data.

2.2 Methods for the measurement of brain signals

When we are discussing human brain perception research, we need to fully realize what type of brain study should be considered for that purpose. The study of the brain has already yielded remarkable findings, and advances in brain research have created a better understanding of the way we function. But how does contemporary science study the brain?

A broad spectrum of different invasive and non-invasive methods is used in the cognitive neurosciences. Each of these methods is used to study a different aspect of the brain. Each has its advantages and disadvantages and the method to be used always depends on the topic being studied.

The brain can be scanned with an axial tomography scan machine which will provide a researcher with multilayered 3-D images. This will help to detect abnormalities in the brain and examine its structure and will demand a specific preparation process and expensive tomography laboratory. Positron emission tomography or PET scans allow us to see the brain's metabolic functioning in 3D images at a cellular level by injecting a subject with a safe dose of radioactive material. This method also demands special preparation procedures and a laboratory [20].

A researcher can use functional magnetic resonance imaging or fMRI technique to measure brain activity by detecting associated changes in blood flow [21]. The FMRI procedure is widely used both in the research and clinical world, demanding laboratory equipment and having ability to localize activity of grey matter to within millimeters

within a time window of a few seconds [21]. This time window is too large to be applicable to the analysis of human brain perception where we have to measure changes within a few milliseconds. The method which allows us to explore human brain perception within this reduced timeframe, is EEG or Electroencephalography.

2.3 Advantages of EEG method

Electroencephalography is the recording of electrical activity along the scalp. EEG measures voltage fluctuations resulting from ionic current flows within the neurons of the brain [22]. In clinical contexts, EEG diagnostic applications generally focus on the spectral content of EEG, the type of neural oscillations that can be observed in EEG signals. In neurology, the main diagnostic application of EEG is in the case of epilepsy [23]. A secondary clinical use of EEG is in the diagnosis of coma, encephalopathy, and brain death. A third clinical use of EEG is for studies of sleep and sleep disorders. EEG can also be used for the diagnosis of tumors, stroke and other focal brain disorders [24], and such anatomical imaging techniques as MRI and CT can solve those problems better due to high (<1 mm) spatial resolution.

The derivatives of the EEG techniques such as evoked potentials (EP), which involves averaging the EEG activity time-locked to the presentation of visual, somatosensory or auditory stimuli and event-related potentials (ERPs), which refer to averaged time-locked to processing of stimuli EEG responses are widely used in cognitive science, cognitive psychology, and psychophysiological research [24].

Despite the disadvantage of limited spatial resolution, EEG is a highly valuable tool for research and diagnosis, especially when millisecond-range temporal resolution is

required which is not possible with CT or MRI; so EEG possesses multiple advantages over other techniques:

- Modern EEG systems are totally non-invasive.
- EEG has very high temporal resolution so EEG can detect changes over milliseconds, which is excellent, considering an action potential takes approximately 0.5-130 milliseconds to propagate across a single neuron, depending on the type of neuron [27]. Other methods, such as PET and fMRI have time resolution between seconds and minutes. EEG is commonly recorded at sampling rates between 250 and 2000 Hz in clinical and research settings, but modern EEG data collection systems are capable of recording at sampling rates above 20,000Hz [26].
- EEG is relatively tolerant of subject movement, unlike most other neuroimaging techniques. The new methods have been presented recently for minimizing, and in some cases even eliminating movement artifacts in EEG data [25].
- EEG is silent, allowing better study of the responses to auditory stimuli, which is extremely important for this study.
- EEG measures the brain's electrical activity directly, while other methods record changes in blood flow (e.g., SPECT, fMRI) or metabolic activity (e.g., PET, NIRS), which are indirect markers of brain electrical activity.
- EEG does not involve exposure to high-intensity (>1 Tesla) magnetic fields, as in some of the other techniques, especially MRI and MRS.
- Hardware costs of EEG are significantly lower than those of most other techniques [28].

Regarding the EEG method in stationary conventional scalp EEG, the recording is obtained by placing electrodes on the scalp with a conductive gel or paste. Many systems typically use electrodes, each of which is attached to an individual wire. Some

systems use caps or nets into which electrodes are embedded; this is particularly common when high-density arrays of electrodes are needed fig.2.3.1 [29].



Fig.2.3.1 EEG system

Electrode locations and names are specified by the International 10–20 system [30] for most clinical and research applications (except when high-density arrays are used), fig 2.3.2.

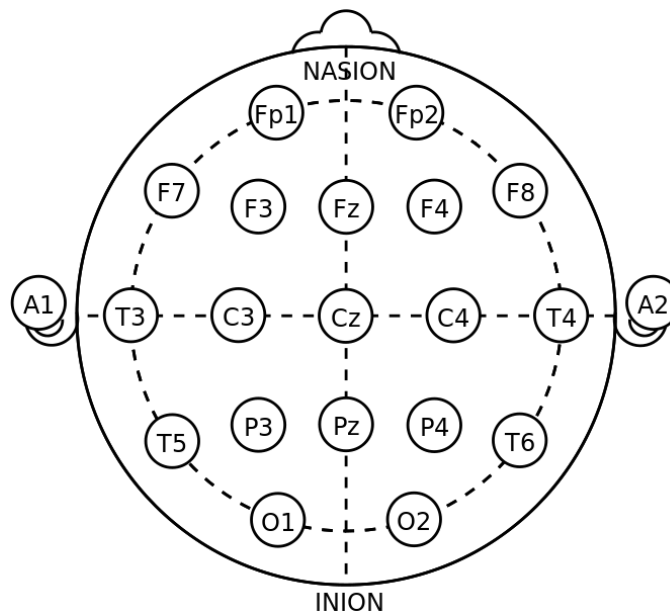


Fig 2.3.2 Electrode locations and names specified by the International 10–20 system.

This system ensures that the naming of electrodes is consistent across laboratories. High-density arrays (typically via cap or net) can contain up to 256 electrodes more-or-less evenly spaced around the scalp. A typical adult human EEG signal is about 10 μV to 100 μV in amplitude when measured from the scalp [31].

All methods mentioned above for collecting brain data are constrained by requirements of laboratory environment. Contemporary cognitive-state or perceptive human brain research sets new challenges and demands to be non-invasive, non-intrusive, non-tethered, and non-stop. Development of the technologies allows us to make another qualitative step in collecting EEG brain data. These technologies enable translation of laboratory oriented neuroscience research to study the human brain in real-world environments. Modern EEG systems are based on dry sensors and mobile/wireless systems for measuring neural and behavioral data from unconstrained subjects in ecologically valid environments fig. 2.3.3 [32]:



Fig. 2.3.3 The EPOC Emotiv neuroheadset



Fig.2.3.4 High-Density Mobile & Wireless EEG systems MINDO-32 and -64

These High-Density Mobile & Wireless EEG systems allow us to use real-time data processing, fig 2.3.4 [33]; pervasive brain or body telemonitoring with multi-tiered fog and cloud computing. One of the critical challenges to be addressed is designing signal-processing techniques capable of finding statistical relationships among the variations in environmental, behavioral, and functional brain dynamics. Therefore methods of classification of EEG data represent significant challenges and are of great importance.

2.4 EEG data review

Brain-related electrical potentials are recorded from the scalp in EEG. The difference in voltage between the electrodes is measured, and due to weakness of the signal (30-100 μ V) it is amplified. Current occurs when neurons communicate fig. 2.4.1. The simplest event is called action potential, and a discharge is caused by fast opening and closing of Na⁺ and K⁺ ion channels in the neuron membrane. If the membrane depolarises to some threshold, the neuron will “fire”. Tracking of these discharges over time reveals the brain activity [34].

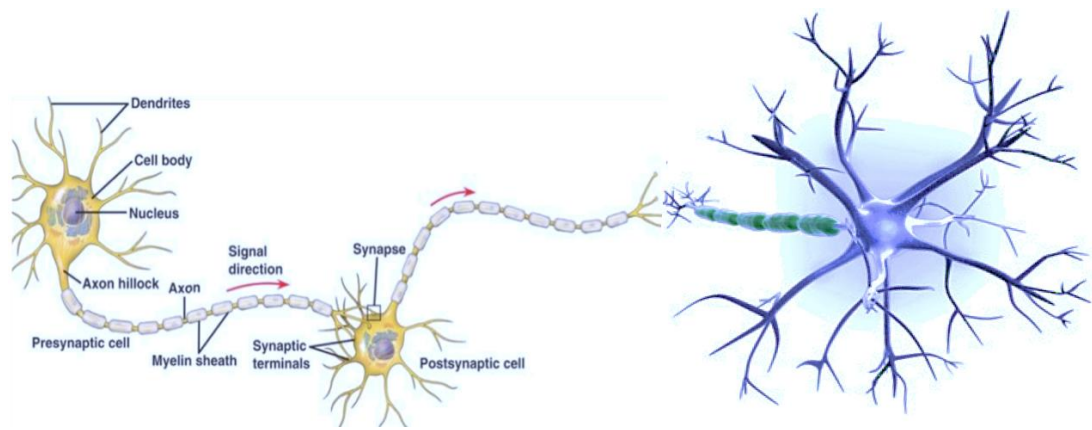


Fig. 2.4.1 Action potentials transferring between neurons through synapse

The EEG is typically described in terms of rhythmic activity. A German scientist Hans Berger, who discovered electroencephalography (EEG) about 80 years ago found that different electrical frequencies could be linked to actions and different stages of consciousness by observing subjects performing different tasks while recording their EEG [34]. That rhythmic activity is divided into bands by frequency. Figure 2.4.2 [35] and tab.2.1 show the frequency bands and their relations to the human brain wave activity.

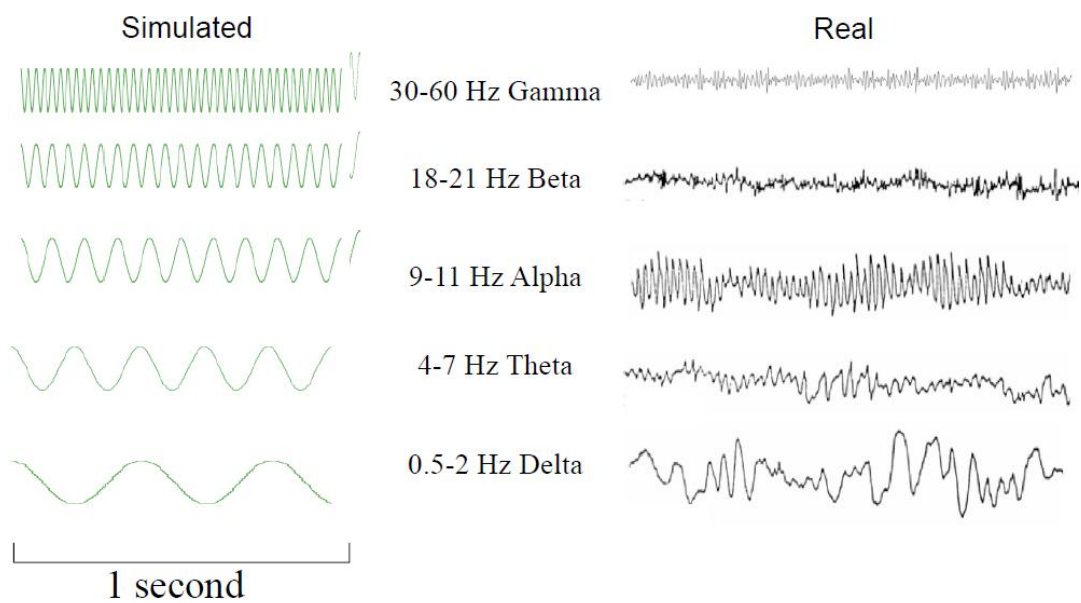
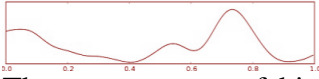
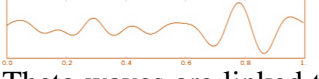
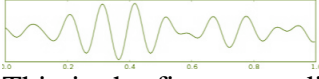
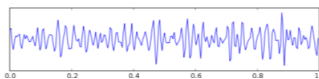


Fig. 2.4.2 Common oscillatory modes in EEG

<i>Signal</i>	<i>Frequency</i>	<i>Properties</i>
Delta	1-3 Hz	 <p>These waves are of high amplitude and low frequency, the slowest waves and occur when sleeping [36]. If these waves occur in the wakeful state, it is thought to indicate physical defects in the brain. Movement can make artificial delta waves, but with an instant analysis (just observing raw EEG records), this can be verified. It is seen in young children normally.</p>
Theta	4-7 Hz	 <p>Theta waves are linked to inefficiency, daydreaming, and the very lowest waves of theta represent the fine line between being awake or in a sleep state. Theta arises from emotional stress, especially frustration or disappointment [37]. It has also been associated with access to unconscious material, creative inspiration and deep meditation. High levels of theta are considered abnormal in adults. This signal is normally observed in young children.</p>
Alpha	8-13 Hz	 <p>This is the first wave discovered on the human brain. It has high amplitude. Alfa waves are associated with relaxation and disengagement. It emerges with eye closing, and attenuates with eye opening and mental exertion.</p>
Beta	14-30 Hz	 <p>Beta waves are often divided into β_1 and β_2 to get a more specific range. The waves are associated with focused concentration and best defined in central and frontal areas. When resisting or suppressing movement, or solving a math task, there is an increase of beta activity [37]. Beta waves can be also called sensorimotor rhythm accruing when arms or hand idle. It could be associated with anxious thinking. In case of cortical damage this wave can be absent.</p>
Gamma	>30 Hz	 <p>Gamma waves are in the frequency range of 31Hz and up. It is thought that it reflects the mechanism of consciousness. The pattern is associated with alertness, working and motor movements Beta and gamma waves together have been associated with attention, perception, and cognition. [38]</p>

Tab. 2.1 Frequency bands related to the human brain wave activity.

Scalp EEG signals appear to be noisy because they each sum a mixture of signals generated in many brain areas, fig 2.4.3 [35]. Poor spatial resolution is one of the main constraints of EEG.

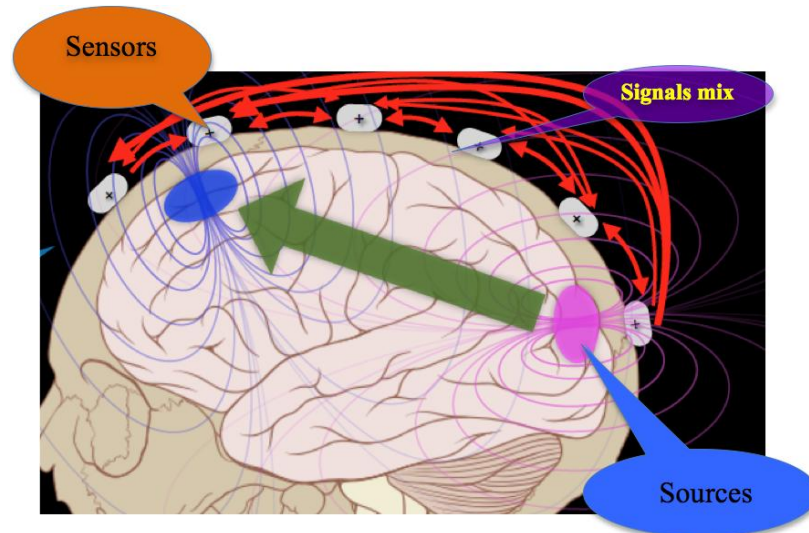


Fig. 2.4.3 Mixture of signals

The generation and modulation of EEG is complex and not well studied. It is mathematically impossible to reconstruct a unique intracranial current source for a given EEG signal, as some currents produce potentials that cancel each other out [39]. This is referred to as the inverse problem. However, much work has been done to produce remarkably good estimates of a localized electric dipole that represents the recorded currents [35].

The nature of the study and the set up tasks let us turn the weak point of poor spatial resolution of EEG into a feature that doesn't prevent solving the problem of personal identification based on a personal subjects perception, on unique brainprints. A unique subjects background will differently activate different brain areas and will allow the NeuCube to build a unique network pattern, which would be possible to recognize and identify. As the performed experiments have shown, the person identification classification completed with a full set of EEG system channels and accomplished with full time stimuli presentation, has a higher level of classification accuracy than in

experiments with selected auditory and /or visual brain area channels only, with shorter stimuli. This fact allows us to make a suggestion that the brain data collected with the use of high-density EEG systems and with presentation relatively long audio/video stimuli will give us a more specific neural network for a certain subject and therefore will allow higher identification accuracy. The limitation in this case would be the computational feasibility or availability of computing resources.

2.5 Methods of classification of EEG data

The analysis of an enormous quantity of spatio-temporal brain data in a format of EEG that has been collected recently presents a serious challenge to researchers. To be able to make a new qualitative step in classification analysis it is important to understand the way the analysis was developed and highlight the core traditional classification models. The most applied method for signal processing and analysis is arguably considered to be the Fourier Transformation and extraction of band powers [40]. The algorithm is based on discrete Fourier transform (DFT) equation 4.1, and by applying that to the EEG signal it makes it possible to separate the EEG rhythms. (Tab.2.1).

Definition of the DFT:

$$X_n = \frac{1}{N} \sum_{k=0}^{N-1} \left(X_k e^{i2k\pi \frac{n}{N}} \right) \quad k=0, \dots, N-1 \quad (2.1)$$

And the inverse of it:

$$X_n = \frac{1}{N} \sum_{k=0}^{N-1} \left(X_k e^{i2k\pi \frac{n}{N}} \right) \quad (2.2)$$

The performance of the DTF is $O(N^2)$, but there is a more efficient algorithm called Fast Fourier Transform (FFT), that can compute the same result in only $O(N \log N)$.

This is a great improvement and one of the reasons why FFT is one of the favourite methods of analyzing EEG signals. There are several categories that cover the most used algorithms in classification systems, and among them are such traditional methods as linear classifiers, nonlinear Bayesian classifiers, nearest neighbor classifiers, neural networks, and a combination of classifiers [40]. We will briefly describe some of them: *Linear Regression* is a statistical approach to modelling the relationship between a scalar dependent variable y and some explanatory variables, fig. 2.5.1. In linear regression data are modelled using linear predictor functions, and unknown model parameters are estimated from the data. The basic form of a linear predictor function $f(i)$ for data point i (consisting of p explanatory variables), for $i = 1, \dots, n$, is

$$f(i) = \beta_0 + \beta_1 x_{i1} + \dots + \beta_p x_{ip}, \quad (2.3)$$

where β_0, \dots, β_p are the regression coefficients, weights, etc. indicating the relative effect of a particular explanatory variable on the outcome. Thus the model takes the form:

$$y_i = \beta_1 x_{i1} + \dots + \beta_p x_{ip} + \varepsilon_i = \mathbf{x}_i^T \boldsymbol{\beta} + \varepsilon_i, \quad i = 1, \dots, n, \quad (2.4)$$

where T denotes the transpose, so that $\mathbf{x}_i^T \boldsymbol{\beta}$ is the inner product between vectors \mathbf{x}_i and $\boldsymbol{\beta}$.

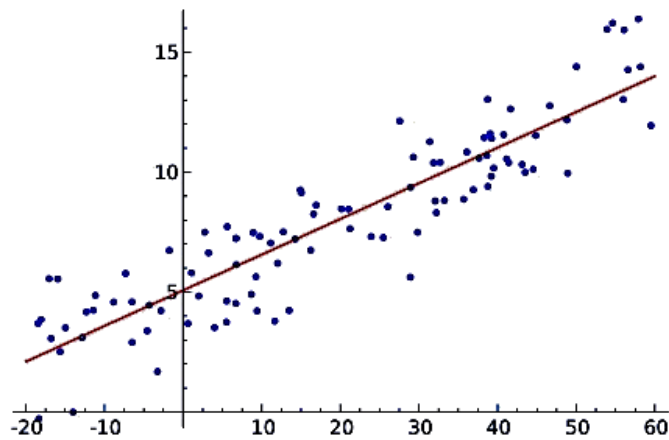


Fig. 2.5.1 Linear Regression

Logistic regression or *logit regression* is a type of probabilistic statistical classification model [41]. Logistic regression measures the relationship between a categorical dependent variable and independent variables, which are usually continuous, by using probability scores as the predicted values of the dependent variable [42]. An explanation of logistic regression begins with an explanation of the logistic function, which always takes on values between zero and one [43].

$$F(t) = \frac{e^t}{e^t + 1} = \frac{1}{1 + e^{-t}}, \quad (2.5)$$

We also define the inverse of the logistic function, the *logit*:

$$g(x) = \ln \frac{\pi(x)}{1 - \pi(x)} = \beta_0 + \beta_1 x, \quad (2.6)$$

and equivalently:

$$\frac{\pi(x)}{1 - \pi(x)} = e^{\beta_0 + \beta_1 x} \quad (2.7)$$

The input is the value of $\beta_0 + \beta_1 x$ and the output is $\pi(x)$. A graph of the logistic function $\pi(x)$ is shown in fig.2.5.2.

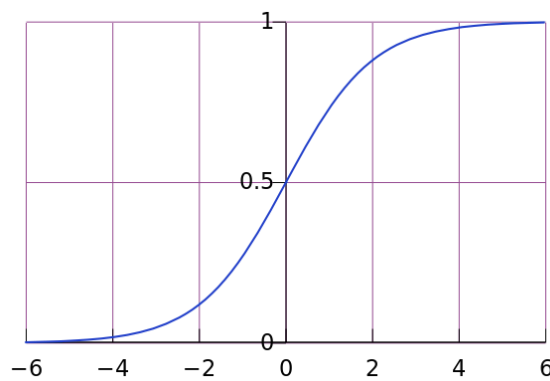


Fig. 2.5.2 The logistic function with $\beta_0 + \beta_1 x$ on the horizontal axis and $\pi(x)$ on the vertical axis.

Support vector machine (SVM) is a concept in computer science for a set of related supervised learning methods that analyze data and recognize patterns, used for classification and regression analysis [43]. The standard SVM takes a set of input data and predicts for each given input which of two possible classes the input is a member of. This makes the SVM a non-probabilistic binary linear classifier. A support vector machine constructs a hyperplane or set of hyperplanes, fig. 2.5.3, in a high- or infinite-dimensional space which can be used for classification, regression, or other tasks.

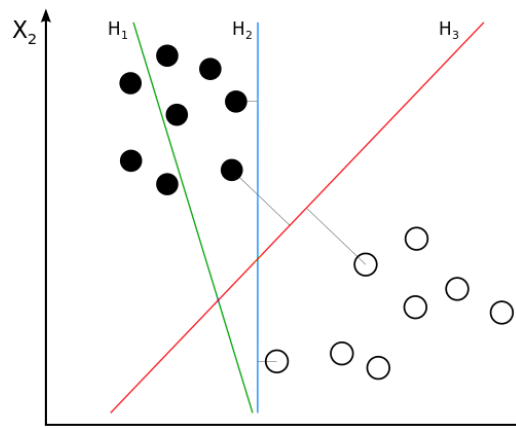


Fig. 2.5.3 Only hyperplane H3 separates classes with the maximum margin.

The Multilayer perceptron (MLP) is a feed forward artificial neural network model that maps sets of input data onto a set of appropriate outputs. An MLP consists of multiple layers of nodes in a directed graph, with each layer fully connected to the next one, fig.2.5.4. Except for the input nodes, each node is a neuron (or processing element) with a nonlinear activation function. The MLP utilizes a supervised learning technique called backpropagation for training the network [44], [45]. MLP is a modification of the standard linear perceptron and can distinguish data that are not linearly separable [46].

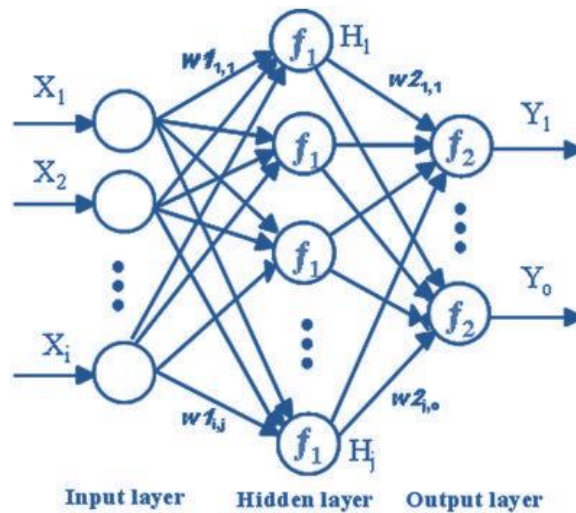


Fig.2.5.4 Multilayer perceptron

Each neuron uses a nonlinear activation function which was developed to model the frequency of action potentials, or firing of biological neurons in the brain. This function is modeled in several ways, but must always be normalizable and differentiable. The two main activation functions used in current applications are both sigmoids, and are described by:

$$\phi(v_i) = \tanh(v_i) \quad \text{and} \quad \phi(v_i) = (1 + e^{-v_i})^{-1}, \quad (2.8)$$

The multilayer perceptron consists of three or more layers, an input and an output layer with one or more hidden layers of nonlinearly-activating nodes. Each node in one layer connects with a certain weight w_{ij} to every node in the following layer. Learning occurs in the perceptron by changing connection weights after each piece of data is processed, based on the amount of error in the output compared to the expected result. This is an example of supervised learning, and is carried out through backpropagation, a generalization of the least mean squares algorithm in the linear perceptron.

Hidden Markov Model (HMM) is a statistical Markov model in which the system being modelled is assumed to be a Markov process with unobserved (hidden) states [47]. A HMM can be considered the simplest dynamic Bayesian network.

The mathematics behind the HMM is closely related to an optimal nonlinear filtering problem/stochastic processes. Hidden Markov models are especially known for their application in temporal pattern recognition such as speech, handwriting, gesture recognition [48] musical score following and bioinformatics.

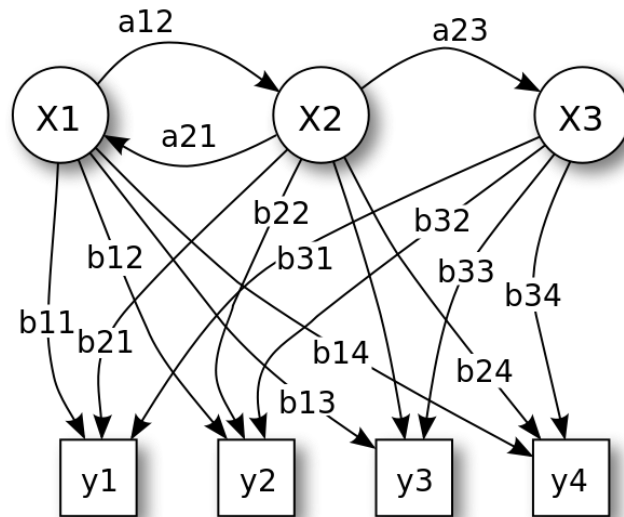


Fig. 2.5.5 Probabilistic parameters of a hidden Markov model, x – states, y - possible observations, a - state transition probabilities, b - output probabilities.

In the standard type of hidden Markov model, fig. 2.5.5, the state space of the hidden variables is discrete, while the observations themselves can either be discrete or continuous, typically from a Gaussian distribution. The parameters of a hidden Markov model are of two types, transition probabilities and emission probabilities, also known as output probabilities. The HMM has a limitation when defining more than a single independent variable. They can only be defined for a process that is a function of a single variable, such as time or one-dimensional position [49]. This limitation makes HMM inadequate for two-dimensional SSTD patterns.

With regards to the combination of classifiers the interactive Matlab toolboxes have to be mentioned. They are: EEGLAB, created for processing continuous and event-related EEG, MEG and other electrophysiological data incorporating independent component analysis (ICA), time/frequency analysis, artifact rejection, event-related statistics, and several useful modes of visualization of the averaged and single-trial data [35];

BCILAB, an open source Matlab toolbox for Brain-Computer Interface research; and Source Information Flow Toolbox (SIFT).

Independent Component Analysis. Decomposing data by ICA or any linear decomposition method, including Principal component analysis (PCA) and its derivatives (PCA is mathematically defined [50] as an orthogonal linear transformation) involves a linear change of basis from data collected at single scalp channels to a spatially transformed "virtual channel" basis. ICA makes a key assumption: that the far-field signals produced by the cortical and non-cortical EEG sources are temporally distinct and, over sufficient input data, near temporally independent of one another. More advanced ICA approaches including complex ICA, if performed on Fourier or wavelet transformed EEG data at 10 Hz, might indeed be able to recover, in some cases, evidence of near cm-scale potential flow patterns within individual cortical alpha source domains. ICA is an effective method for removing stereotype data artifacts including eye blinks and lateral eye movements, muscle activities, electrode or line noise, and pulse artifacts [51], fig. 2.5.6.

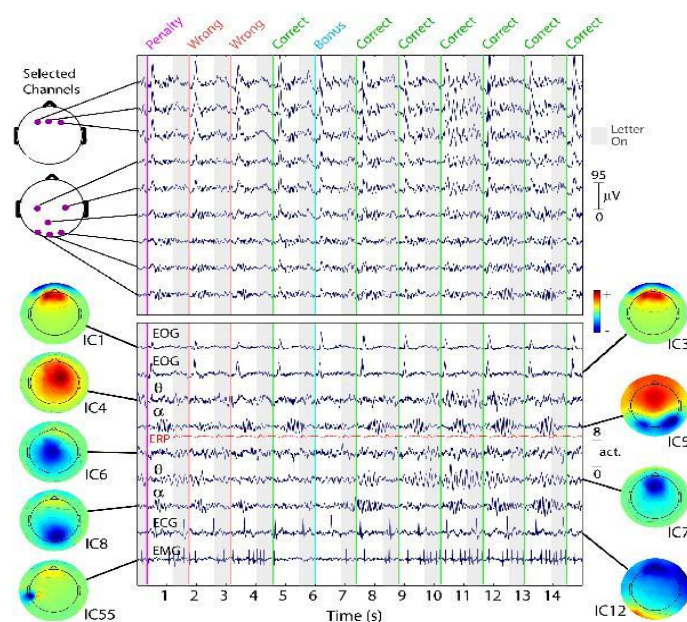


Fig. 2.5.6 Fifteen seconds of EEG data at 9 (of 100) scalp channels (top panel) with activities of 9 (of 100) independent components (ICs, bottom panel). While nearby electrodes (upper panel) record highly similar mixtures of brain and non-brain activities, ICA component activities (lower panel) are temporally distinct.

BCILAB is an EEGLAB plugin for the design, prototyping, testing, experimentation with, and evaluation of Brain-Computer Interfaces (BCIs), and other systems in the same computational framework [35]. Most of *BCILAB*'s functionality is contained in (plugin) components, of which there are five types. Most plugin types reside in their own directory and are automatically identified and loaded by *BCILAB*.

Signal Processing components are implemented as single MATLAB functions that translate input signals into output signals; they can be adaptive or static, linear or non-linear, causal or non-causal, they can operate both in real time or offline, and on continuous or epoched data - thus they can implement arbitrary processing, as long as the inputs and outputs are both signals. Signals are represented as extended EEGLAB datasets. The majority of signal processing components serve to filter the input signals (e.g., spatially, spectrally, or in time), thereby discarding unwanted information and "amplifying" information of interest, i.e., improving the signal/noise ratio of the data. Other filters may implement more specialized processing, such as re-representing the data in a more interpretable basis (ICA, sparse reconstruction, or the Fourier transform). Feature extraction components take off where signal processing ends. They accept epoched or continuous signals and output sequences of feature vectors, thereby transforming segments of data into some abstract domain (referred to as the feature space). Feature extraction often simplifies the data and can drastically reduce its dimensionality. The processing may be static or adaptive, and, if adaptive, it frequently uses information about the value of the variables to be predicted (called supervised learning). Typical algorithm choices are certain simple mathematical transformations (e.g., PCA, wavelet decomposition, etc.).

Machine learning components come in two parts, one to learn a predictive model from some data, and the other to apply a previously learned model to data, in order to make predictions. The learning function ultimately summarizes the data (the pre-processed

example data gathered in the calibration session). BCI paradigm components are MATLAB functions that tie together all stages of a BCI approach, including any signal processing, feature extraction, machine learning functions, as well as their default parameters or allowed parameter ranges, fig. 2.5.7 [52].

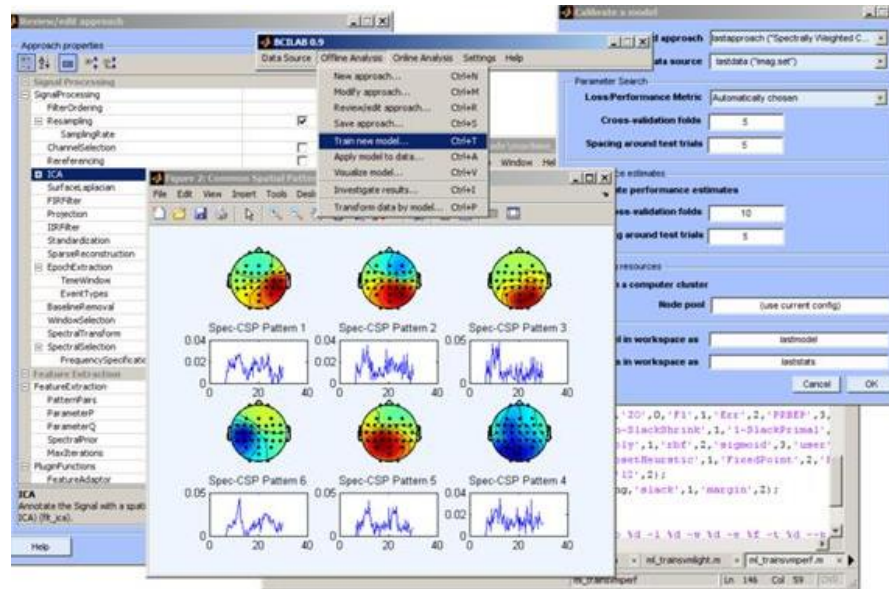


Fig. 2.5.7. EEGLAB BCI tool.

Source Information Flow Toolbox (SIFT) is an EEGLAB-compatible toolbox for analysis and visualization of multivariate causality and information flow between sources of electrophysiological (EEG/ECOG/MEG) activity [53]. It consists of a suite of command-line functions with an integrated Graphical User Interface for easy access to multiple features. There are currently four modules: data preprocessing, model fitting and connectivity estimation, statistical analysis, and visualization.

Methods currently implemented include: Preprocessing routines; Time-varying (adaptive) multivariate autoregressive modeling (granger causality; directed transfer function (DTF, dDTF); partial directed coherence (PDC, GPDC, PDCF, RPDC); multiple and partial coherence; event-related spectral perturbation (ERSP) etc);

Bootstrap/resampling and analytical statistics; a suite of programs for interactive visualization of information flow dynamics across time and frequency (with optional 3D visualization in MRI-coregistered source-space), fig. 2.5.8.

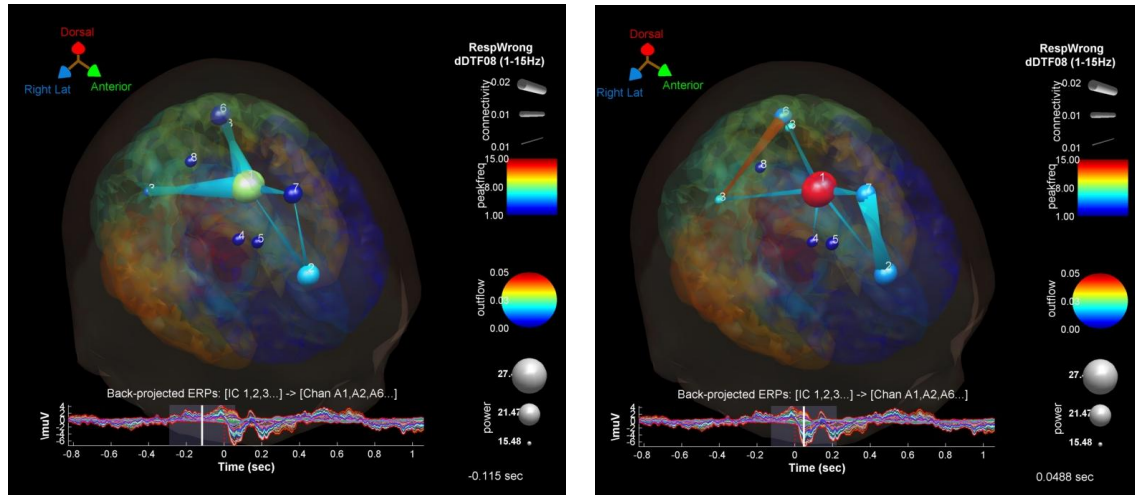


Fig. 2.5.8 Still images of SIFT 3D visualization / brainmovie.

2.6 Summary

The nature of EEG brain data is spatio- or spectro- temporal and it is an extremely difficult task for machine learning to analyse the data successfully. Another feature which is especially problematic for analysis is the tight correlation between spatial and temporal components of the SSTD. As mentioned above, traditional methods of EEG data analysis have been widely used but with limited success [54] for the classification of EEG data [40, 55, 56, 57]. This gives priority to either the spatial-, or the temporal component of the data, but does not take into account their dynamic interaction. In addition, they were able to accommodate multimodal STBD and prior information about the source of this data.

As there are no universal traditional classification methods for EEG brain data analysis, the new techniques, inspired by nature, should be explored further.

Chapter 3

Introduction to SNN

3.1 What is ASNN?

The first artificial neural network (ANN), which is a computational mathematical model that is capable of machine learning and pattern recognition, was defined by its first inventor Alexander Bain [58] in 1873 in his book “*Mind and Body. The Theories and Their Relation*”. It was defined as a model inspired by the brain. The Spiking Neural Networks (SNN) were proposed by Alan Lloyd Hodgkin and Andrew Huxley in 1952. Recent SNN models, developed by W. Gerstner, W. Kisler [59] and Izhikevich [60] became the third generation of neural network models, increasing the level of realism in neural simulation [61].

It is still impossible to reproduce the exact functioning mechanism of the biological neuron, the full brain functionality is still a mystery for us. Even a single neuron process is extremely complex, fig.3.1.1[62].

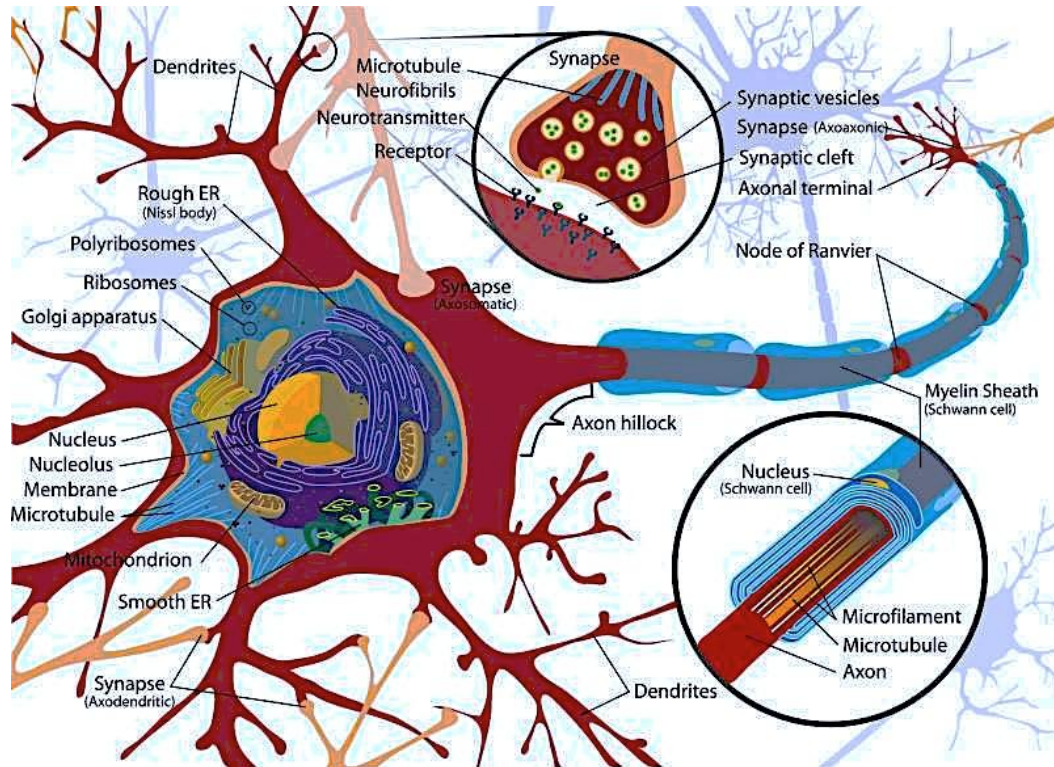


Fig.3.1.1: Schematics of a biological neuron illustrating signal propagation and synapsis.

The brain represents and processes information in the form of many trains of temporal electrical potentials that can be considered binary events (spikes) and are transferred between neurons through synaptic connections. Through learning from data the synaptic connections are modified to reflect more precisely the timing of the data from the sensory inputs. To avoid any prior assumptions on neural computation, the processing and exchange of information between neurons should be carried out at the level of spikes [59]. SNNs are made up of artificial neurons that use trains of spikes to represent and process pulse coded information [61]. SNNs use trains of spikes for internal information representation [63]. This is one of the principles of brain-inspired spiking neural networks [64] resulting in the consideration of SNNs as the new generation of neural network models with additional capabilities in a range of fields such as spatio-

temporal spheres (e.g. time series), complex networks with several thousand neurons and areas requiring biological fidelity.

In summary, Artificial Spiking Neural Networks (ASNN) consist of neuronal models with network structure and connectivity which encode information into spikes and use learning algorithms to dynamically respond to new input signals.

3.2 SNN models

Traditional ANN's neural models consisted of synaptic weights and an activation / transfer function. The artificial neuron abstraction could be expressed mathematically as:

$$y_j = \varphi \sum_i w_{ij} x_i \quad (3.1)$$

where y_j and x_i are the neuronal output and input signals respectively, φ is the activation function and w_{ij} represents the synaptic connection weight between neurons i and j .

Biological neurons are described by ion currents that are transmitted through the cell membrane when neurotransmitters activate the ion channels in the cell. Many models have been proposed in order to simulate a biologically realistic neuron, among them are such models as Hodgkin-Huxley's model [65], Spike Response Models (SRM) [59], Integrate-and-Fire Models [61]; [59] Izhikevich models [66, 67, 68, 69]. We briefly highlight the main characteristics of some of them.

Hodgkin-Huxley is based on the experiments on the giant axon of the squid, Hodgkin and Huxley found three different ion channels: sodium, potassium and Cl^- ions leak current [65, 16, 17]. In mathematical terms, this model can be described as an electric circuit (see fig.3.2.1) having a capacitance (C), batteries (E), and current sources (I).

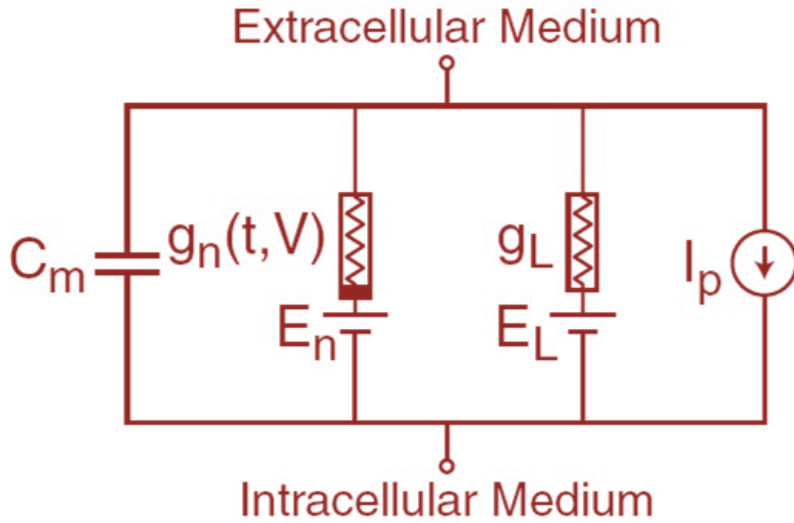


Fig.3.2.1 Hodgkin-Huxley type models represent the biophysical characteristic of cell membranes. The lipid bilayer is represented as a capacitance (C_m). Voltage-gated and leak ion channels are represented by nonlinear (g_n) and linear (g_L) conductances, respectively. The electrochemical gradients driving the flow of ions are represented by batteries (E), and ion pumps and exchangers are represented by current sources (I_p). Adapted from Hodgkin and Huxley [65].

The current applied over time ($I(t)$), (fig.3.2.1), may be distributed as a capacitive current (I_C) which charges the capacitor (C), and the current (I_k) of each ion channel is:

$$I(t) = I_C(t) + \sum_k I_k(t) \quad (3.2)$$

where the \sum_k represents the sum of all ion channels. The capacitor (C) can be defined as $C = Q/u$, where Q and u are the charge and voltage across the capacitor. Thus, charging capacitive current can be represented as

$$I_C = C \frac{du}{dt} \quad (3.3)$$

According to Eq.3.2 and Eq.3.3:

$$C \frac{du}{dt} = - \sum_k I_k(t) + I(t) \quad (3.4)$$

Therefore, Eq.2.4 can be used to represent Hodgkin-Huxley's three ion channel model as:

$$\sum_k I_k(t) = g_{Na} m^3 h (u - E_{Na}) + g_K n^4 h (u - E_K) + g_L (u - E_L) \quad (3.5)$$

where E_{Na} , E_K and E_L are reversal potentials obtained from empirical experiments. The gating variables m , n and h evolve according to the differential equation

$$\dot{x} = \alpha_x(u)(1 - x) - \beta_x(u)x \quad (3.6)$$

where x represents m , n or h and α_x , β_x denote exponential function that can be adjusted in order to simulate a specific neuron. It can be seen that the Hodgkin-Huxley model can reproduce electrophysiological measurements very accurately. However, due to the model's complexity, it is computationally expensive, making it inappropriate for simulating large networks of spiking neurons.

Leaky Integrate and Fire Model (LIF) or the leaky integrate-and-fire neuron is one of the best-known examples of a formal spiking neuron model, fig.3.2.2. Generalizations of the leaky integrate-and-fire model include the nonlinear integrate-and-fire model. All integrate-and-fire neurons can either be stimulated by external current or by synaptic input from presynaptic neurons.

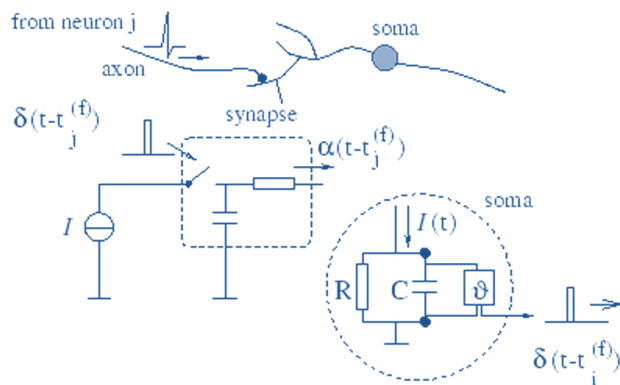


Fig. 3.2.2. Schematic diagram of the integrate-and-fire model. The basic circuit is the module inside the dashed circle on the right-hand side. A current $I(t)$ charges the RC circuit. The voltage $u(t)$ across the capacitance (points) is compared to a threshold ϑ . If $u(t) = \vartheta$ at time $t_i^{(f)}$ an output pulse $\delta(t - t_i^{(f)})$ is generated. Left part: A presynaptic spike $\delta(t - t_j^{(f)})$ is low-pass filtered at the synapse and generates an input current pulse $\alpha(t - t_j^{(f)})$ [72].

A LIF neuron is a simplified Hodgkin-Huxley model where all the ion channels are represented with a single current [72]. The basic circuit of an integrate-and-fire model consists of a capacitor C in parallel with a resistor R driven by a current $I(t)$; see fig. 3.2.2 The driving current can be split into two components, $I(t) = I_R + I_C$. The first component is the resistive current I_R , which passes through the linear resistor R . It can be calculated from Ohm's law as $I_R = u/R$ where u is the voltage across the resistor. The second component I_C charges the capacitor C . From the definition of the capacitance as $C = q/u$ (where q is the charge and u the voltage), we find a capacitive current $I_C = C du/dt$. Thus, according to Eq.3.3 and $I_R = u/R$ (Ohm's law) we get

$$I(t) = \frac{u(t)}{R} + C \frac{du}{dt} \quad (3.7)$$

On introducing a time constant $\tau_m = RC$ and R in Eq.3.7, we yield the standard form

$$\tau_m \frac{du}{dt} = -u(t) + RI(t) \quad (3.8)$$

where u is the membrane potential, $I(t)$ is the input current, τ_m is the membrane time constant of the neuron and R represents soma membrane resistance. Apart from the stimulation by the external current $I(t) = I_{ext}(t)$ over time, in a network the neurons can also be stimulated by presynaptic neuron j . The synaptic input of neuron i is the weighted sum over all the currents generated by the presynaptic neurons and can be represented as:

$$I_i(t) = \sum_j w_{ij} \sum_f \alpha(t - t_j^{(f)}) \quad (3.9)$$

where weight w_{ij} reflects the strength of the synapses from neuron j to neuron i , $t_j^{(f)}$ represents the firing time of neuron j , while α represents the time course of the postsynaptic current. The LIF models were successfully used use in large-scale networks providing efficient simulation due to their relative simplicity.

Spike Response Model (SRM) is a generalization of the leaky integrate-and-fire model, or the LIF model can be considered as a special case of the general SRM that defines the spike dynamics. In SRM the state of the neuron i is defined by a single parameter $u_i(t)$ (membrane potential) [73,74, 75, 76, 77]. In the absence of spikes, the variable u_i is at its resting value, $u_{\text{rest}} = 0$. The function ϵ describes the time course of the response to an incoming spike, and w_{ij} represents synaptic efficacy. If after the summation of the effects of several incoming spikes u_i reaches the threshold ϑ , an output spike fires. The form of the action potential and the after-potential is described by the function η and the linear response of the membrane for external input current I_{ext} is represented by kernel function k . Supposing a neuron i has fired its last spike at time \hat{t}_i , then after firing the evolution of u_i is given by

$$u_i(t) = \eta(t - \hat{t}_i) + \sum_j w_{ij} \sum_f \epsilon_{ij}(t - \hat{t}_i, t - t_j^{(f)}) + \int_0^{\infty} k(t - \hat{t}_i, s) I_{\text{ext}}(t - s) ds \quad (3.10)$$

Compared to the LIF model, the membrane threshold of SRM is not fixed but may depend on $t - \hat{t}_i$, therefore

$$\vartheta \rightarrow \vartheta(t - \hat{t}_i) \quad (3.11)$$

Due to its simplicity the SRM is appropriate for simulating a large number of neurons in a network.

3.3 Reservoir NN framework

Reservoir computing (RC) is a neural network based computational framework where the input signal is fed into a fixed (random) dynamical system called a reservoir resulting in mapping of the input to a higher dimension. RC is an approach to design, train, and analyse recurrent neural networks (RNNs). It yields computational and sometimes analytical models for biological neural networks. What distinguishes reservoir computing from other views on recurrent neural networks are the fundamental principles that can be summarized as follows: using a large, random RNN or reservoir, such that when driven by input signals, each unit in the RNN creates its own nonlinear transform of the input; output signals are produced from the excited RNN by some readout mechanism, typically a simple linear combination of the reservoir signals; outputs can be trained in a supervised way, typically by linear regression of the teacher output on the tapped reservoir signals [78].

Reservoir computing includes a number of independently found approaches based on this fundamental idea, these are Liquid State Machines [79], [80], Echo State Networks [81] Backpropagation Decorrelation and Temporal Recurrent Networks [82]. The reservoir comprises a group of recurrently connected neurons. The connectivity is generally random, and the units are typically nonlinear. On the whole, the activity in the reservoir is driven by the input and is also influenced by the past. The reservoir's dynamical input output mapping provides a crucial benefit over the simple time delay neural networks. This approach theoretically allows for real time computation on continuous input streams in parallel. Each neuron is stimulated by time varying inputs from external sources as well as from other neurons. The recurrent connectivity turns the time varying input into a spatio-temporal pattern of activations in the network nodes [80]. The reservoir system is partially biologically plausible, since parts of the cerebral

cortex have been found to carry out sensory integration in small and homogeneous columns of neurons [84].

Reservoir computing for SSNs is now regarded as an established paradigm due to feasibility of the computational methods for practical applications, and as a model for some of the processes in the human brain. Some of the core concepts of reservoir computation are briefly explained below.

Echo State Networks (ESNs) proposed by Jaeger [81] is a recurrent neural network with a sparsely connected hidden layer. The connectivity and weights of hidden neurons are randomly assigned and are fixed. The weights of output neurons can be learned so that the network can reproduce specific temporal patterns. For training the ESNs, a linear readout function is often sufficient for achieving good performance when employed for practical applications. This is because of the algebraic properties inherent in the recurrent neural network that is ESNs. The term dynamical reservoir refers to untrained recurrent neural network component of ESNs, and its reservoir states are termed echoes since the state reflects the input history [81]. The main interest of this network is that although its behaviour is non-linear, the only parameters are the weights of the output layer. The error function is thus quadratic with respect to the parameter vector and can be differentiated easily to a linear system. The use of weighted sum and nonlinearity type of simulated analogue-valued neurons such as the $\tanh()$ nonlinearity function makes ESNs different from other reservoir computing models [85]. Since the readout from the echo state networks is linear, most often for batch training, a linear regression method is used for computing the output weights and a similarly computationally inexpensive method such as least squares algorithms are employed for the online training approach [86].

Liquid State Machines (LSMs) was proposed by Maass, Natschläger, and Markram [87] and is another reservoir method. LSM consists of a large collection of nodes or neurons. Each node receives time varying input from external sources / inputs as well as from other nodes which are randomly connected to each other. The recurrent nature of the connections turns the time varying input into a spatio-temporal pattern of activations in the network nodes. The spatio-temporal patterns of activation are read out by linear discriminant units. Compared to the ESNs which were framed on the basis of theoretical computational principles, the Liquid State Machine was developed on the basis of computational neuroscience. The foundation of Liquid State Machine allows the reservoir system to correspond to the computational properties of neural microcircuits [88].

3.4 Summary

SNN methods and engineering systems have been recently developed for the following subjects: learning from data [89,64, 65,67]; system design and implementation [90, 91]; encoding continuous input data into spike trains, such as the silicon retina and the silicon cochlea sensory devices [92, 93]; neurogenetic computation [94, 95]; high performance and neuromorphic engineering systems and supercomputers [96, 97]. There is a number of promising features of SNN such as: compact representation of space and time; fast information processing; time-based and frequency-based information representation. Information processing methods based on SNN, such as: methods for transformation of continuous input signals into spike trains; computational models of spiking neurons; methods for connecting and learning in SNN support the paradigm for STBD. Although numerous models of SNNs and their applications have

been developed, they have not been fully successful when used for solving large scale, complex AI problems of classification, temporal and string sequence pattern recognition and associative memory [95].

Looking for new inspiration, the developers of the latest SNN models are enhancing them with probabilistic parameters and evolving features. [98].

Lately, novel SNN methods for spatio-temporal pattern recognition were developed [99]. Among them are two types of evolving SNN classifiers – the Dynamic Evolving Spiking Neural Network (deSNN) [101] and SPAN (Spike Pattern Association Neuron) [100] and pilot applications for moving object recognition and for simple EEG data classification, recently proposed by the Kasabov framework for STBD – NeuCube [18] which will be used for purposes of classification of spatio-temporal EEG brain perception data. The main principles and the framework of the NeuCube as well as the more detailed methodology for EEG spatio-temporal data classification in the NeuCube environment will be explained later in chapter 4 of this study.

Chapter 4

The NeuCube based methodology of the study

4.1 The NeuCube objectives and challenges

The brain is a complex integrated spatio-temporal information-processing machine, which deals extremely well with the most common data collected to measure brain signals and brain activities- spatio-temporal data. [18].

Over recent decades a vast amount of information about structural and functional characteristics of the human brain has been accumulated [102, 103, 104, 105, 106]. That enormous quantity of Spatio-Temporal Brain Data (STBD) includes Electroencephalogram (EEG) [40, 55, 56, 57], Magneto encephalograph data (MEG) [107], functional Magnetic Resonance Imaging (fMRI) [108, 109, 110, 111] gene expression data related to brain states [112], etc. The analysis of this type of data

however still presents a challenge to researchers. Such traditional methods as Multiple Linear- and Logistic Regression, Support Vector Machines (SVM), Multilayer Perceptron Neural Networks, Hidden Markov Models, rule-based systems, and some others have been used with limited success [54] for the classification of EEG data [40, 55, 56, 57]. All these methods accentuate either the spatial-, or the temporal component of the data, but do not take into account their dynamic interaction. They can't accommodate multimodal STBD and prior information about the source of this data.

Although there are still no universal computational models to integrate all different types of data into a single model to analyze brain processes and to recognize brain signal patterns, the new EU FP7 Marie Curie IIF EvoSpike project develops methods and tools for spatio and spectro-temporal pattern recognition [18]. Within this project Kasabov proposed a new evolving spiking model called NeuCube for the creation of concrete models to map, learn and understand STBD. The NeuCube is 3D evolving Neurogenetic Brain Cube of spiking neurons that is an approximate map of structural and functional areas of interest of an animal or human brain. Similar to the human brain which processes information through the activation of complex spatio-temporal pathways involving many brain areas, the NeuCube is attempting to simulate the same principles in a computer model resulting in an improved accuracy of brain signal pattern recognition and discovery of new knowledge.

Summarizing the following principles that are to be utilized in the NeuCube architecture: ability to accommodate and integrate various STBD; spatial structure mapping the areas of the brain where STBD is collected; spiking information processing paradigm used in the model to represent and to process the STBD; brain-like learning rules using in the model to learn STBD; evolving ability to learn, recognize and add incrementally new STBD patterns, thus following brain cognitive development

principle; ability to keep a spatio-temporal associative memory which is a subject to be explored, interpreted and to be represented as a spatio-temporal finite automation.

To train NeuCube different types of brain SSTD can be used including EEG, fMRI, video-, image- and sound data and complex multimodal data. In this study EEG brain data were used to evaluate the feasibility of the NeuCube for classification of human brain perception of video & audio stimuli in a format of STBD.

4.2 The NeuCube Main Principles and Framework for STBD

The main idea of the NeuCube is the creation of a multi-modular integrated system, different modules of which consist of different neuronal types and genetic parameters. The parameters relate to different parts of the brain and different functions of interest such as: vision, sensory information processing, sound recognition or motor-control etc. The whole system works in an integrated mode for brain signal pattern recognition. A concrete NeuCube architecture model would have been built for every specific problem (as classification of EEG signals; recognition of fMRI data; BCI; emotional cognitive robotics, etc) and would have a specific structure and a set of algorithms depending on the problem or application [18].

A NeuCube model learns from STBD and creates connections between clusters of neurons that establish chains or trajectories of neuronal activity [113]. After performing learning, a NeuCube model can reproduce these trajectories working as an associative memory, even if only part of the input STBD or the stimuli data is presented. The NeuCube framework can be used as a predictive system of brain activities, discovering functional pathways from data and can be used to predict certain events. Analysis of the internal structure of a model after training can reveal important spatio-temporal relationships ‘hidden’ in the data. NeuCube can be used for personalized modeling

purposes allowing the integration in one model of various brain data and other information related to a certain subject.

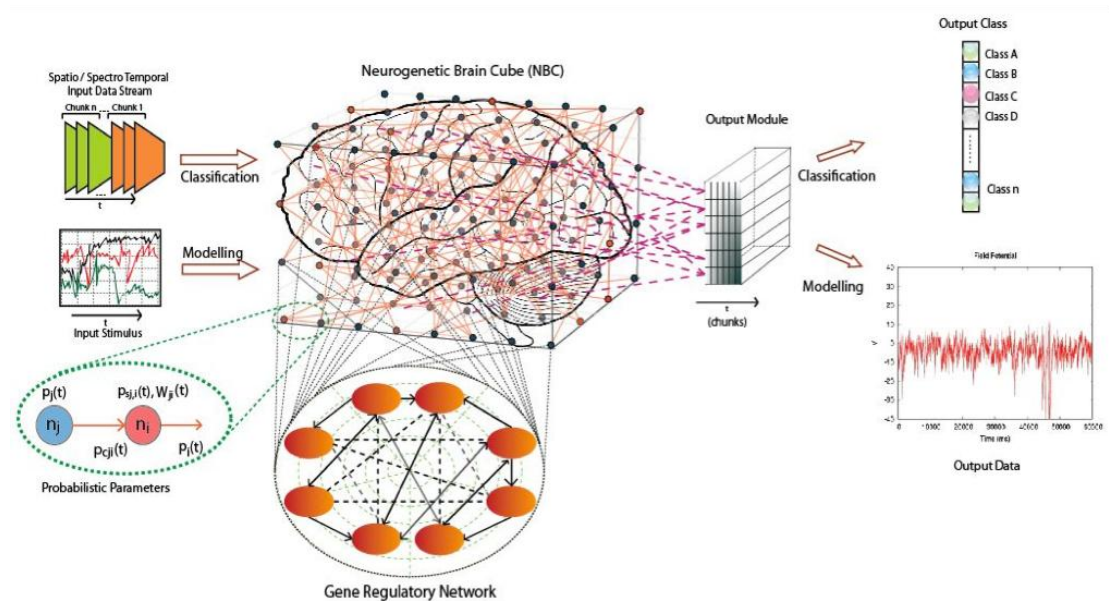


Fig. 4.2.1. A schematic diagram of a general NeuCube architecture, consisting of: input encoding module; NeuCube module; output function module; gene regulatory networks (GRN) module (optional)

A block diagram of the general EvoSpike NeuCube architecture is shown in fig.4.2.1 [18], [113]. Consisting of three levels a NeuCube architecture includes a NeuCube module at the middle level, gene regulatory networks (GRN) at the lowest level, and a classification or evaluation module at the highest level. Neurons from the NeuCube are connected to neurons of the output module in a two-way mode, so that the state of the NueCube can be recognized, classified and interpreted in the Output Module and the result of this can further influence activity of the neurons in the NeuCube as a feedback. In detail the functional modules of the NeuCube are the following:

- Input information encoding module;
- 3D SNN reservoir module (SNNr) or Neurogenetic Brain Cube (NBC) module;
- Output function module / classification module;
- Gene regulatory networks (GRN) module, (optional).

The steps of the process of creating a NeuCube model for a certain STBD are the following:

1. Encoding the STBD into spike sequences: continuous value input information is encoded into trains of spikes;
2. Constructing and training, in an unsupervised mode, a recurrent 3D SNN reservoir (SNNr) to learn the spike sequences that represent individual input patterns;
3. Constructing and training, in a supervised mode, an evolving SNN classifier to learn to classify different dynamic patterns of the SNNr activities that represent different input patterns from SSTD that belong to different classes;
4. Optimizing the model through several iterations of steps 1 to 3 above for different parameter values until maximum accuracy is achieved.
5. Recalling the model on new data.

We briefly describe the NeuCube modules.

4.3 The NeuCube module architecture

Input data encoding module where continuous value input data can be transformed into spikes so that the current value of each input variable (in our case it is EEG channel, but it might be pixel or fMRI voxel) is entered into a population of neurons that emit or transfer input into trains of spikes. The input information is distributed through a large population of neurons and is represented by spike time relatively. The quantity of information that can be transmitted by this type of code increases with the number of neurons in the population. Spike emitting is based on the level of the membership degree of the input to their receptive fields. This method is called *population rank coding* [114] reflecting the principle: the higher the membership degree, the earlier a spike is generated, fig.4.3.1.

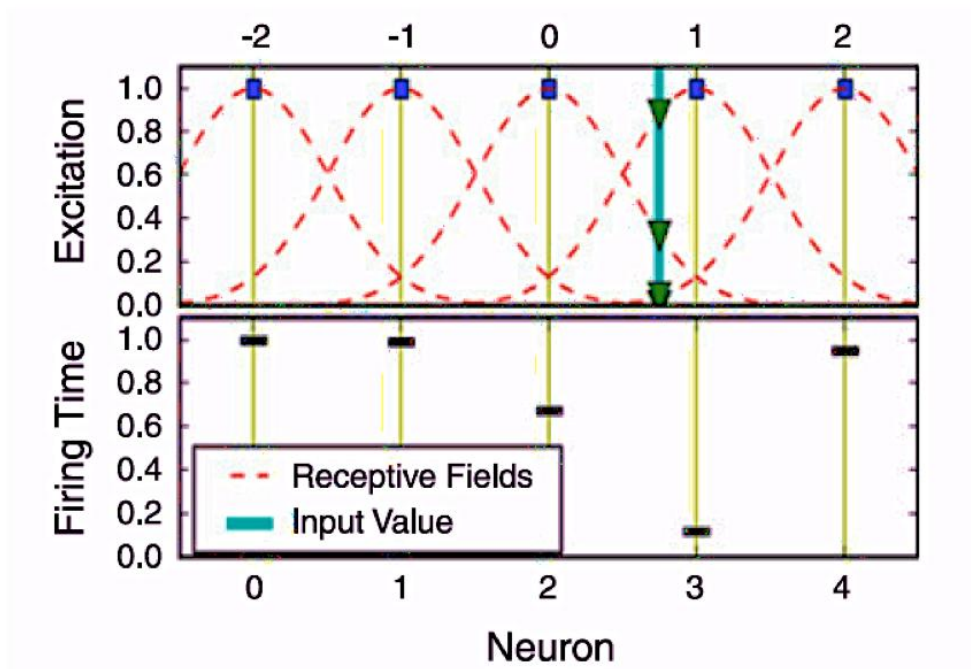


Fig.4.3.1 Population rank order coding of input information

Another method of encoding of input data is the Address Event Representation (AER) [115]. This method is based on thresholding the difference between two consecutive values of the same input variable over time, fig.4.3.2 and fig.4.3.3. This method is used when the input data is a stream and only the changes in consecutive values can be processed (as video and sound stream data).

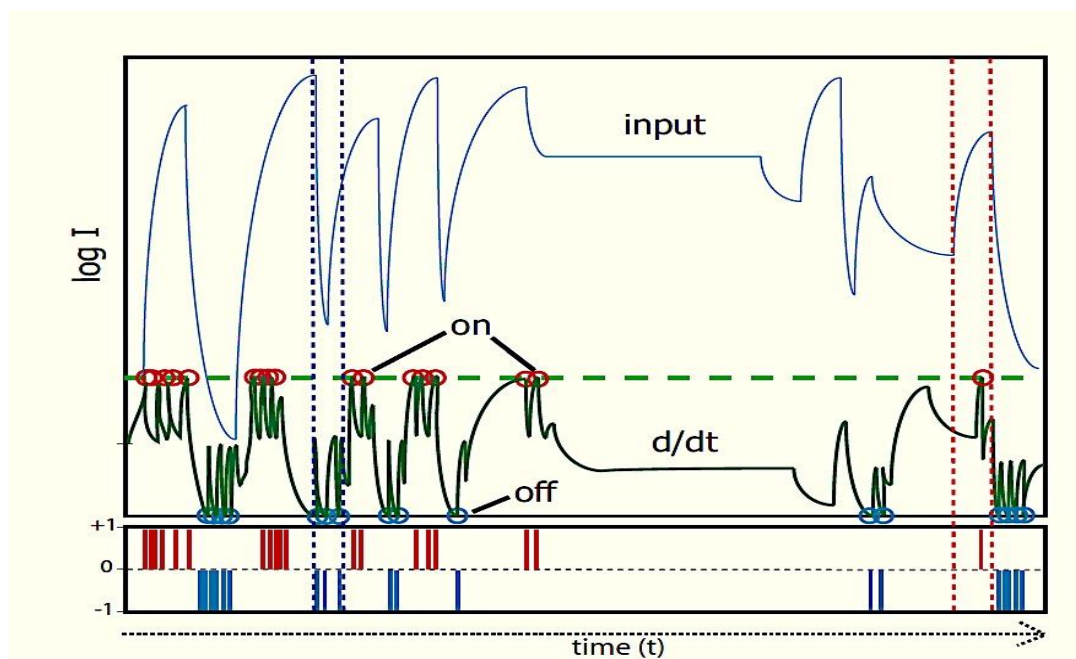


Fig.4.3.2 AER of continuous value time series input data into spike trains, the idealized pixel encoding and reconstruction of video data.

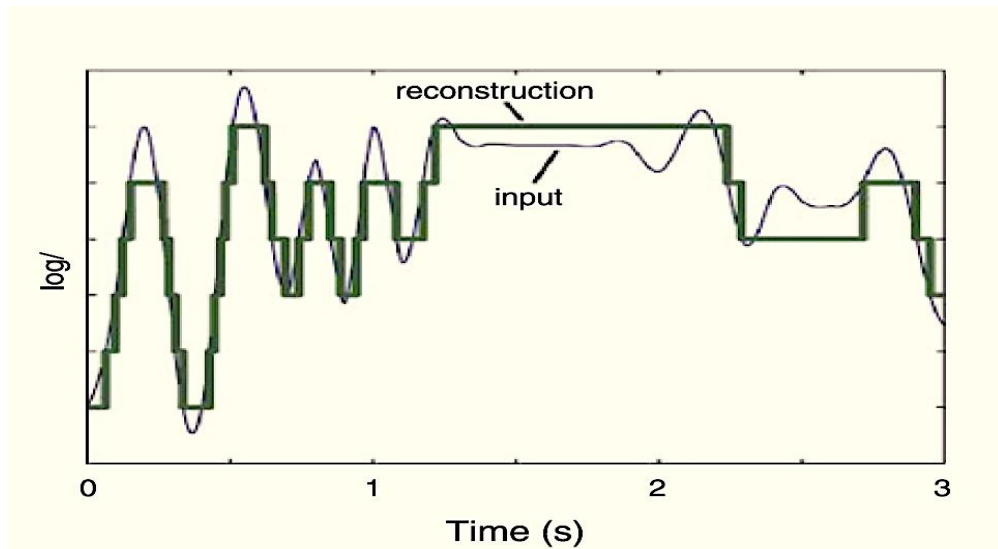


Fig.4.3.3 AER of continuous value time series, the idealized pixel reconstruction of video data.

A spike encoder method called Ben's Spike Algorithm (BSA) has been used for EEG data transformation into spike trains [116]. The benefit of using BSA is that the frequency and amplitude features are smoother in comparison to some other algorithms, and the smoother threshold optimization curve, the less susceptible the algorithm to changes in the filter and the threshold, fig.4.3.4.

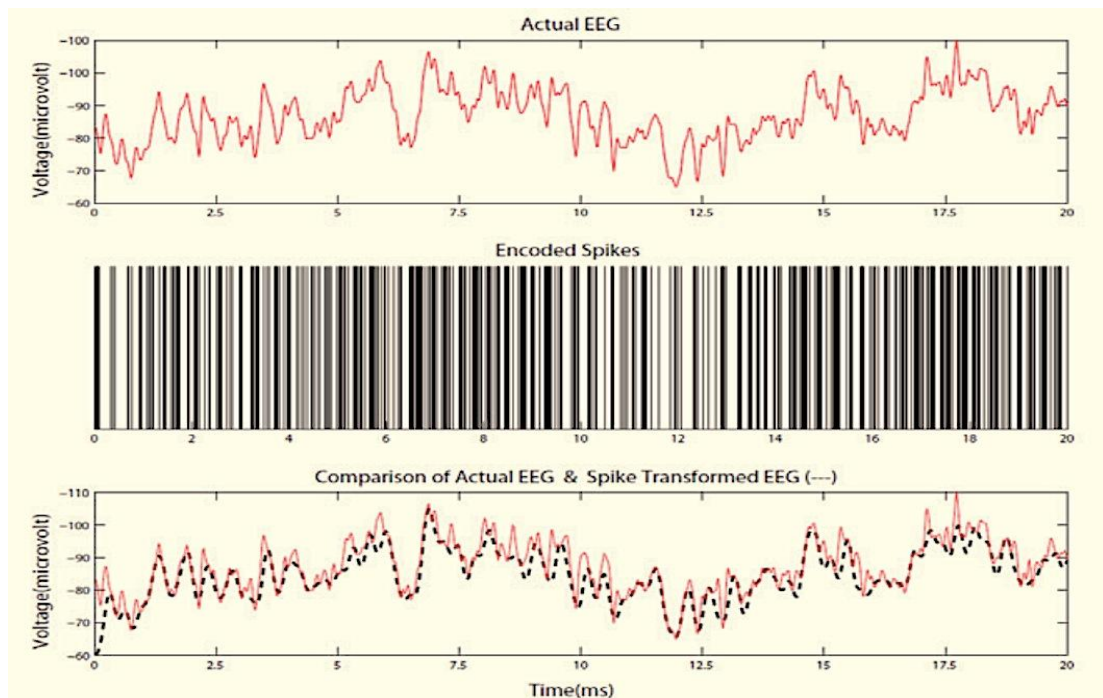


Fig.4.3.4. Actual one EEG channel signal (top); the spike representation of the above figure obtained using BSA (middle); and the bottom –the actual one EEG channel signal (red) plus superimposed with representation of the reconstructed EEG signal from the BSA encoded spikes (dashed).

Any of the mentioned above spike encoders may be realized in the NeuCube, the choice will depend on the existing problem. The transformed spike series input data is mapped into spatially located neurons from the SNNr. Here the brain data sequences in their temporal order are continuously fed into spatially located neurons in the SNNr that represent brain areas where data is collected.

3D SNN reservoir module (SNNr) or Neurogenetic Brain Cube (NBC) module is an approximate map of relevant brain regions for which STBD, and/or relevant genetic information available which has a 3D spiking neuronal structure. Small world connections are used for initialization, where neurons within a functional area of interest from the cube (e.g. visual area) are more densely connected than neurons across areas, depending on the distance between the neurons [117]. The initial structure of the SNNr is defined based on the available brain data and the problem, but this structure can be evolving through the creation of new neurons and new connections based on the STBD using the ECOS principles [118]. The new neurons are connected with the rest following the initial small-world principle.

Fig. 4.3.5 (a)–(c) illustrate the spiking activity (a) and connectivity of 1471 neurons SNNr before training (b) and after training—(c) on SSTD. It can be seen that as a result of training new connections have been created that represent spatio-temporal interaction between input variables captured in the SNNr from the data.

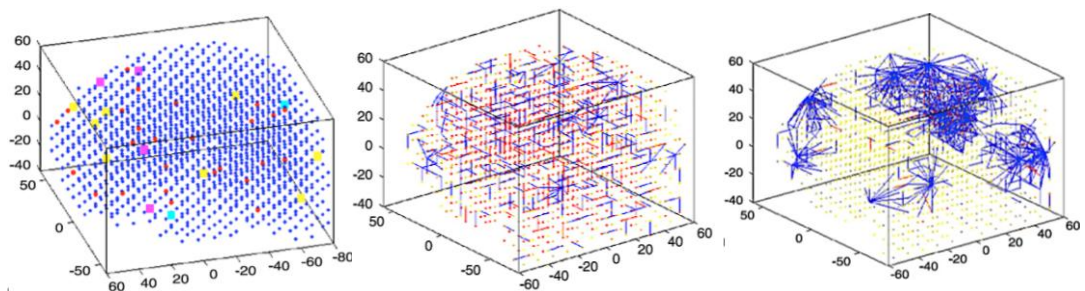


Fig.4.3.5 Visualization of connectivity and spiking activity of a SNNr: (a) spiking activity—active neurons are represented in red color and large size; (b) connectivity before training – small world connections – positive connections are represented in blue and negative—in red; (c) connectivity after training.

In this implementation, the SNNr has a 3D structure connecting leaky-integrate and fire model (LIFM) spiking neurons with recurrent connections, fig. 4.3.6 and 4.3.7.

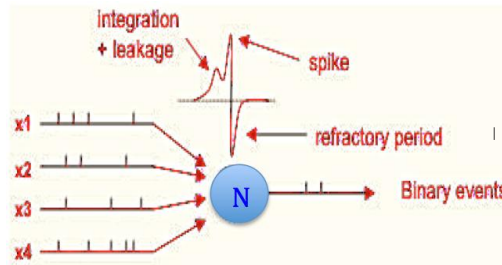


Fig.4.3.6. The structure of the LIFM

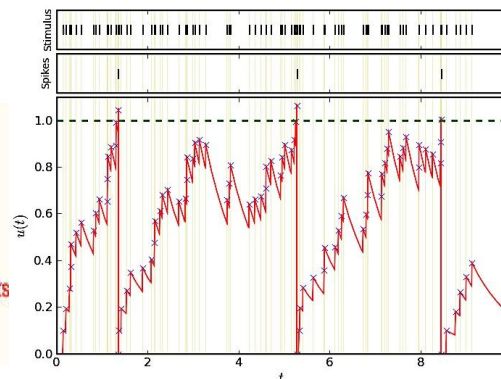


Fig.4.3.7. Functionality of the LIFM

The input STBD is propagated through the SNNr and a method of unsupervised learning is applied, such as Spike Timing Dependent Plasticity (STDP). The neuronal connections are adapted and the SNNr learns to generate specific trajectories of spiking activities when a particular input pattern is entered.

Different learning rules for SNN have been already introduced. The STDP learning rule [119] utilizes Hebbian plasticity [120] in the form of long-term potentiation (LTP) and depression (LTD). Based on the timing of post-synaptic action potential in relation to the pre-synaptic spike efficacy of synapses the connection weight is strengthened or weakened. If the difference in the spike time between the pre-synaptic and post-synaptic neurons is negative, this means that pre-synaptic neuron spikes first, then the connection weight between the two neurons increases, otherwise it decreases. Connected neurons, trained with STDP learning rule, learn consecutive temporal associations from data. New connections can be generated based on the activity of consecutively spiking neurons.

The rank-order learning rule [121] uses important information from the input spike trains, namely the rank of the first incoming spikes on the neuronal synapses, fig.4.3.8. It establishes a priority of inputs (synapses) based on the order of the spike arrival on these synapses for a particular pattern. Used in SNN the rank-order learning has

advantages in being fast one-pass learning (as it uses the extra information of the order of the incoming spikes) and asynchronous data entry.

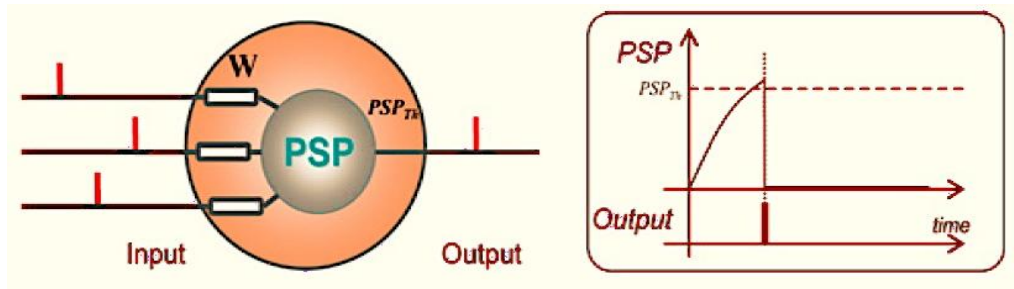


Fig. 4.3.8 Rank-order learning neuron

The dynamic eSNN (deSNN) [122] combines rank-order and temporal (e.g. STDP) learning rules. The initial values of synaptic weights are set according to the rank-order learning assuming the first incoming spikes are more important than the rest. The weights are further modified to accommodate following spikes activated by the same stimulus, with the use of a temporal learning rule—STDP.

SPAN is an algorithm for both classification and spike pattern association [123]. The connection weights of a neuron are updated after the presentation of the whole spatio-temporal spiking pattern, rather than spike-by-spike as it is in the deSNN model. SPAN learns to generate an output spike at a certain time, or a pattern of temporally distributed spikes over time, when a certain spatio-temporal pattern of input spikes is recognized.

All these briefly described learning principles can be implemented in the NeuCube. Different types of neurons and learning rules can be used in different areas of the evolving NeuCube architecture.

Output function module / classification module: After the SNNr is trained on the STBD in an unsupervised model, the same input data is propagated again through the SNNr, pattern by pattern, the state of the SNNr is measured for each pattern and an output classifier is trained to recognize this state in a predefined output class for this input pattern. Feedback connections from the Output Module to the NeuCube are possible to establish reinforcement learning. In this realisation, all spiking neurons from the

NeuCube are connected to each of the output neurons. Two different methods are developed in the EvoSpike project: deSNN for classification of NeuCube states; SPAN for generating motor control signals in response to certain patterns of activity of the NeuCube. The recall procedure can be performed using different recall algorithms applying different methods:

(1) The first method is called eSNNm (deSNNm). A spike sequence (the response of the trained SNNr) is propagated to all trained output neurons and the first neuron that spikes defines the output. The assumption is that the neuron that best matches the input pattern will spike earlier, based on the PSP threshold (membrane potential).

(2) The second method, called eSNNs (deSNNs), implies the creation of a new output neuron in the eSNN for each new input pattern from the SNNr and then comparing the connection weight vector of the new one to the already existing neurons using Euclidean distance. The closest output neuron in terms of synaptic connection weights is the ‘winner’. This method uses the principle of transductive reasoning and nearest neighbour classification in the connection weight space. It compares spatially distributed synaptic weight vectors of a new neuron that captures a new input pattern with an existing neuron.

The main advantage of the eSNN compared with other supervised or unsupervised learning and classification SNN models, that makes the eSNN suitable for on-line learning and early prediction of temporal events, is the importance of the order in which input spikes arrive, and its low computational cost.

Gene regulatory networks (GRN) module, (optional) The GRN module uses as a main principle the analogy between biological facts about the relationship between spiking activity and gene/protein (neuro-transmitter, neuro-receptor, ion channel, neuro-modulator) dynamics in order to control the learning and spiking parameters in a SNN. Biological support of this can be found in numerous publications (e.g. [124, 125]).

Chapter 5

Experimental case study of EEG STBD classification in the NeuCube model with audio stimuli

5.1 Audio perception review

The second main source of incoming information for a human is the information obtained via the auditory system. The primary auditory cortex is the first region of the cerebral cortex to receive auditory input. The auditory cortex is the most highly organized processing unit of sound in the brain. This cortex area is the neural crux of hearing, and—in humans—language and music. The auditory cortex is divided into three separate parts: the primary, secondary, and tertiary. These structures are formed

concentrically around one another, with the primary cortex in the middle and the tertiary cortex on the outside [126], fig.2.1.1 and fig.2.1.2.

The primary auditory cortex is a region of the brain that processes sound contributing to our ability to hear. Corresponding roughly with Brodmann areas 41 and 42 of the cerebral cortex [127], it is located on the temporal lobe, and performs the basics of hearing—pitch and volume. Besides receiving input from the ear and lower centers of the brain, the primary auditory cortex also transmits signals back to these areas, fig.5.1.1 (a) and (b).

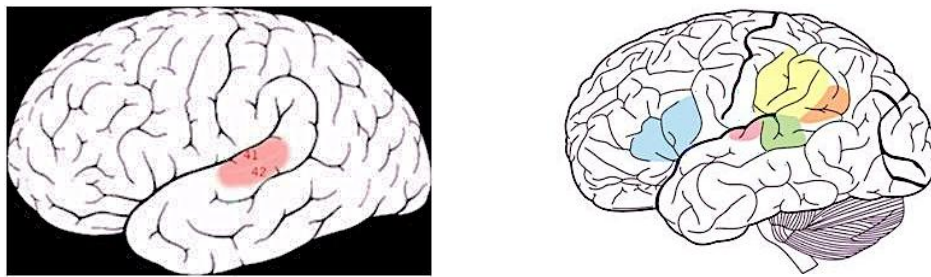


Fig.5.1.1 (a) Brodmann areas 41 & 42 of the human brain; (b) The Primary Auditory Cortex is highlighted in magenta, and has been known to interact with all areas highlighted on this neural map.

Neurons in the auditory cortex are organized according to the frequency of sound to which they respond best. Neurons at one end of the auditory cortex respond best to low frequencies; neurons at the other respond best to high frequencies. There are multiple auditory areas (much like the multiple areas in the visual cortex), which can be distinguished anatomically and on the basis that they contain a complete "frequency map." The purpose of this frequency map (known as a tonotopic map) is not yet clearly defined, and is likely to reflect the fact that the cochlea is arranged according to sound frequency. The auditory cortex is involved in tasks such as identifying and segregating auditory "objects" and identifying the location of a sound in space [128]. Human brain scans have indicated that a peripheral unit of this brain region is active when trying to

identify musical pitch. Individual cells are consistently excited by sounds at specific frequencies, or multiples of that frequency.

In the hearing process, multiple sounds are absorbed simultaneously. The role of the auditory system is to decide which components form the sound link. Many have surmised that this linkage is based on the location of sounds. However, there are numerous distortions of sound when reflected off different mediums, which makes this possibility unlikely. Instead, the auditory cortex forms groupings based on more reliable fundamentals; in music; for example, this would include harmony, timing, and pitch [129], [83].

The primary auditory cortex is located in the temporal lobe. There are additional areas of the human cerebral cortex that are involved in processing sound, in the frontal and parietal lobes. The auditory cortex is composed of fields, which differ from each other in both structure and function [130].

When each instrument of a symphony orchestra or the jazz band plays the same note, the quality of each sound is different — but the musician perceives each note as having the same pitch. The neurons of the auditory cortex of the brain are able to respond to pitch. This location of a pitch-selective area has also been identified in recent functional imaging studies in humans [131, 132].

Areas of brain activation for reading and listening comprehension are highlighted in fig.5.1.2 [133].

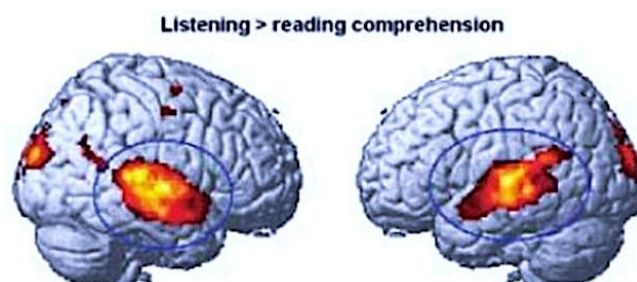


Fig.5.1.2. Areas of brain activation for reading and listening comprehension

Studies suggest that individuals are capable of automatically detecting a difference or anomaly in a melody such as an out of tune pitch which does not fit with their previous music experience. The findings of Brattico et al. suggest that there is automatic and rapid processing of melodic properties in the secondary auditory cortex [134]. The findings that pitch incongruities were detected automatically, even in processing unfamiliar melodies, suggests that there is an automatic comparison of incoming information with long term knowledge of musical scale properties, such as culturally influenced rules of musical properties (common chord progressions, scale patterns, etc.) and individual expectations of how the melody should proceed. The better understanding of the origin of human inherited long-term knowledge is seen as one of importance in future research.

5.2 EEG NeuCube model and mapping structure

EEG brain data can be obtained with the use of a wide range of different wired and wireless recording tools. The problem of mapping is vital for any existing device and it is attempting to be solved based on a universal internationally recognized system [135]. All EEG channels of any device are spatially distributed on the scalp. An example of the positioning of 64 EEG channels on a human head and channel representation in a 3D space is shown in Fig.5.2.1 (a and b).

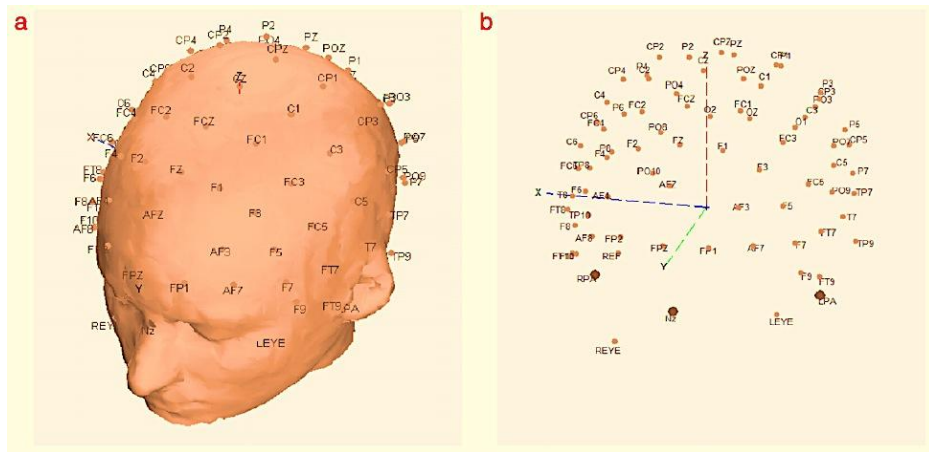


Fig.5.2.1 Positioning of 64 EEG channels on a human head (a); EEG channels representation in a 3D space (b)

The spatially defined positions of the channels can be mapped into a SNNr using different approaches. One of them is using the Talairach template, fig.5.2.2.

The neurons in the SNNr are located following the same (x, y, z) coordinates of the Talairach template and the EEG channels are mapped according to the standard mapping given in the “*Anatomical locations of international 10–10 EEG cortical projections into Talairach coordinates*” [135]. The same coordinates are used in a SNNr of a NeuCube model. The spiking sequences that represent EEG channels, after transformation of continuous value signals into spike trains, are entered into the correspondingly located neurons before a training procedure (e.g. STDP) is applied.

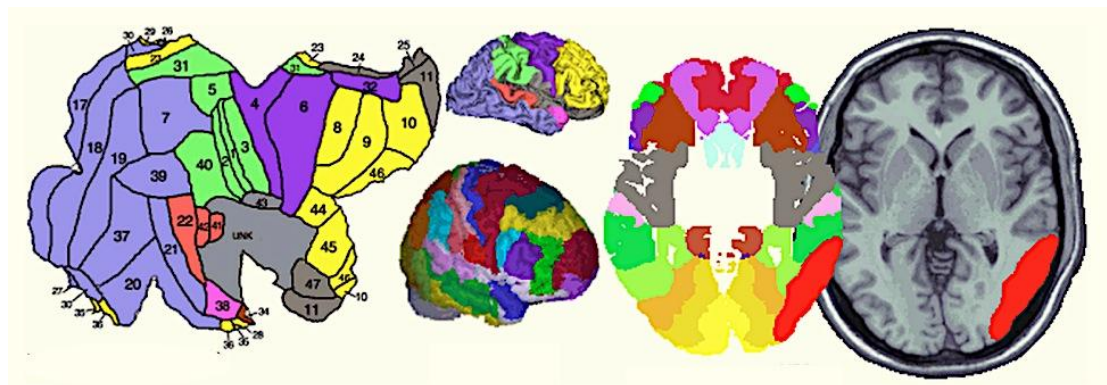


Fig.5.2.2 The Talairach template development and mapping

The whole NeuCube framework employed in this study for classification of STBD based on evolving probabilistic spiking neural network reservoir (epSNNr) paradigm is presented in fig.5.2.3. At first, each channel of spatial-temporal data (EEG) is transformed into trains of spikes by the encoder module. An AER input data encoding method is used for this study. Then the trains of spikes are distributed into spatiotemporal filter which employs the reservoir paradigm of LIFM neurons, located according to the Talairach template and the Koessler [135] mapping.

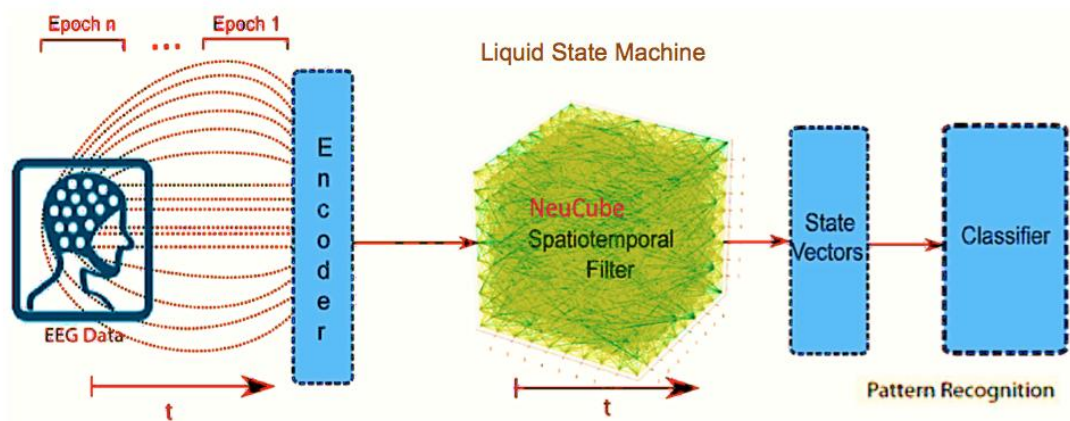


Fig.5.2.3 The whole framework for classification of STBD

STDP learning is applied in the NeuCube to establish the connection weights of spatial-temporal patterns of pathway connectivity. Then the states are fed into a classifier for training and testing the classification performance using a pre-defined type of classifier. For the purposes of further experimental optimisation of a certain NeuCube model different classifiers were tested (deSSNm, deSNNs, SPAN) within the set of experiments and the results of this tuning will be given later in this chapter.

A NeuCube model was trained and tested with the parameters shown in the NeuCube screenshot, fig.5.2.4.

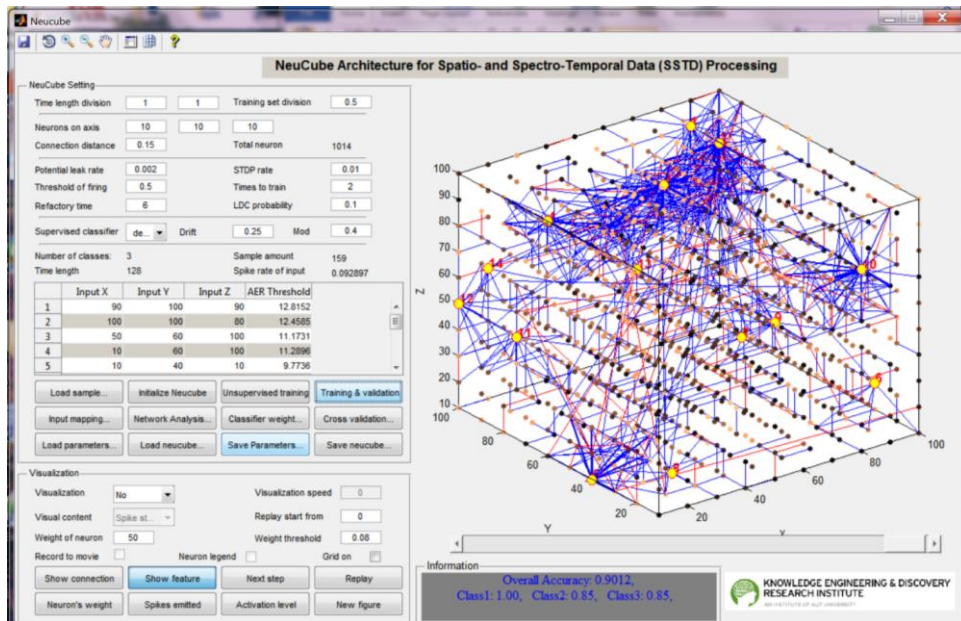


Fig.5.2.4 The NeuCube.

5.3 EEG brain perception data and experiment description

The experimental case study of EEG perception STBD classification with audio stimuli in a NeuCube model was performed using the EEG data collected using a 14-channel EEG recording device [32] and original software, fig.5.3.1. The Emotiv EEG recording device has 14 EEG channels labeled based on the “Anatomical locations of international 10–10 EEG cortical projections into Talairach coordinates” [135] which are: AF3, F7, F3, FC5, T7, P7, O1, O2, P8, T8, FC6, F4, F8, AF4; plus 2 reference channels which offer optimal positioning for accurate spatial resolution.

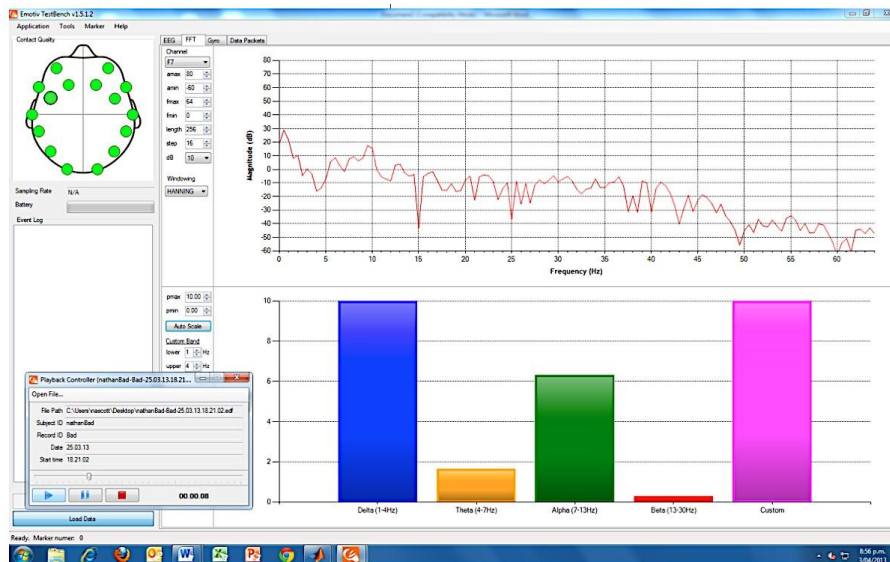


Fig.5.3.1 Emotiv software GUI screenshot

The following audio stimuli were prepared for experiments to represent specific aspects of the nature of human art and of human art perception. The set of three audio stimuli were composed: the first and the second stimuli were using two ingeniously structured pieces of classical music of the 16th century and the third stimuli was composed from unstructured chaotic irritating noise, mostly of industrial origin:

- 1) 85 seconds extract from the Ich ruf' zu dir, Herr Jesu Christ (BWV 639) by Johann Sebastian Bach; (related further in the chapter as “M1”)
- 2) 54 seconds extract from the Wachet auf, ruft uns die Stimme (BWV 140) by Johann Sebastian Bach; (related further in the chapter as “M2”)
- 3) 30 seconds of unstructured chaotic irritating industrial noise; (related further in the chapter as “N”).

The juxtaposition of two contrast stimuli was used as a base for experiments. The core meaning of this juxtaposition should be understood as a contradiction between two polar notions, which in human perception is defined as “harmony”, and “chaos”. They are represented here with an exemplar of highly structured canonical religious music used as music for meditation by many generations of people, and an exemplar of amorphous

irritating industrial noise; these stimuli are labeled “M1” for the first music pattern, “M2” for the second music pattern and “N” for noise consecutively.

The EEG data was recorded from a small group of healthy male and female subjects in the age category of 20 – 40 years old. All the experiments with audio perception were recorded with closed eyes, in order to avoid EEG artifacts from blinking. The recorded data was not used previously. The length of a whole session of each of three stimuli (M1 of 85 sec, M2 of 54 sec and N of 30 sec) was later divided into equal samples of 1 sec length due to a certain experiment objectives. The data was collected and classified following four scenarios each of which set distinct goals:

Scenario 1: The primary goal for the Scenario 1 was defined as classification of subjects based on their perception of one of the stimuli M1, M2 or N. Each of the three experiments performed within this scenario was utilizing one of these stimuli.

Experiment 4-1 classified subjects 1, 2, 3 and was based on stimulus M1 presented to 3 subjects; contained 3 classes:

Class #	Subject	Stimulus	Class Accuracy %
1	1	M1	100
2	2	M1	93.33
3	3	M1	93.33

Overall accuracy of experiment is **95.55%**.

Experiment 4-2 classified subjects 1, 2, 3 and was based on stimulus N presented to 3 subjects; contained 3 classes:

Class #	Subject	Stimulus	Class Accuracy %
1	1	N	79.67
2	2	N	68.40
3	3	N	74.81

Overall accuracy of experiment is **74.29%**.

Experiment 4-3 classified subjects 1, 2, 3 and was based on stimulus M2 presented to 3 subjects; contained 3 classes:

Class #	Stimulus	Subject	Class Accuracy %
1	1	M2	96.30
2	2	M2	98.43
3	3	M2	92.54

Overall accuracy of experiment is **95.75%**.

Scenario 2: The primary goal for the Scenario 2 was defined as classification of stimuli based on perception of one of the subjects 1, 2 or 3.

Experiment 9-1 classified stimuli M1, M2, N and was based on Subject 1 perception of the stimuli; contained 3 classes:

Class #	Stimulus	Subject	Class Accuracy %
1	M1	1	73.49
2	N	1	35.93
3	M2	1	83.67

Overall accuracy of experiment is **64.36%**.

Experiment 9-2 classified stimuli M1, M2, N and was based on Subject 2 perception of the stimuli; contained 3 classes:

Class #	Stimulus	Subject	Class Accuracy %
1	M1	2	80.00
2	N	2	48.93
3	M2	2	66.67

Overall accuracy of experiment is **65.2%**.

Experiment 9-3 classified stimuli M1, M2, N and was based on Subject 3 perception of the stimuli; contained 3 classes:

Class #	Stimulus	Subject	Class Accuracy %
1	M1	3	96.30
2	N	3	26.67
3	M2	3	81.40

Overall accuracy of experiment is **68.12%**.

Scenario 3: The primary goal for the Scenario 3 was more complex and defined as classification of the stimuli M1, M2 and N based on mixed samples of perception of all three subjects 1, 2 and 3.

Experiment 14 classified the stimuli M1, M2, N and was based on the mixed samples of perception of all three subjects 1, 2, 3; contained 3 classes:

Class #	Stimulus	Subject	Class Accuracy %
1	M1	1 2 3	60.59
2	N	1 2 3	28.89
3	M2	1 2 3	58.53

Overall accuracy of experiment is **49.34%**.

Scenario 4: The primary goal for the Scenario 4 was more complex and defined as classification of the subjects 1, 2 and 3 based on the mixed samples of all three stimuli M1, M2 and N perception.

Experiment 14-1 classified subjects 1, 2, 3 was based on the mixed samples of all three stimuli M1, M2 and N perception; contained 3 classes:

Class #	Subject	Stimulus	Class Accuracy %
1	1	M1 N M2	65.87
2	2	M1 N M2	61.23
3	3	M1 N M2	73.55

Overall accuracy of experiment is **66.88%**.

Summarizing the experiments with audio stimuli we can see that the level of classification accuracy is noticeably high with overall accuracy up to 95.75% and for

selected classes up to 100%, which illustrates the feasibility of the NeuCube architecture for classification of EEG brain data related to perception of audio art or music. The highest 95% accuracy of classification of subjects also shows the feasibility of person identification based on the proposed methodology of using the structured audio stimulus as a “security key”. The level of accuracy of only 74% is also obtained on classification of subjects, but with irregular noise stimulus in a role of “security key”. Such a low level of accuracy confirms our supposition of a lesser level of personification of human perception of chaotic structures; in other words the human perception of irregular noise is more “irregular” as well, which makes the NeuCube identification process less reliable.

The results of classification of stimuli also support this assumption with significant difference in classification accuracy: between 83% of average accuracy for music stimulus M1 and only 37% of average accuracy for noise stimulus N.

The full analysis of results of audio experiments will be given later in this chapter in the conclusion section 5.5.

5.4 Visualization of EEG recorded data

For the visualization purposes of the recorded EEG brain data different tools were used. The primary visualization tool is the embedded visualization function of the NeuCube that allows us following the processing of the EEG data in “live” mode step by step, and finally showing the full network representing the certain processed EEG data, fig.5.4.1.

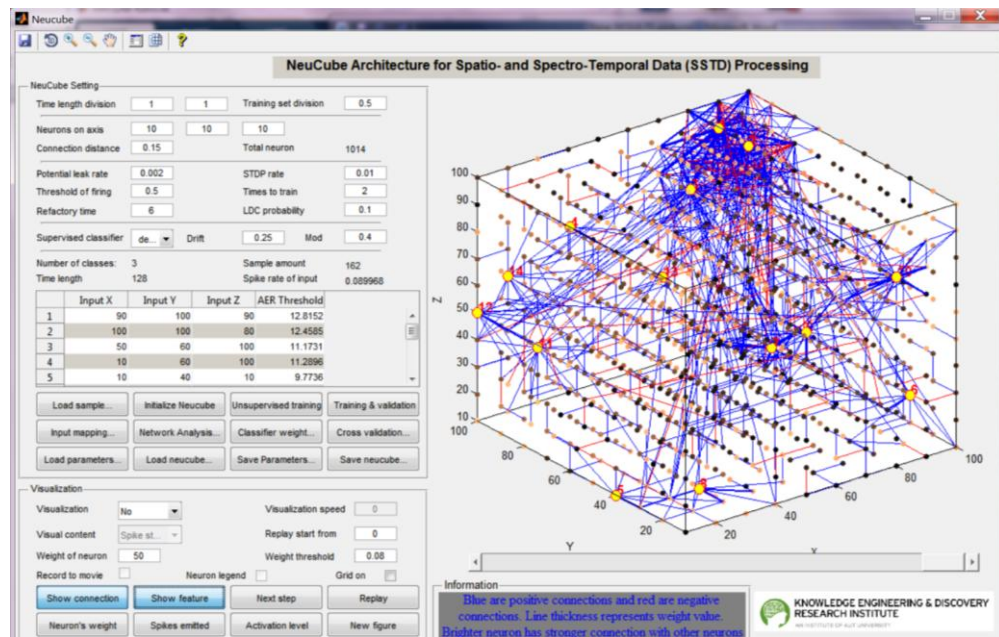


Fig.5.4.1 NeuCube Exp 4-3 visualization of connectivity and spiking activity after training of a SNNr; positive connections are represented in blue and negative—in red;

The network is highlighting the specific brain areas that relate to the Emotiv 14 channels [135] and shown as yellow circles with numbers from 1 to 14. The intensity of excitation of the brain areas that relatively correlated with the mentioned above channels can be evaluated due to the density of network activity represented by blue and red connections between neurons. The NeuCube is building the unique network for every dataset collected on a certain stimulus. By comparing different experiment visualizations, we can study the difference between networks built for different stimuli. We can therefore explore deeper the brain reaction on various stimuli while taking in account the high level of simplification of the existing system. Fig. 5.4.2 and fig.5.4.3

illustrate the difference in levels of complexity of the networks built for two experiments with three types of stimuli, and also the difference in brain areas involved in processing.

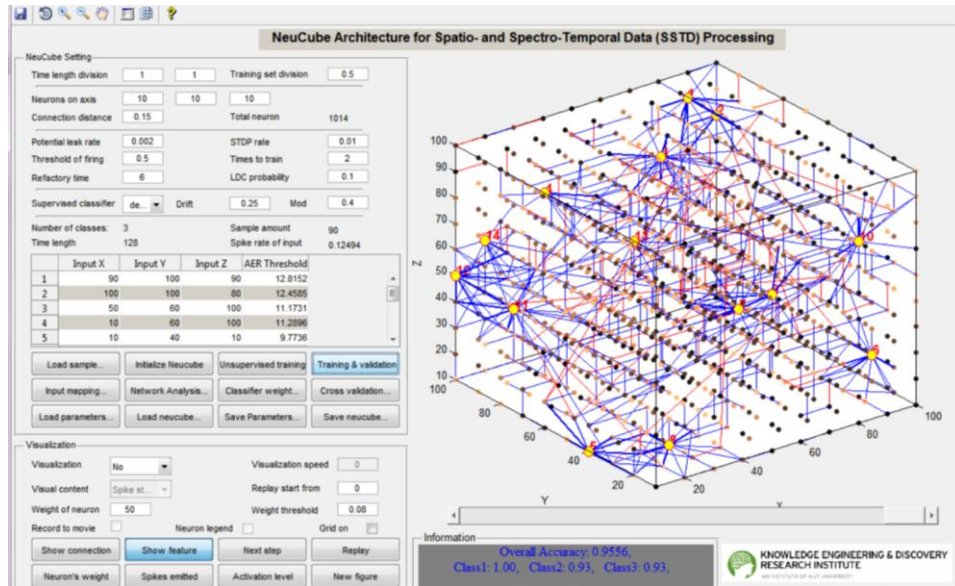


Fig.5.4.2 The visualization of simple network of *Experiment 4-1* for classification of three subjects 1, 2, and 3 with stimuli length of 1 sec.

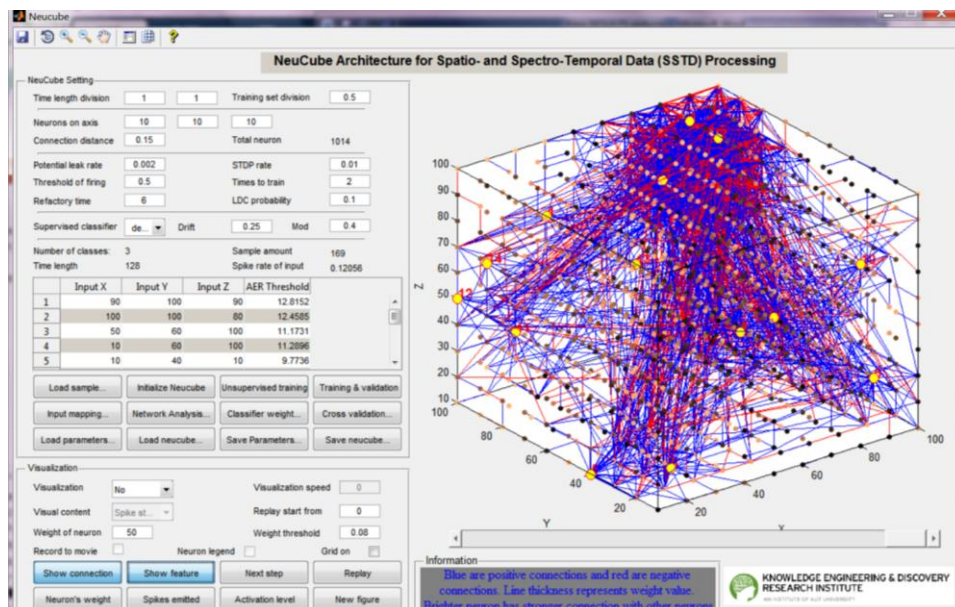


Fig.5.4.3 The visualization of more complex *Experiment 14* which classified the stimuli M1, M2, N and based on the mixed samples of perception of all three subjects 1, 2, 3 in each class with stimuli length of 1sec.

Another visualization tool used is the EEGLAB [35], an interactive Matlab toolbox for processing continuous and event-related EEG, MEG and other electrophysiological data. Below there are the EEGLAB visualizations of the measured EEG data (all 14 channels) represented as 2 or 3 dimensional EEG scalp maps of prepared dataset / EEG epochs. The first set, fig.5.4.4, is representing the subject 1 brain activity recorded with structured music stimulus M1:

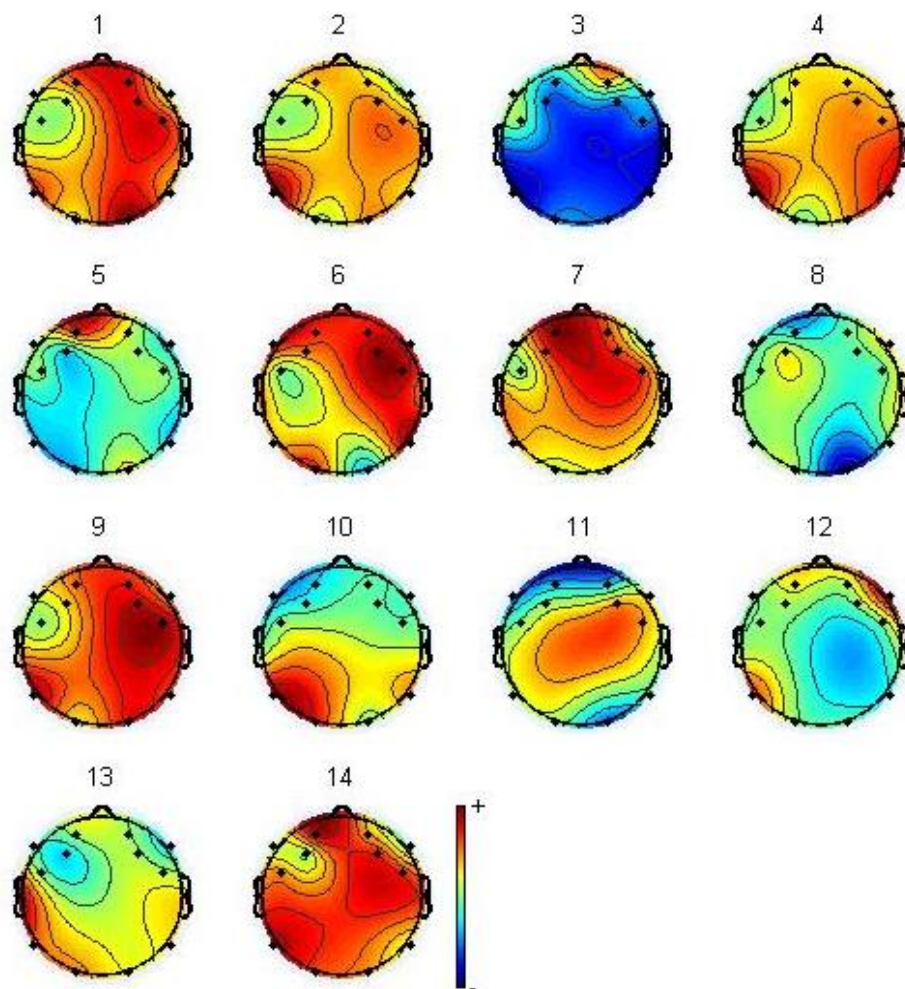


Fig.5.4.4 2D EEG scalp maps of dataset EEG epochs; subject 1, stimulus M1

Fig.5.4.5 is representing the subject 1 brain activity recorded with irritating industrial noise stimulus N:

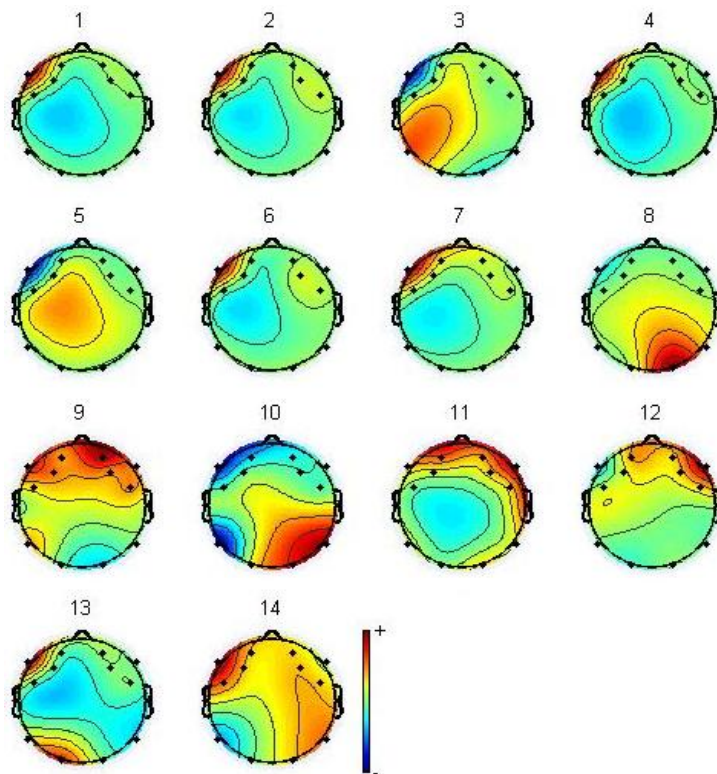


Fig.5.4.5. 2D EEG scalp maps of dataset EEG epochs; subject 1, stimulus N.

3D visualization can be seen in fig.5.4.6 representing the subject 1 brain activity recorded with structured music stimulus M2:

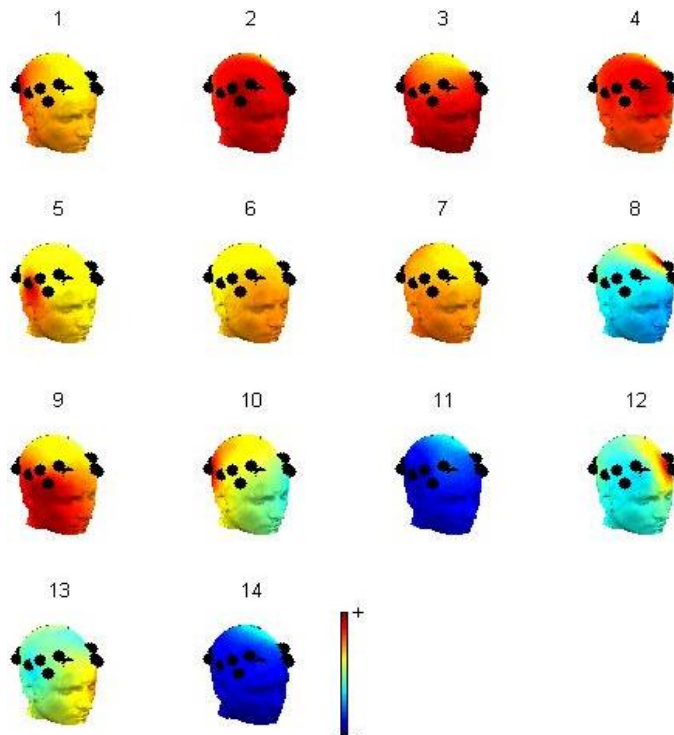


Fig.5.4.6 3D visualization of subject 1, music stimulus M2

The EEGLAB plots of the normalized spectrogram are widely used in the EEG literature to visualize continuous and event-related changes in spectral power over time in a broad frequency range [136]. The color at each image pixel then indicates power (in dB) at a given frequency. For computation, EEGLAB widely uses the short-time Fourier transform, a sinusoidal wavelet (short-time DFT) transform that provides a specified time and frequency resolution.

If we look at the plots of specifically chosen channels representations T7 and T8 which correspond roughly with Brodmann areas 41 and 42 auditory cortex areas, fig.5.4.7 represents the spectral power and frequency resolution of EEG data with M1 music stimuli and fig.5.4.8 is representation of that for N Noise stimuli. The spectral power and frequency of the plots are significantly different. This might reflect the difference in human perception of structured versus chaotic stimuli.

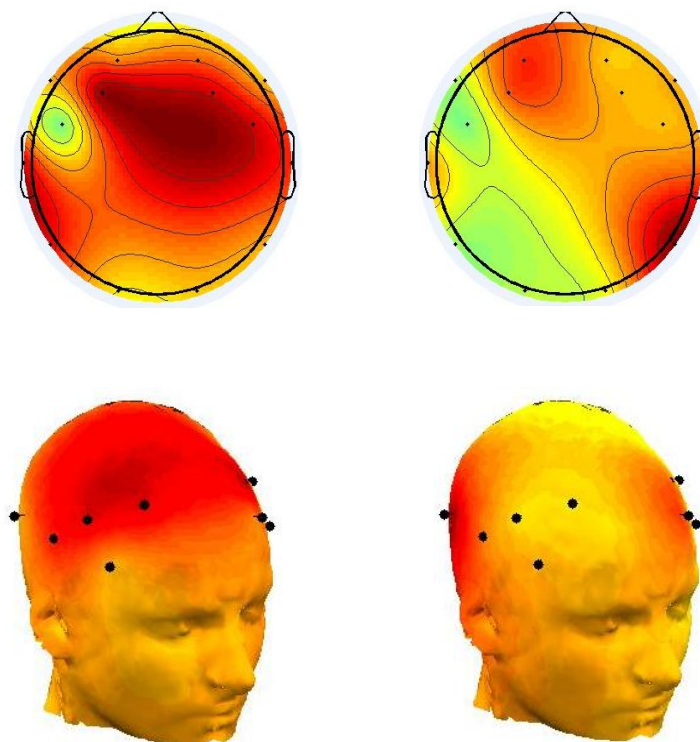


Fig.5.4.7 2D and 3D plotting of sensor T7 and sensor T8 which are corresponding roughly with Brodmann areas 41 and 42 /auditory cortex areas; recorded with M1/Music stimuli

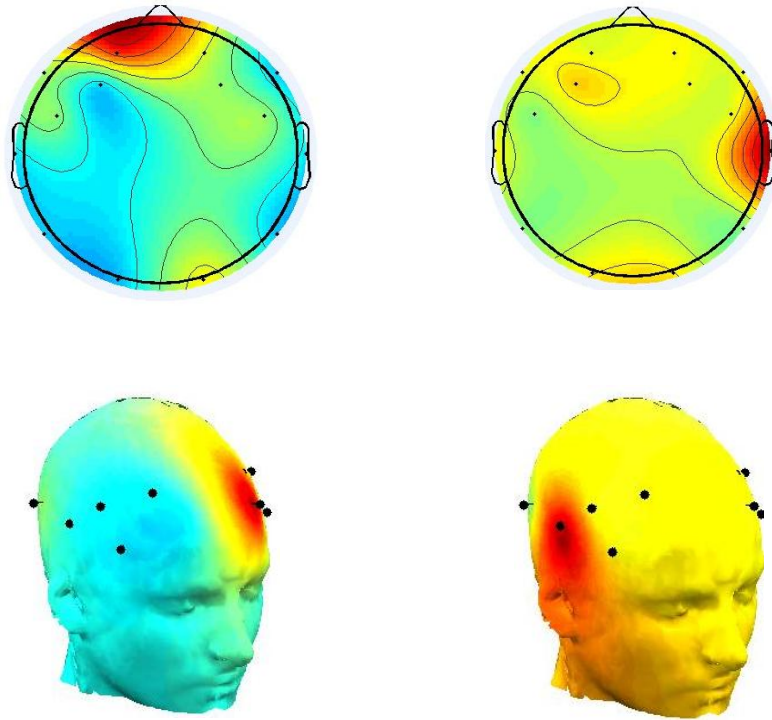


Fig.5.4.8 2D and 3D plotting of sensor T7 and sensor T8 which are corresponding roughly with Brodmann areas 41 and 42 /auditory cortex areas; recorded with N Noise stimuli

Finally for illustration of training and testing processes running in the NeuCube the following reservoir-like Spike state visualization are presented, fig.5.4.9

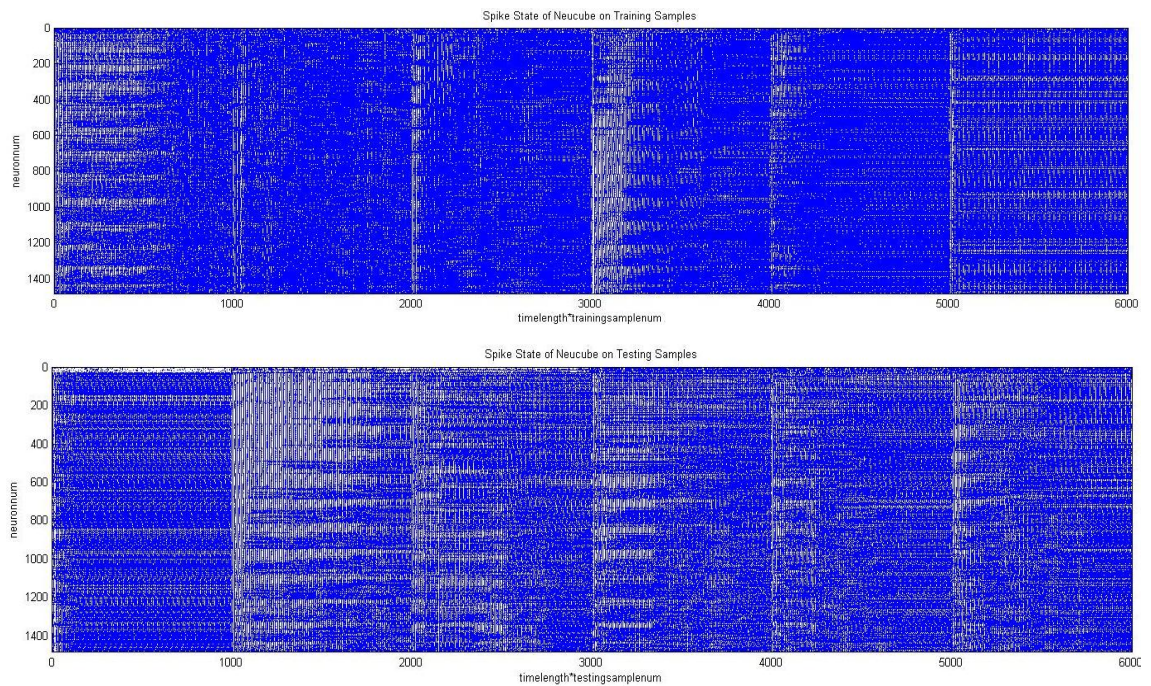


Fig.5.4.9 Spike state of NeuCube on training (up) and testing (bottom) samples.

5.5 Conclusion

The classification accuracy analysis based on the sets of described above experiments, performed on the application of the specific group of audio stimuli proposed for a small group of subjects, led to the following conclusions.

The performed experiments, which are utilizing the features of a novel software frame of the NeuCube show the feasibility of solving assigned tasks of human perception classification.

The level of classification accuracy reached in the experiments appeared to be noticeably high with maximums of overall accuracy for selected experiments rising to 95.75% and for selected classes up to 100%.

The highest accuracy of 100% for selected classes and 95.75% of overall accuracy is reached in the experiments designed for classification of subjects (or personal identification).

The accuracy of experiments designed for classification of stimuli drops considerably to its minimums of 68% for selected classes and to 74.29% for overall accuracy of an experiment.

Within the experiments of subjects' classification we may obviously highlight the descent of accuracy on Noise stimulus for all subjects. This illustrates the problematic issues when we are classifying perception of chaotic audio noise, so human perception of noise tends to be more "noisy" and therefore more difficult to classify than structural music perception.

In the analysis of complicated experiments designed for classification of subjects and for classification of stimuli but with classes consisted of mixed samples (scenarios 3 and 4), we can see the absolute minimum of accuracy fallen to 49.34% in the classification of stimuli (experiment 14); while the similarly designed experiment 14-1 for the classification of subjects still shows relatively higher accuracy of 66.88%.

The next step in this study will be the evaluation of the NeuCube classification feasibility with utilization of video stimuli.

Chapter 6

Experimental case study of EEG STBD classification in the NeuCube model with video stimuli

6.1 Visual perception review

The visual cortex of the brain is the part of the cerebral cortex responsible for processing visual information. It is located in the occipital lobe, in the back of the brain. The primary visual cortex is anatomically equivalent to Brodmann area 17. The extrastriate cortical areas consist of Brodmann area 18 and Brodmann area 19 [127]. There is a visual cortex in each hemisphere of the brain. The left hemisphere visual cortex receives signals from the right visual field and the right visual cortex from the left visual field, fig.6.1.1.

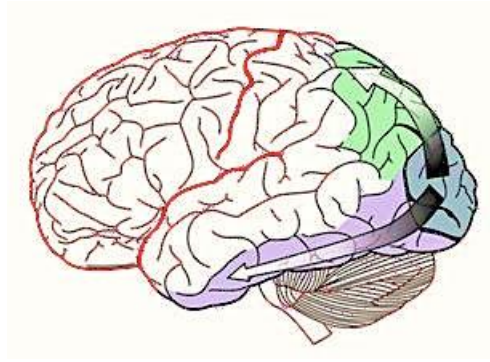


Fig.6.1.1. The visual dorsal stream (green) and ventral stream (purple) are shown. Much of the human cerebral cortex is involved in vision.

Arguably the visual information is delivering about 80 percent of the total information stream which is received by humans. It is still not clear enough when the visual function has triggered, for example, newborns show a preference for following moving faces within the first 30 minutes of life [137] expressing quite mature ability for face recognition. Obviously visual perception is a key point in human ability to perceive incoming information.

6.2 EEG brain perception data and experiment description

To obtain EEG brain perception data of visual areas of human brain the same equipment and EEG recording device and software was used as for the experiments with audio stimuli [32], with addition of a monitor to present the video stimuli.

The core reasons for preparation of video stimuli were kept the same: collecting human brain perception data recorded on contradictory stimuli representing the notions “harmony” versus “chaos”.

The sets of video stimuli (moving images) for experiments were prepared to represent archetypal and patterned aspects of human art. Two video samples were produced: the first was using ancient human art patterns of Tibetan mandalas, fig.6.2.1 (b). [14]; the second stimulus employed natural objects, snow crystals or snowflakes [15] fig.1.3.1(a) and fig.6.2.1(a), which have been used as inspiration art models and as decoration patterns by many generations of humans. As a contradiction to structured/patterned stimuli the third was composed from works of modern abstract art of V. Kandinsky, S. Dali, A. Warhol [16], fig.6.2.2 (a and b).

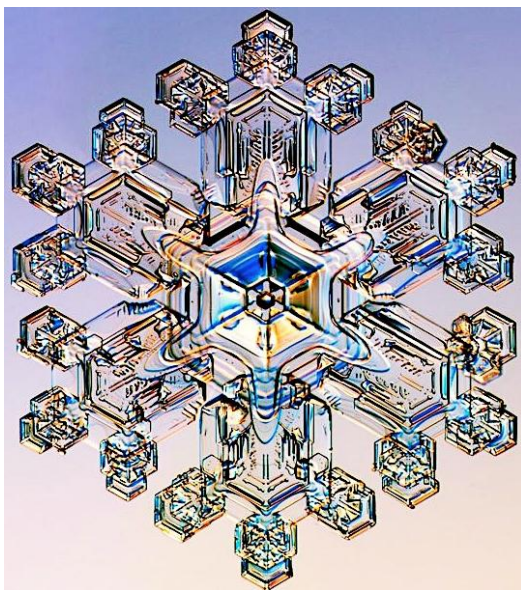


Fig.6.2.1.(a) Natural snowflake crystal; (b) Tibetan mandala Chakrasamvara;



Fig.6.2.2.(a) abstract art of V. Kandinsky; (b) surrealism art work of S. Dali

The video stimuli were labeled “P1” for the first patterned sample with mandalas, “P2” for the second patterned sample with snowflakes, and “A” for abstract art sample.

The EEG data was recorded from a small group of healthy male and female subjects in the age category of 20 – 40 years old. The recorded data was not used previously. The length of a whole session of each of three stimuli (P1 of 85 sec, P2 of 54 sec and A of 30 sec) was later divided into equal samples of 1 sec length. The data was collected and classified following five scenarios each of which set distinct goals:

Scenario 1: The primary goal for the Scenario 1 was defined as classification of subjects based on their perception of one of the stimuli P1, P2 or A. Each of the experiments performed within this scenario was utilizing only one of these stimuli.

Experiment 2-1 classified subjects 1, 2, 3 and was based on stimulus P1 presented to subjects; contained 3 classes:

Class #	Subject	Stimulus	Class Accuracy %
1	1	P1	98.75
2	2	P1	100
3	3	P1	100

Overall accuracy of experiment is **99.58%**.

Experiment2-2 classified subjects 1, 2, 3 and was based on stimulus A presented to subjects; contained 3 classes:

Class #	Subject	Stimulus	Class Accuracy %
1	1	A	96.80
2	2	A	96.97
3	3	A	89.76

Overall accuracy of experiment is **94.51%**.

Experiment 2-3 classified subjects 1, 2, 3 and was based on stimulus P2 presented to subjects; contained 3 classes:

Class #	Stimulus	Subject	Class Accuracy %
1	1	P2	98.84
2	2	P2	100
3	3	P2	99.55

Overall accuracy of experiment is **99.46%**.

Scenario 2: The primary goal for the Scenario 2 was defined as classification of stimuli based on perception of one of the subjects 1, 2 or 3.

Experiment 12-1 classified stimuli P1, P2, A and was based on Subject 1 perception of the stimuli; contained 3 classes:

Class #	Stimulus	Subject	Class Accuracy %
1	P1	1	98.00
2	A	1	78.90
3	P2	1	91.48

Overall accuracy of experiment is **89.46%**.

Experiment 12-2 classified stimuli P1, P2, A and was based on Subject 2 perception of the stimuli; contained 3 classes:

Class #	Stimulus	Subject	Class Accuracy %
1	P1	2	71.18
2	A	2	70.03
3	P2	2	83.62

Overall accuracy of experiment is **74.94%**.

Experiment 12-3 classified stimuli P1, P2, A and was based on Subject 3 perception of the stimuli; contained 3 classes:

Class #	Stimulus	Subject	Class Accuracy %
1	P1	3	91.01
2	A	3	74.87
3	P2	3	80.05

Overall accuracy of experiment is **81.98%**.

Scenario 3: The primary goal for the Scenario 3 was more complex and defined as classification of the stimuli P1, P2, A based on mixed samples of perception of all three subjects 1, 2 and 3.

Experiment 13-1 classified the stimuli P1, P2, A and was based on the mixed samples of perception of all three subjects 1, 2, 3; contained 3 classes:

Class #	Stimulus	Subject	Class Accuracy %
1	P1	1 2 3	79.19
2	A	1 2 3	69.44
3	P2	1 2 3	67.94

Overall accuracy of experiment is **72.19%**.

Scenario 4: The primary goal for the Scenario 4 was more complex and defined as classification of the subjects 1, 2 and 3 based on the mixed samples of all three stimuli P1, P2 and A perception.

Experiment 13-2 classified subjects 1, 2, 3 was based on the mixed samples of all three stimuli P1, P2 and A perception; contained 3 classes:

Class #	Subject	Stimulus	Class Accuracy %
1	1	P1 A P2	84.95
2	2	P1 A P2	90.10
3	3	P1 A P2	77.23

Overall accuracy of experiment is **84.09%**.

Scenario 5: The primary goal for the Scenario 5 was the most complex and defined as classification of the combination of a certain subject plus a certain stimulus.

Experiment 13: two contradictory stimuli P1 and A were presented to three subjects 1, 2, 3; the experiment contained 6 classes:

Class #	Subject/Stimulus	Class Accuracy %
1	1/P1	89.97
2	2/P1	73.16
3	3/P1	83.78
4	1/A	40.20
5	2/A	68.20
6	3/A	73.02

Overall accuracy of experiment is **71.38%**.

Summarizing the video stimuli we can state the following:

1) Despite the relative variability in accuracy of video stimuli experiments, we can confirm again the feasibility of perception classification and would like to emphasize that this is similar to the audio experiments general trend. The classification accuracy on patterned stimuli is higher than on unstructured.

2) The second general tendency is that average accuracy of experiments with video stimuli is higher than in experiments with audio stimuli.

The detailed analysis will be given later in the summary section 6.4.

6.3 Visualization of EEG recorded data

The same visualization tools are used for video stimuli perception, the EEGLAB toolbox for processing continuous and event-related EEG, fig.6.3.1 and fig.6.3.2.

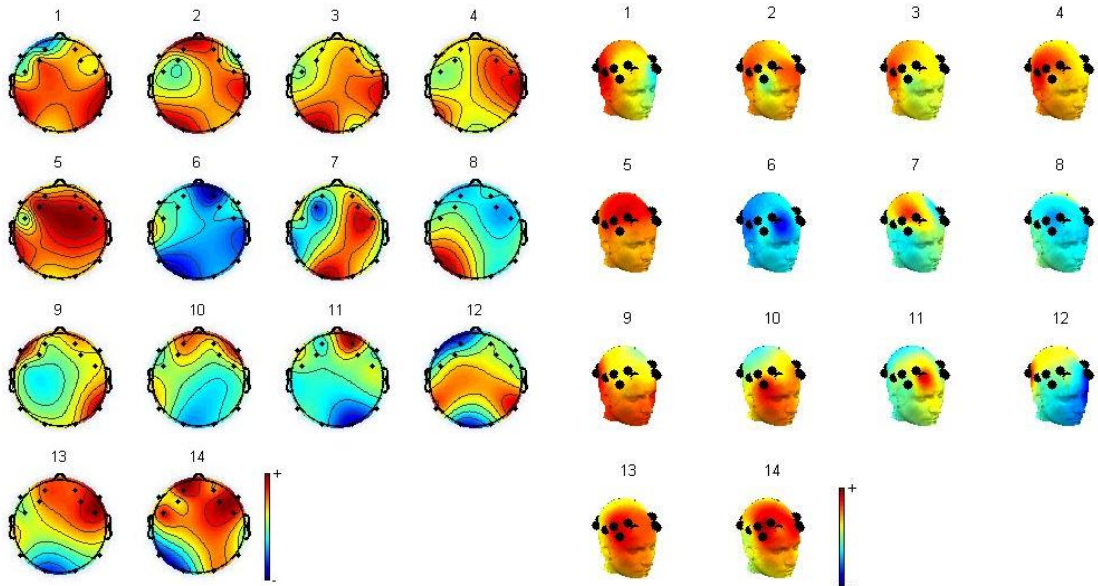


Fig.6.3.1 2D EEG scalp maps of dataset EEG epochs; subject 1, P2 Patterned video stimulus

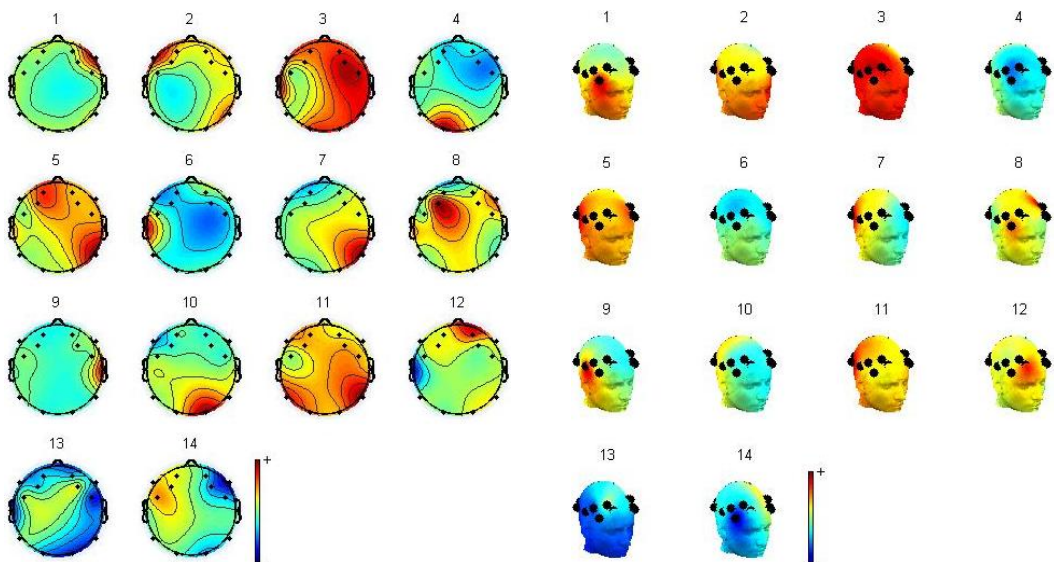


Fig.6.3.2 2D EEG scalp maps of dataset EEG epochs; subject 1, A Abstract video stimulus

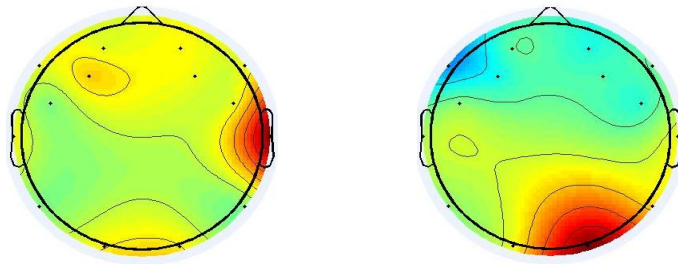


Fig.6.3.3 2D plotting of sensor O1 and sensor O2 that are corresponding roughly with visual dorsal and ventral stream areas; recorded with A/Abstract video stimuli

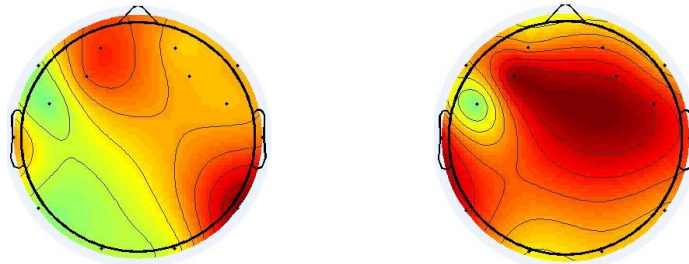


Fig.6.3.4 2D plotting of sensor O1 and sensor O2 that are corresponding roughly with visual dorsal and ventral stream areas; recorded with P2/Patterned video stimuli

Attempts to analyze the spectral power and frequency resolution of EEG data, comparison of visualizations of EEG data collected on video stimuli is looking noticeably less clear than collected on audio stimuli. It might reflect the fact of more complex structure of visual perception, and numerous brain areas involved into visual perception brain processing. Similar conclusions might be assumed with the NeuCube visualizations, fig.6.3.5. The networks built on video perceptions have more complex structure in general.

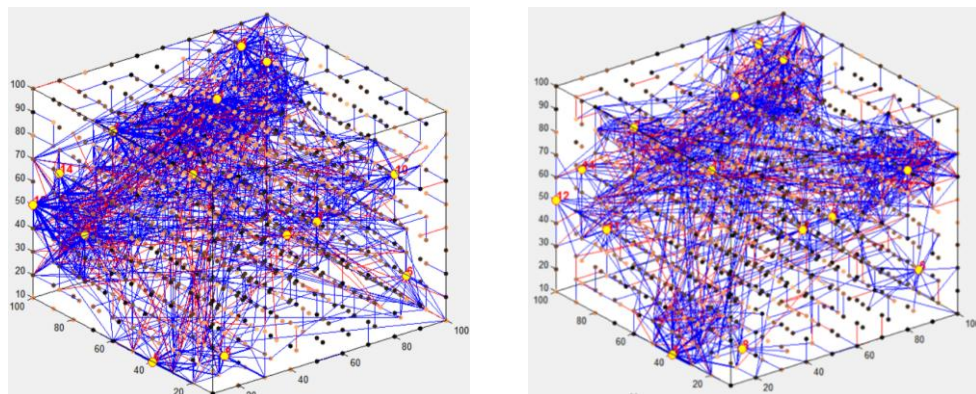


Fig.6.3.5 NeuCube visualizations of *Experiment 2-1* (left) and *Experiment 2-2* (right) EEG data classification of subjects with video stimuli.

6.4 Summary

Analyzing the classification accuracy of the whole set of the experiments performed with the use of three types of video stimuli (two different patterned stimuli P1 and P2 and one unstructured abstract stimulus A) we may mention that in general the classification accuracy of perception of video samples is higher if compared with the classification accuracy obtained with the use of audio stimuli. While the general tendency in reaching higher results in the experiments designed for classification of subjects to compare with the experiments for classification of stimuli remained the same (up to 99.58% for subjects compared with only 89.46% for stimuli), there is a noticeable distinction.

The classification of subjects based on the Abstract stimulus A has reached fairly high accuracy of 94.51% and it's just slightly lower accuracy obtained on patterned and structural stimuli P1 and P2. This fact should be investigated further but as we presume, the color component plays one of the most important roles in visual perception, therefore the choice of the stimulus A abstract art samples haven't met the assigned requirements for this sort of stimuli to be totally noisy and chaotic. Thus this fact should be taken into account for further study. Here we have to mention that the perception of irregular with bright clear colors video art samples might be classified possibly with a higher level of accuracy, which suggests further investigation and additional experiments.

The perception accuracy on combinations of audio and video (in a single stimulus) will be explored in chapter 7.

Chapter 7

Experimental case study of EEG STBD classification in the NeuCube model with mixed audio/video stimuli

7.1 EEG brain perception data and experiment description

Collecting of EEG brain perception data of visual and auditory areas of human brain demands the same equipment and EEG recording device and software that was used for the experiments with video stimuli [32].

The main ideas of collecting human brain perception data recorded on contradictory stimuli representing the notions of harmony versus chaos were also kept for the combined audio/video stimuli.

The suggestion was made about the possibility to gain higher accuracy of classification of perception with stimuli presented as combination of audio and video components being logical extensions of each other. In other words, for the patterned video stream the structural classical music was chosen as combination and for the amorphous noise sample the abstract shapeless art works were chosen as video component:

The audio/video stimuli were combined and labeled in the following way:

- 1) 85 seconds extract from the Ich ruf' zu dir, Herr Jesu Christ (BWV 639) by Johann Sebastian Bach was completed with mandalas video (related further in the chapter as "PM1");
- 2) 54 seconds extract from the Wachet auf, ruft uns die Stimme (BWV 140) by Johann Sebastian Bach was completed with snow crystals video (related further in the chapter as "PM2");
- 3) 30 seconds of unstructured chaotic irritating industrial noise was completed with abstract art video (related further in the chapter as "AN").

The EEG data was recorded from several healthy male and female subjects in the age category of 20 – 40 years. The recorded data was not used previously. The length of a whole session of each of three stimuli (PM1 of 85 sec, PM2 of 54 sec and AN of 30 sec) was later divided into equal samples of 1 sec length. The data was collected and classified following five scenarios each of which set distinct goals:

Scenario 1: The primary goal for the Scenario 1 was defined as classification of subjects based on their perception of one of the stimuli PM1, PM2 or AN. Each of the experiments performed within this scenario was utilizing only one of these stimuli.

Experiment 1-1 classified subjects 1, 2, 3 and was based on stimulus PM1 presented to subjects; contained 3 classes:

Class #	Subject	Stimulus	Class Accuracy %
1	1	PM1	100
2	2	PM1	95.19
3	3	PM1	100

Overall accuracy of experiment is **98.40%**.

Experiment 1-2 classified subjects 1, 2, 3 and was based on stimulus AN presented to subjects; contained 3 classes:

Class #	Subject	Stimulus	Class Accuracy %
1	1	AN	79.06
2	2	AN	87.67
3	3	AN	83.02

Overall accuracy of experiment is **83.25%**.

Experiment 1-3 classified subjects 1, 2, 3 and was based on stimulus PM2 presented to subjects; contained 3 classes:

Class #	Stimulus	Subject	Class Accuracy %
1	1	PM2	100
2	2	PM2	100
3	3	PM2	100

Overall accuracy of experiment is **100%**.

Scenario 2: The primary goal for the Scenario 2 was defined as classification of stimuli based on perception of one of the subjects 1, 2 or 3.

Experiment 5-1 classified stimuli PM1, PM2, AN and was based on Subject 1 perception of the stimuli; contained 3 classes:

Class #	Stimulus	Subject	Class Accuracy %
1	PM1	1	80.37
2	AN	1	69.07
3	PM2	1	86.67

Overall accuracy of experiment is **78.70%**.

Experiment 5-2 classified stimuli PM1, PM2, AN and was based on Subject 2 perception of the stimuli; contained 3 classes:

Class #	Stimulus	Subject	Class Accuracy %
1	PM1	2	75.56
2	AN	2	40.00
3	PM2	2	72.09

Overall accuracy of experiment is **62.55%**.

Experiment 5-3 classified stimuli P1, P2, A and was based on Subject 3 perception of the stimuli; contained 3 classes:

Class #	Stimulus	Subject	Class Accuracy %
1	PM1	3	84.07
2	AN	3	72.67
3	PM2	3	86.09

Overall accuracy of experiment is **80.94%**.

Scenario 3: The primary goal for the Scenario 3 was more complex and defined as classification of the stimuli PM1, PM2, AN based on mixed samples of perception of all three subjects 1, 2 and 3.

Experiment 7 classified the stimuli PM1, PM2, AN and was based on the mixed samples of perception of all three subjects 1, 2, 3; contained 3 classes:

Class #	Stimulus	Subject	Class Accuracy %
1	PM1	1	50.25
		2	
		3	
2	AN	1	36.25
		2	
		3	
3	PM2	1	70.31
		2	
		3	

Overall accuracy of experiment is **52.27%**.

Scenario 4: The primary goal for the Scenario 4 was more complex and defined as classification of the subjects 1, 2 and 3 based on the mixed samples of all three stimuli PM1, PM2, AN perception.

Experiment 7-1 classified subjects 1, 2, 3 was based on the mixed samples of all three stimuli PM1, PM2, AN perception; contained 3 classes:

Class #	Subject	Stimulus	Class Accuracy %
1	1	PM1 AN PM2	84.44
2	2	PM1 AN PM2	84.00
3	3	PM1 AN PM2	86.43

Overall accuracy of experiment is **84.96%**.

Scenario 5: The primary goal for the Scenario 5 was the most complex and defined as classification of the combination of a certain subject plus a certain stimulus.

Experiment 8: two contradictory stimuli PM1 and AN were presented to three subjects 1, 2, 3; the experiment contained 6 classes:

Class #	Subject/Stimulus	Class Accuracy %
1	1/PM1	100
2	2/PM1	85.13
3	3/PM1	94.06
4	1/AN	67.54
5	2/AN	80.05
6	3/AN	73.76

Overall accuracy of experiment is **83.42%**.

7.2 EEG data samples' length experiment

A separate classification session was performed on the same audio/video stimuli but with different sample length arrangements.

The length of a whole session of each of three stimuli (PM1 of 85 sec, PM2 of 54 sec and AN of 30 sec) was divided into equal samples of 10 sec length versus 1 sec in all previous experiments. The aim of this experiment was to define any possible influence of the sample length on the level of accuracy. The suggestion was made about a possible direct dependence of the level of accuracy on the length of data sample.

Scenario 1/10: The primary goal for the Scenario 1/10 was defined as classification of subjects based on their perception of one of the stimuli PM1, PM2 or AN. Each of the experiments performed within this scenario was utilizing only one of these stimuli.

Experiment 15-1 classified subjects 1, 2, 3 and was based on stimulus PM1 presented to subjects; contained 3 classes:

Class #	Subject	Stimulus	Class Accuracy %
1	1	PM1	100
2	2	PM1	100
3	3	PM1	100

Overall accuracy of experiment is **100%**.

Experiment 15-2 classified subjects 1, 2, 3 and was based on stimulus AN presented to subjects; contained 3 classes:

Class #	Subject	Stimulus	Class Accuracy %
1	1	AN	100
2	2	AN	83.66
3	3	AN	91.60

Overall accuracy of experiment is **91.75%**.

Experiment 15-3 classified subjects 1, 2, 3 and was based on stimulus PM2 presented to subjects; contained 3 classes:

Class #	Stimulus	Subject	Class Accuracy %
1	1	PM2	100
2	2	PM2	100
3	3	PM2	100

Overall accuracy of experiment is **100%**.

Scenario 2/10: The primary goal for the Scenario 2/10 was defined as classification of stimuli based on perception of one of the subjects 1, 2 or 3.

Experiment 16-1 classified stimuli PM1, PM2, AN and was based on Subject 1 perception of the stimuli; contained 3 classes:

Class #	Stimulus	Subject	Class Accuracy %
1	PM1	1	96.60
2	AN	1	73.88
3	PM2	1	97.31

Overall accuracy of experiment is **89.26%**.

Experiment 16-2 classified stimuli PM1, PM2, AN and was based on Subject 2 perception of the stimuli; contained 3 classes:

Class #	Stimulus	Subject	Class Accuracy %
1	PM1	2	81.39
2	AN	2	61.54
3	PM2	2	95.00

Overall accuracy of experiment is **79.31%**.

Experiment 16-3 classified stimuli P1, P2, A and was based on Subject 3 perception of the stimuli; contained 3 classes:

Class #	Stimulus	Subject	Class Accuracy %
1	PM1	3	95.13
2	AN	3	74.36
3	PM2	3	98.33

Overall accuracy of experiment is **89.27%**.

Scenario 3/10: The primary goal for the Scenario 3/10 was the most complex and defined as classification of the combination of a certain subject plus a certain stimulus.

Experiment 17: two contradictory stimuli PM1 and AN were presented to three subjects 1, 2, 3; the experiment contained 6 classes:

Class #	Subject/Stimulus	Class Accuracy %
1	1/PM1	100
2	2/PM1	94.14
3	3/PM1	83.09
4	1/AN	81.10
5	2/AN	47.70
6	3/AN	70.15

Overall accuracy of experiment is **79.36%**.

The top overall accuracy of 100% for classification of subjects is reached here with combined patterned audio plus video stimulus PM2. The extending of the duration of the stimuli has increased the accuracy level and allowed us to extend the 100% accuracy on both patterned stimuli PM1 and PM2 and also to obtain the highest accuracy for irregular stimulus AN. The highest accuracy is also achieved for stimuli classification experiments as well as in the complex experiments with 6 classes (concurrent classification of subjects and stimuli).

The detailed analysis of the results will be given later in this chapter in the summary section 7.5.

7.3 Special case of EEG STBD classification in the NeuCube model with mixed audio/video contradictory pairs stimuli

To verify the suggestion made earlier about the possibility of obtaining higher accuracy of classification with mixed audio/video stimuli combined as being logical extensions of each other, (combinations of structural video stream with structural classical music versus amorphous noise samples with shapeless abstract art), the following experiments with “broken pairs” stimuli were performed. The previously used polarizing or contradictory logic for pairs of audio plus video combinations was changed to opposite, and new pairs were composed and labeled in the following way:

1) 54 seconds extract from the Wacht auf, ruft uns die Stimme (BWV 140) by Johann Sebastian Bach was combined with shapeless abstract art video (related further in the chapter as “AM”).

2) 30 seconds of unstructured chaotic irritating industrial noise was completed with snow crystals video (related further in the chapter as “PN”);

The EEG data was recorded from a small group of healthy male and female subjects in the age category of 20 – 40. The length of a whole session of each of two stimuli (PN of 54 sec and AM of 30 sec) was later divided into equal samples of 1 sec length. The data was collected and classified following three scenarios:

Scenario 1: The primary goal for the Scenario 1 was defined as classification of subjects based on their perception of one of the new “broken pairs” stimuli, PN or AM.

Experiment 3-1 classified subjects 1, 2 and was based on stimulus PM1 presented to subjects; contained 2 classes:

Class #	Subject	Stimulus	Class Accuracy %
1	1	PN	83.32
2	2	PN	72.34

Overall accuracy of experiment is **77.83%**.

Experiment 3-2 classified subjects 1, 2 and was based on stimulus AN presented to subjects; contained 2 classes:

Class #	Subject	Stimulus	Class Accuracy %
1	1	AM	71.31
2	2	AM	72.46

Overall accuracy of experiment is **71.88%**.

Scenario 2: The primary goal for the Scenario 2 was defined as classification of stimuli based on perception of one of the subjects 1, 2.

Experiment 11-1 classified stimuli PN, AM and was based on Subject 1 perception of the stimuli; contained 2 classes:

Class #	Stimulus	Subject	Class Accuracy %
1	PN	1	55.77
2	AM	1	35.18

Overall accuracy of experiment is **45.47%**.

Experiment 11-2 classified stimuli PM1, PM2, AN and was based on Subject 2 perception of the stimuli; contained 2 classes:

Class #	Stimulus	Subject	Class Accuracy %
1	PN	2	53.29
2	AM	2	49.09

Overall accuracy of experiment is **51.19%**.

Scenario 3: The primary goal for the Scenario 3 was more complex and defined as classification of the stimuli PN and AM based on mixed samples of perception of both two subjects 1 and 2.

Experiment 10 classified the stimuli PN and AM and was based on the mixed samples of perception of both two subjects 1, 2; contained 2 classes:

Class #	Stimulus	Subject	Class Accuracy %
1	PN	1 2	35.72
2	AM	1 2	60.05

Overall accuracy of experiment is **47.88%**.

Experiment 10-1 classified subjects 1, 2, was based on the mixed samples of both two stimuli PN and AM perception; contained 2 classes:

Class #	Subject	Stimulus	Class Accuracy %
1	1	PN AM	47.02
2	2	PN AM	61.08

Overall accuracy of experiment is **54.05%**.

The experiments of this section with mixed contradictory pairs stimuli has shown the instability of classification and accuracy volatility. Similar experiments should be repeated in future research to investigate the nature of these findings.

7.4 Visualization of EEG recorded data

For visualization purposes of EEG brain data perception of audio/video stimuli the novel software EEGLAB tool SIFTS [138] was used. The visualization feature allows us to simulate step by step the flow of the signals, which activate certain brain areas so that all the brain states combined one by one into the “brainmovie” will let us watch time dependent brain signal processing. Below selected pictures of the “brainmovie” are shown, fig.7.4.1.

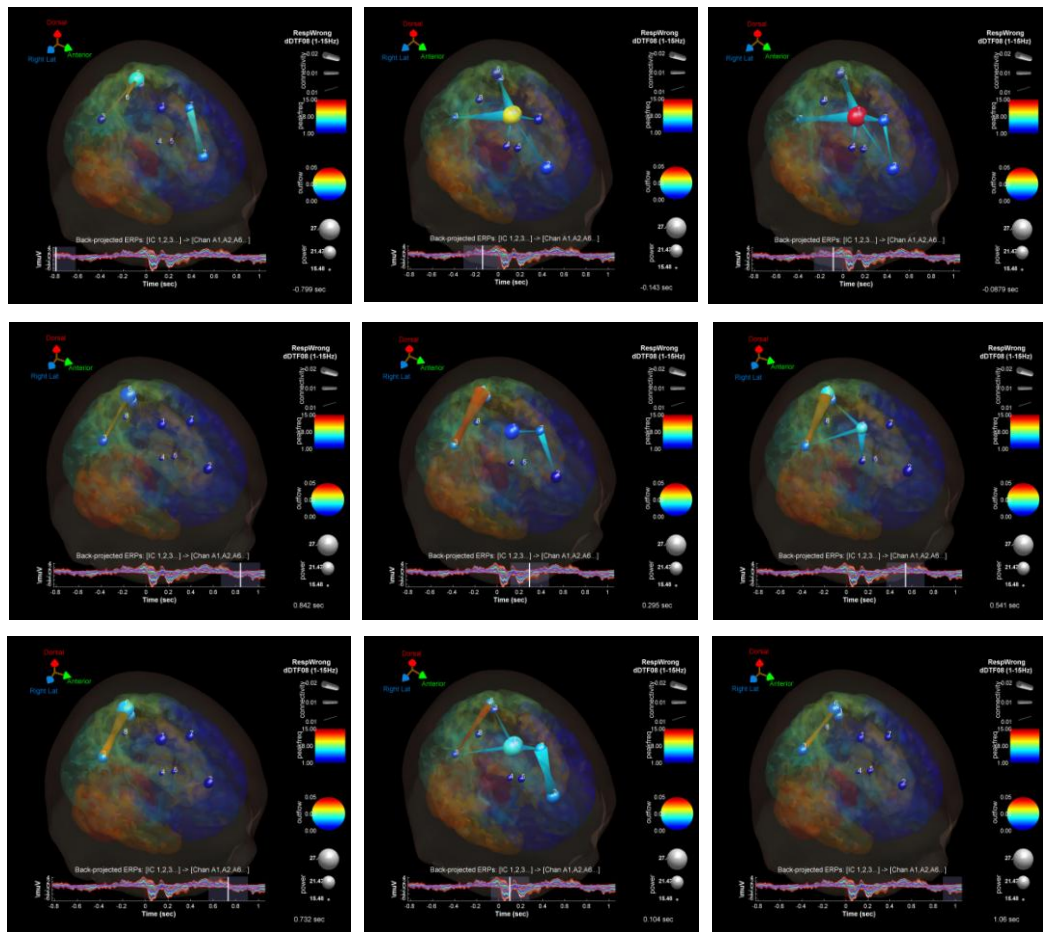


Fig.7.4.1 BrainMovie3DVisualization of EEG data with mixed audio/video 1/MP2 patterned stimuli; SIFT Matlab/EEGLAB plugin

For illustration of the complexity of the NeuCube processing of complicated experiments 8 and 17 (with classification of the combination of a certain subject plus a certain stimulus), fig 7.4.2 shows the network produced by the NeuCube after the training of the system.

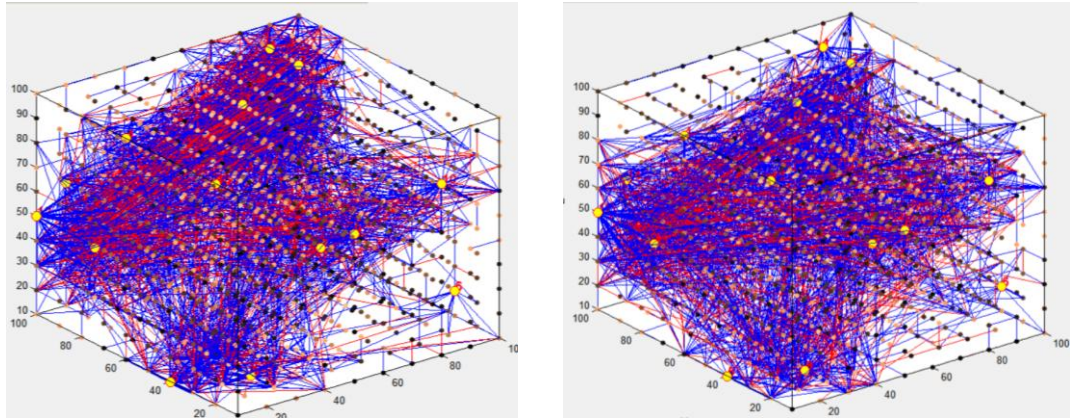


Fig 7.4.2. The NeuCube network after training of complicated experiments 8 and 17.

7.5 Summary

The analysis of the results obtained using a combination of audio and video samples in a single stimulus confirms the existing tendency: gaining higher classification accuracy in the experiments designed for classification of subjects in comparison with the experiments for classification of stimuli.

In this set of experiments with video/audio stimuli we achieved the highest percentage of accuracy - 100% for selected classes and for overall accuracy for classification of subjects. However we have to mention that the addition of Noise audio to the Abstract video (in the stimulus AN) decreases an achievement of “pure video” A stimulus accuracy dropping it from 94.51% (for A) to 83.25% (for AN). It may illustrate the negative influence of Noise audio component on the combined audio/video AN stimulus.

We observed unexpectedly low accuracy results for stimuli classification in complex scenarios (mix of 3 subjects data) e.g. the lowest 36.25% for the AN (Abstract/Noise) stimulus. These were compensated with surprisingly high accuracy in the most complex experiment design with 6 classes (experiments 8 and 17) gaining there 100% accuracy for one class in each experiment with overall accuracy of 83.42% and 79.36% respectively. The relative success of those fairly complicated experiments lets us make a suggestion of feasibility of “subjects plus stimuli” concurrent classification.

As articulated above in this chapter the assumption about a direct dependence in level of accuracy on a duration of a stimulus was confirmed with experiments 15-1, 15-2, 15-3, 16-1, 16-2, 16-3 and 17, where the duration of the proposed stimuli was increased from 1 sec to 10 sec which produced an increase in the accuracy for the whole range of these experiments.

The special case of experiments 3-1, 3-2, 10, 10-1, 11-1 and 11-2 with contradictory pairs of audio/video stimuli has also confirmed the assumption about lesser classification abilities of contradictorily combined stimuli. The highest accuracy reached in these experiments was only 77.83% compared to 100% in similar experiments but with logically combined audio and video components. The stimuli classification on contradictory pairs gave an even worse result of 45.47% against 80.94% on logical stimuli. It is drastically lower, especially taking into account the fact of only 2 existing classes in contradictory experiment design. This case illustrates the instability of brain perception of information consisting of contradictory components (e.g. audio versus video) and as a result a high volatility of classification accuracy.

Chapter 8

Conclusion and future work

The range of performed experiments gives us the possibility to make several conclusions. First of all the results of experiments have shown the feasibility of using human brain data recorded as plain EEG brain data on specific stimuli for purposes of data classification and in particular for person identification. Classification of human brain perception data of a number of subjects recorded with the use of video, audio and combination of audio and video stimuli performed on the Neucube software tool has shown promisingly high levels of accuracy.

A methodology for spatio-temporal EEG brain data classification, based on the collected auditory data, in the NeuCube 3D SNN environment has been developed and a paper had been submitted to the 20th ICONIP conference (November 2013) in Daegu, Korea.

A methodology for visual STBD and combined auditory and visual STBD data classification has been proposed and a paper is in preparation to be published by Springer later in 2014.

A methodology for person identification has been successfully tested and a procedure of using specific audio, video and mixed stimuli with the function of a security key for the authentication process has been proposed. The term of brainprints is offered by analogy with fingerprints and prospectively having the ability to supply similar functionality but with a higher level of security. The obtained classification results also allow us to make initial evaluation of stimuli regarding its appropriateness for the authentication purposes. The combination of structured music audio with patterned video sample has provided a stimulus with its best qualities necessary for consistent and trustworthy person identification. Therefore we may define an “ideal” stimulus which would possess the best qualities of a security code providing the appropriate level of accuracy of classification and being relatively fast. It would be a sample of highly structural audio combined with dedicated video string of reasonably long duration (still feasible for fast computation, in a range of seconds).

Most problematic for person identification, appeared to be the stimuli of chaotic irregular noise in the audio only format. Classification of human perception recorded showed a minimum of 68.4% accuracy. For the identification of stimuli these noisy samples were critically problematic with a sharp decline to 28.89%.

The experiments with scenarios of stimuli identification demonstrated the feasibility of this type of classification although reaching in general lower classification accuracy.

We have to mention some limitations of this study such as: limited amount of available perception data, and the availability of only 14 channels EEG equipment. These limitations have constrained the possibility of the study to some extent. For the prospective future research new opportunities will be opened with accessibility of the

full 64 channels EEG equipment. Also to prove proper repeatability of the classification accuracy the experiments should be performed with a larger number of subjects. Another aspect that should be addressed in a future work is the analysis of classification accuracy dependence on the length of data samples used for experiments with an objective of defining a possible minimum optimal length for a data sample.

At last, regarding the evaluation of the NeuCube feasibility for classification of plain EEG data we have to state its success even for classification of complex data given the task to identify combinations of subjects and stimuli together.

While the level of accuracy was less stable in that case, the further research would be beneficial.

Summarizing, we may say that the classification of human brain perception is only one of the very first steps on the way of human creativity research. Evaluation and verification of the hypothesis of the patterned nature of human inspiration and creativity will demand many experiments to be performed and vast amounts of data to be collected. To define any special cases in human perception, to differentiate the perception of archetypical symbols, discussed in chapter 1, we will need to explore deeply the streams of human perception with a wide range of experimental methods.

Another important aspect for future research involves experimenting with dynamic network processing within the 3D SNN NeuCube environment and that should define new horizons for this field of research.

References

1. Haykin, S. (1994). *Neural Networks: A Comprehensive Foundation*. New York: Macmillan. 35-38.
2. Azevedo, F. A., Carvalho, L. R., Grinberg, L. T., Farfel, J. M. M., Ferretti, R. E., Leite, R. E., Herculano-Houzel, S. (2009, April). Equal numbers of neuronal and nonneuronal cells make the human brain an isometrically scaled-up primate brain. *The Journal of comparative neurology*, 513 (5), 532–541. doi: 10.1002/cne.21974179
3. The DANA foundation, <http://www.dana.org>.
4. Schacter, Daniel (2011). *Psychology*. Worth Publishers. 65-73
5. Gregory, Richard. "Perception" in Gregory, Zangwill (1987) pp. 598–601.
6. Bernstein, Douglas A. (5 March 2010). *Essentials of Psychology*. Cengage Learning. pp. 123–124.
7. <http://www.britannica.com/EBchecked/topic/289766/human-intelligence>.
8. *Intelligence: A Multidisciplinary Journal*, 1997. 27-36.
9. McCarthy, John; Minsky, Marvin; Rochester, Nathan; Shannon, Claude; A Proposal for the Dartmouth Summer Research Project on Artificial Intelligence, (1956),
10. Russell, Stuart J.; Norvig, Peter (2003), *Artificial Intelligence: A Modern Approach* (2nd ed.), Upper Saddle River, New Jersey: Prentice Hall, 48-52.
11. Kurzweil, Ray (2005). *The Singularity is Near*. Penguin Books, 39-42.
12. NRC, (United States National Research Council) (1999). "Developments in Artificial Intelligence". *Funding a Revolution: Government Support for Computing Research*. National Academy Press. 78-94.
13. Malewitsch K. *Suprematismus — Die gegenstandslose Welt*. Ubertragen von Hans von Riesen. Koln: Verlag M.DuMont Schauberg 1962, S. 27-29.
14. John Ankerberg, John Weldon, *Encyclopedia of New Age Beliefs: The New Age Movement*, p. 343-357.
15. <http://www.its.caltech.edu/~atomic/>; SnowCrystals.com
16. Elger, D., *Abstract Art*, TASCHEN, 2013, 13-76.
17. Frackowiak, R. S. (2004). Human brain functions. *International Journal of Computer Applications*, 40(1), 18-24.
18. Kasabov, N., NeuCube EvoSpike Architecture for Spatio-Temporal Modelling and Pattern Recognition of Brain Signals, in: Mana, Schwenker and Trentin (Eds) *ANNPR*, Springer LNAI 7477, 2012, 225-243.
19. Makeig, S.; Kothe, C.; Mullen, T.; Bigdely-Shamlo, N., *Evolving Signal Processing for Brain–Computer Interfaces*, *Proceedings of the IEEE* (Volume: 100, Issue: Special Centennial Issue) 2012. P. 1567-1584
20. Bailey, D.L; D.W. Townsend, P.E. Valk, M.N. Maisey (2005). *Positron Emission Tomography: Basic Sciences*. Secaucus, NJ: Springer-Verlag. P 11-13
21. *Clinical Research for Surgeons*. Mohit Bhandari, Anders Joensson. p. 293
22. Niedermeyer E. and da Silva F.L. (2004). *Electroencephalography: Basic*

- Principles, Clinical Applications, and Related Fields. Lippincot Williams & Wilkins. ISBN 0-7817-5126-8, p.13
23. Atlas of EEG & Seizure Semiology. B. Abou-Khalil; Musilus, K.E.; Elsevier, 2006.p.112
 24. <http://www.nlm.nih.gov/medlineplus/ency/article/003931.htm>
 25. O'Regan, S; Faul, S; Marnane, W (2010). "Automatic detection of EEG artefacts arising from head movements". 2010 Annual International Conference of the IEEE Engineering in Medicine and Biology. p. 6353–6.
 26. Hämäläinen, Matti; Hari, Riitta; Ilmoniemi, Risto J.; Knuutila, Jukka; Lounasmaa, Olli V. (1993). "Magnetoencephalography-theory, instrumentation, and applications to noninvasive studies of the working human brain". *Reviews of Modern Physics* 65 (2): 413–97.
 27. Anderson, J. (22 October 2004). *Cognitive Psychology and Its Implications (Hardcover) (6th ed.)*. New York, NY: Worth. p. 17. ISBN 0-7167-0110-3.
 28. Vespa, Paul M.; Nenov, Val; Nuwer, Marc R. (1999). "Continuous EEG Monitoring in the Intensive Care Unit: Early Findings and Clinical Efficacy". *Journal of Clinical Neurophysiology* 16 (1): 1–13. doi:10.1097/00004691-199901000-00001. PMID 10082088.
 29. <http://www.mrn.org/collaborate/egi-eeeg-system/>
 30. Towle, Vernon L.; Bolaños, José; Suarez, Diane; Tan, Kim; Grzeszczuk, Robert; Levin, David N.; Cakmur, Raif; Frank, Samuel A.; Spire, Jean-Paul (1993). "The spatial location of EEG electrodes: Locating the best-fitting sphere relative to cortical anatomy". *Electroencephalography and Clinical Neurophysiology* 86 (1): 1–6. doi:10.1016/0013-4694(93)90061-Y. PMID 7678386.
 31. Aurlien, H; Gjerde, I.O; Aarseth, J.H; Eldøen, G; Karlsen, B; Skeidsvoll, H; Gilhus, N.E (2004). "EEG background activity described by a large computerized database". *Clinical Neurophysiology* 115 (3): 665–73. doi:10.1016/j.clinph.2003.10.019. PMID 15036063.
 32. <http://emotiv.com/>
 33. L. D. Liao, I J. Wang, S. F Chen, J. Y. Chang, and C. T. Lin, "Design, Fabrication and Experimental Validation of a Novel Dry Contact Sensor for Measuring Electroencephalography Signals without Skin Preparation," *Sensors*, Vol.11, pp.5819-5834, 2011. (IF: 1.821, 11/58 or 18.97% of INSTRUMENTS & INSTRUMENTATION)
 34. Kropotov, J. D. (2009). *Quantitative EEG, Event-Related Potentials And Neurotherapy*. 525 B Street, Suite 1900, San Diego, CA 92101-4495, USA: Elsevier Inc.
 35. http://sccn.ucsd.edu/wiki/EEGLAB_2013_UCSD
 36. Hammond, D. C. (2006). What is Neurofeedback? *Journal of Neurotherapy*, 10:4, p.11.
 37. Zhang, Y., Chen, Y., Bressler, S. L., & Ding, M. (2009). Response preparation and inhibition: The role of the cortical sensorimotor beta rhythm. *Neuroscience*, 156:1, 238–246.
 38. Rangaswamy, M., Porjesz, B., Chorlian, D. B., Wang, K., Jones, K. a., Bauer, L. O., et al. (2002, October). Beta power in the EEG of alcoholics. *Biological psychiatry*, 52(8), 831–42. Available from <http://www.ncbi.nlm.nih.gov/pubmed/12372655>
 39. Niedermeyer E. and da Silva F.L. (2004). *Electroencephalography: Basic Principles, Clinical Applications, and Related Fields*. Lippincot Williams & Wilkins. ISBN 0-7817-5126-8.113-127.

40. Lotte, F., M. Congedo, A. Lécuyer, F. et al., A review of classification algorithms for EEG-based brain-computer interfaces, *J. Neural Eng.*, 2007; 4(2):1-15. Available from <http://www.ncbi.nlm.nih.gov/pubmed/17409472>.
41. Christopher M. Bishop (2006). *Pattern Recognition and Machine Learning*. Springer. p. 205.
42. Hosmer, David W.; Lemeshow, Stanley (2000). *Applied Logistic Regression* (2nd ed.). Wiley. ISBN 0-471-35632-8
43. T.Joachims, *SVM Light Support Vector Machine*, 2002, <http://svmlight.joachims.org>.
44. Rosenblatt, Frank. x. *Principles of Neurodynamics: Perceptrons and the Theory of Brain Mechanisms*. Spartan Books, Washington DC, 1961
45. Rumelhart, David E., Geoffrey E. Hinton, and R. J. Williams. "Learning Internal Representations by Error Propagation". David E. Rumelhart, James L. McClelland, and the PDP research group. *Parallel distributed processing: Explorations in the microstructure of cognition, Volume 1: Foundations*. MIT Press, 1986.
46. Cybenko, G. 1989. Approximation by superpositions of a sigmoidal function *Mathematics of Control, Signals, and Systems*, 2(4), 303–314.
47. Baum, L. E.; Petrie, T. (1966). "Statistical Inference for Probabilistic Functions of Finite State Markov Chains". *The Annals of Mathematical Statistics* 37 (6): 1554–1563. doi:10.1214/aoms/1177699147. Retrieved 28 November 2011.
48. Thad Starner, Alex Pentland. *Real-Time American Sign Language Visual Recognition From Video Using Hidden Markov Models*. Master's Thesis, MIT, Feb 1995, Program in Media Arts.
49. Trentin, E., & Gori, M. (2001). A survey of hybrid ANN/HMM models for automatic speech recognition. *Neurocomputing*, 37(1-4), 91–126.
50. Jolliffe I.T. *Principal Component Analysis*, Series: Springer Series in Statistics, 2nd ed., Springer, NY, 2002, XXIX, 487 p. 28 illus. ISBN 978-0-387-95442-4
51. Onton J. Makeig S. Information-based modeling of event-related brain dynamics, Elsevier Progress in Brain Research book series, Eds. Neuper & Klimesch, February, 2006 p.11-24
52. Kothe C., Makeig S, BCILAB: a platform for brain-computer interface development, *Journal of neural engineering* 10 (5) 2013, IOP Publishing, p. 056014
53. Mullen, T, Delorme, A, Kothe, C, Makeig, S "An Electrophysiological Information Flow Toolbox for EEGLAB" Society for Neuroscience Conference, San Diego, CA, USA, 2010
54. Gerstner, W., Sprekeler, H., Deco, G. Theory and simulation in neuroscience, *Science*, 2012; 338:60-65.
55. Ghosh-Dastidar, S., Adeli, H. Improved Spiking Neural Networks for EEG Classification and Epilepsy and Seizure Detection, *Integrated Computer-Aided Eng.*, 2007; 14(3): 187-212.
56. Fiasché, M., S. Schliebs, L. Nobili, Integrating Neural Networks and Chaotic Measurements for Modelling Epileptic Brain, A.Villa (Eds.): *Proc. ICANN2012*, Springer LNCS 7552, 2012; 653–660.
57. Craig, D.A., H.T. Nguyen, Adaptive EEG Thought Pattern Classifier for Advanced Wheelchair Control, *Engineering in Medicine and Biology Society, Proc. EMBS'07*, 2007; 2544-2547.
58. Wilkes, A. L., & Wade, N. J. (1997). Bain on neural networks. *Brain and Cognition*, 33(3), 295 - 305. doi: DOI:10.1006/brcg.1997.0869.
59. Gerstner, W., & Kistler, W. M. (2002a). *Spiking neuron models*. Cambridge

University Press.

60. Izhikevich, E. M. (2003). Simple model of spiking neurons. *IEEE transactions on neural networks*, 14(6), 1569–1572.
61. Maass, W., & Bishop, C. M. (Eds.). (1999). *Pulsed neural networks*. Cambridge, MA, USA: MIT Press.
62. <http://en.wikipedia.org>
63. Huguenard, J. R. (2000, August 15). Reliability of axonal propagation: the spike doesn't stop here. *Proceedings of the National Academy of Sciences of the United States of America*, 97(17), 9349–9350. Retrieved from <http://view.ncbi.nlm.nih.gov/pubmed/10944204>
64. Thorpe, S., J. Gautrais, Rank order coding, *Computing neuroscience: Trends in research*, 1998;13:113–119.
65. Hodgkin, A. L., & Huxley, A. F. (1952). A quantitative description of membrane current and its application to conduction and excitation in nerve. *Journal of Physiology*, 117, 500–544.
66. Izhikevich, E. M. (2004, Sept.). Which model to use for cortical spiking neurons? *IEEE Transactions on Neural Networks*, 15(5), 1063-1070. doi: 10.1109/TNN.2004.832719
67. Izhikevich, E. M. (2006). Polychronization: Computation with Spikes. *Neural Comput.*, 18 (2), 245–282. doi: <http://dx.doi.org/10.1162/089976606775093882>
68. Izhikevich, E. M. (2007). *Dynamical systems in neuroscience: the geometry of excitability and bursting*. MIT Press.
69. Izhikevich, E. M., & Edelman, G. M. (2008, March). Large-scale model of mammalian thalamocortical systems. *Proceedings of the National Academy of Sciences*, 105(9), 3593–3598. doi: 10.1073/pnas.0712231105
70. Hodgkin, A. L., & Huxley, A. F. (1952a). Currents carried by sodium and potassium ions through the membrane of the giant axon of *Loligo*. *Journal of Physiology*, 116(4), 449-472.
71. Hodgkin, A. L., & Huxley, A. F. (1952b). The dual effect of membrane potential on sodium conductance in the giant axon of *Loligo*. *Journal of Physiology*, 116(4), 497-506.
72. Stein, R. B. (1967). Some models of neuronal variability. *Biophysical journal*, 7 (1), 37–68.
73. Hill, A. (1936). Excitation and accommodation in nerve. *Proceedings of the Royal Society of London. Series B, Biological Sciences*, 119 (814), 305–355.
74. Brillinger, D. R. (1992). Nerve cell spike train data analysis: a progression of technique. *Journal of the American Statistical Association*, 87 (418), 260–271.
75. Gerstner, W. (1995, Jan). Time structure of the activity in neural network models. *Phys. Rev. E*, 51 (1), 738–758. doi: 10.1103/PhysRevE.51.738
76. Keat, J., Reinagel, P., Reid, R. C., & Meister, M. (2001). Predicting every spike: a model for the responses of visual neurons. *Neuron*, 30 (3), 803–817.
77. Jolivet, R., Lewis, T. J., & Gerstner, W. (2004). Generalized integrate-and-fire models of neuronal activity approximate spike trains of a detailed model to a high degree of accuracy. *Journal of Neurophysiology*, 92 (2), 959–976.
78. Dominey, P. (1995). Complex sensory-motor sequence learning based on recurrent state representation and reinforcement learning. *Biological Cybernetics*, 73(3), 265–274.
79. Natschläger, T., Maass, W., & Markram, H. (2002). The liquid computer: A novel strategy for real-time computing on time series. *Special issue on Foundations of Information Processing of TELEMATIK*, 8 (1), 39–43.
80. Maass, W., Natschläger, T., & Markram, H. (2002). Real-time computing

- without stable states: A new framework for neural computation based on perturbations. *Neural computation*, 14 (11), 2531–2560.
81. Jaeger, H. (2001b). The echo state approach to analysing and training recurrent neural networks-with an erratum note. Technical report GMD report, 148.
 82. Steil, J. (2004). Backpropagation-decorrelation: Online recurrent learning with $O(n)$ complexity. In *Neural networks, 2004. Proceedings 2004 IEEE international joint conference on* (Vol. 2, pp. 843–848).
 83. Lauter, Judith L; P Herscovitch, C Formby, MERaichle (1985). "Tonotopic organization in human auditory cortex revealed by positron emission tomography". *Hearing Research* (Elsevier B.V.) 20 (3): 199–205. doi:10.1016/0378-5955(85)90024-3. PMID 3878839
 84. Kandel, E., Schwartz, J., & Szwed, T. (1991). *Principles of neural science*.
 85. Jaeger, H., Lukoševičius, M., Popovici, D., & Siewert, U. (2007). Optimization and applications of echo state networks with leaky-integrator neurons. *Neural Networks*, 20 (3), 335–352.
 86. Jaeger, H., & Haas, H. (2004). Harnessing nonlinearity: Predicting chaotic systems and saving energy in wireless communication. *Science*, 304 (5667), 78–80.
 87. Maass, W., Natschläger, T., & Markram, H. (2002). Real-time computing without stable states: A new framework for neural computation based on perturbations. *Neural computation*, 14 (11), 2531–2560.
 88. Maass, W., Natschläger, T., & Markram, H. (2004). Computational models for generic cortical microcircuits. *Computational neuroscience: A comprehensive approach*, 18, 575.
 89. Song, S., K. Miller, L. Abbott et al., Competitive hebbian learning through spike-timing-dependent synaptic plasticity, *Nature Neuroscience*, 2000; 3: 919–926.
 90. Belatreche, A., Maguire, L. P., McGinnity, M. *Advances in Design and Application of Spiking Neural Networks*. *Soft Comput.*2006; 11(3): 239-248.
 91. Gerstner, W. What's different with spiking neurons? *Plausible Neural Networks for Biological Modelling*, in: H.Mastebroek, H. Vos (Eds.), Kluwer Academic Publishers, 2001; 23- 48.
 92. Lichtsteiner, P., Posch, C., Delbruck, T. A 128×128 120dB 30mW Asynchronous Vision Sensor that Responds to Relative Intensity Change, *ISSCC Digest of Technical Papers*, 2006; 508-509
 93. Liu, S.C., Delbruck, T. Neuromorphic sensory systems, *Curr. Opinion in Neurobiology*, 2010; 20(3):288-295.
 94. Benuskova, L, N. Kasabov, *Computational neuro-genetic modelling*, Springer, New York (2007).
 95. Kasabov, N. (2010). To spike or not to spike: A probabilistic spiking neuron model. *Neural Networks*, 23 (1), 16–19.
 96. Furber, S. To Build a Brain, *IEEE Spectrum*, 2012; 49(8): 39-41.
 97. Indiveri, G., Horiuchi, T.K. *Frontiers in neuromorphic engineering*, *Frontiers in Neuroscience*, 2011; 5:1-2.
 98. Schliebs, S., Defoin-Platel, M., & Kasabov, N. (2009). Integrated feature and parameter optimization for an evolving spiking neural network: Exploring heterogeneous probabilistic models. *Neural Networks*, 22 (5-6), 623–632.
 99. Kasabov, N., *Evolving Spiking Neural Networks and Neurogenetic Systems for Spatio- and Spectro-Temporal Data Modelling and Pattern Recognition*, Springer-Verlag Berlin Heidelberg 2012, J. Liu et al. (Eds.): *IEEE WCCI 2012, LNCS 7311*, pp. 234–260.
 100. Mohemmed, A., S.Schliebs, S.Matsuda, N. Kasabov, SPAN: Spike Pattern Association Neuron for Learning Spatio-Temporal Sequences, *Int. J. of Neural*

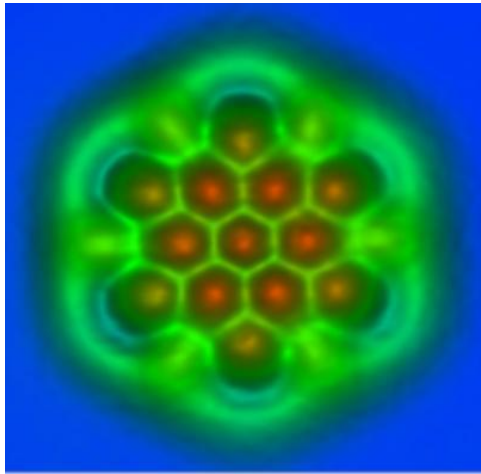
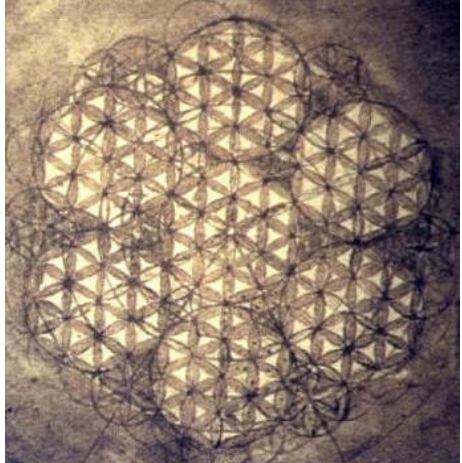
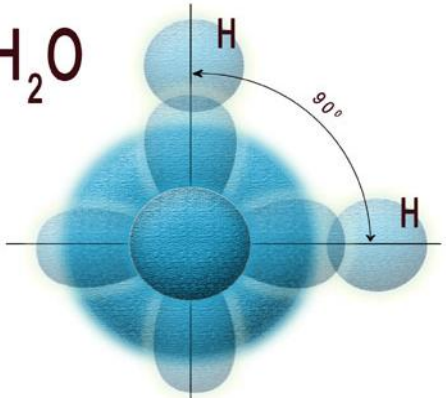
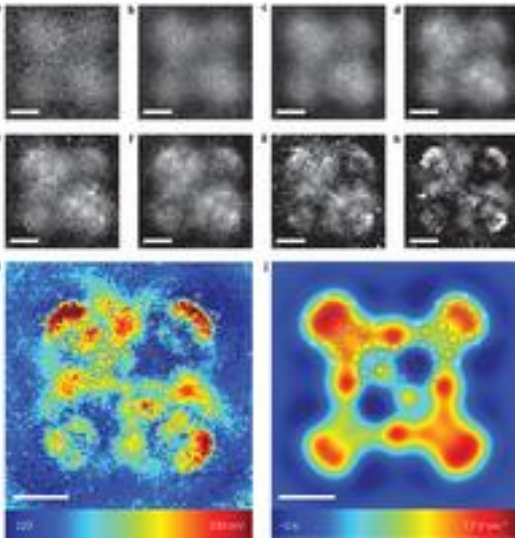
Systems, 2012;

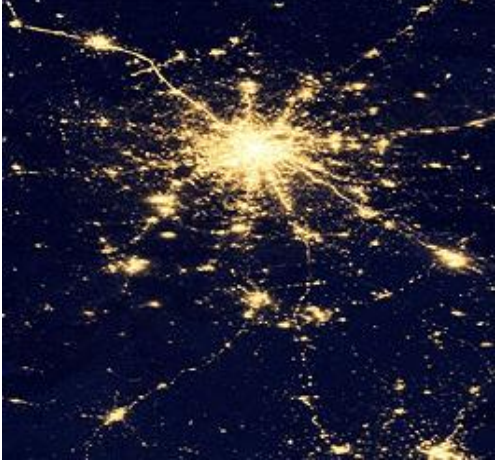
101. Kasabov, N., Dhoble, K., Nuntalid, N., G. Indiveri, Dynamic Evolving Spiking Neural Networks for On-line Spatio- and Spectro-Temporal Pattern Recognition, *Neural Networks*, 2013; 41:188-201. 22 (4): 1-16.
102. Zilles, K., K. Amunts, Centenary of Brodmann's map — conception and fate, *Nature Reviews Neuroscience*, 2010; 11:139-145.
103. Talairach, J., P. Tournoux, and Co-planar Stereotaxic Atlas of the Human Brain: 3-Dimensional Proportional System - an Approach to Cerebral Imaging, Thieme Medical Publishers, NY (1988).
104. Evans A. C., D. L. Collins, S. R. Mills et al, 3D statistical neuroanatomical models from 305 MRI volumes, *Proc. IEEE-Nuclear Science Symp. Medical Imaging Conference*, 1993; 1813-1817.
105. Toga, A., P. Thompson, S. Mori, et al. Towards multimodal atlases of the human brain, *Nature Reviews Neuroscience*, 2006; 7: 952-966.
106. Abeles, M. *Corticonics*, Cambridge University Press, NY (1991).
107. Stam, C. J. Functional connectivity patterns of human magnetoencephalographic recordings: a small-world network? *Neurosci. Lett.* , 2004; 355: 25–28.
108. De Charms R. C., Applications of real-time fMRI, *Nature Reviews Neuroscience*, 2008; 9:720-729.
109. Chen, Z. J., He, Y., Rosa-Neto, et al, Revealing modular architecture of human brain structural networks by using cortical thickness from MRI. *Cereb. Cortex*, 2008; 2374–2381.
110. Mitchel, T., Hutchinson, R. et al, Learning to Decode Cognitive States from Brain Images, *Machine Learning*, 2004; 57:145-175.
111. Broderson, K., Wiech, K., Lomakina, E. et al, Decoding the perception of pain from fMRI using multivariate pattern analysis, *NeuroImage*, 2012; 63:1162-1170.
112. Hawrylycz, M., et al, An anatomically comprehensive atlas of the adult human brain transcriptome, *Nature*, 2012; 489: 391-399.
113. Kasabov, N., NeuCube: A spiking neural network architecture for mapping, learning and understanding of spatio-temporal brain data. *Neural Networks*, 52 (2014) 62–76.
114. Bohte, S. M. (2004). The evidence for neural information processing with precise spike-times: a survey. *Natural Computing*, 3.
115. Delbruck, T. (2007). jAER open source project. <http://jaer.wiki.sourceforge.net>.
116. Nuntalid, N., Dhoble, K., & Kasabov, N. (2011). EEG classification with BSA spike encoding algorithm and evolving probabilistic spiking neural network. In *LNCS:vol. 7062*
117. Verstraeten, D., Schrauwen, B., D'Haene, M., Stroobandt, D.: An experimental unification of reservoir computing methods. *Neural Networks* 20(3), 391–403 (2007)
118. Kasabov, N. (2007). *Evolving connectionist systems: the knowledge engineering approach*. London: Springer, (first edition 2002).
119. Song, S., Miller, K., Abbott, L., et al. (2000). Competitive Hebbian learning through spike-timing-dependent synaptic plasticity. *Nature Neuroscience*, 3, 919–926.
120. Hebb, D. (1949). *The organization of behavior*. New York: John Wiley and Sons.
121. Thorpe, S., & Gautrais, J. (1998). Rank order coding. *Computational Neuroscience:Trends in Research*, 13, 113–119.
122. Kasabov, N., Dhoble, K., Nuntalid, N., & Indiveri, G. (2013). Dynamic evolving spiking neural networks for on-line spatio- and spectro-temporal pattern

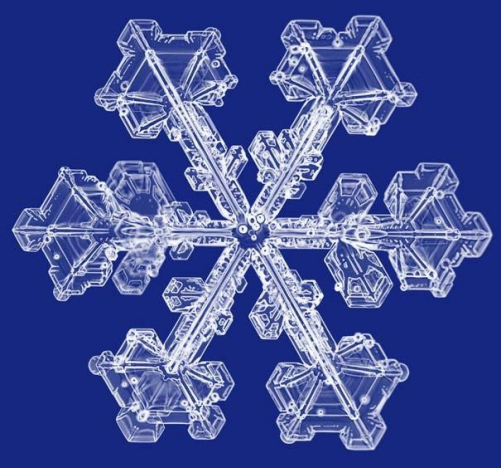
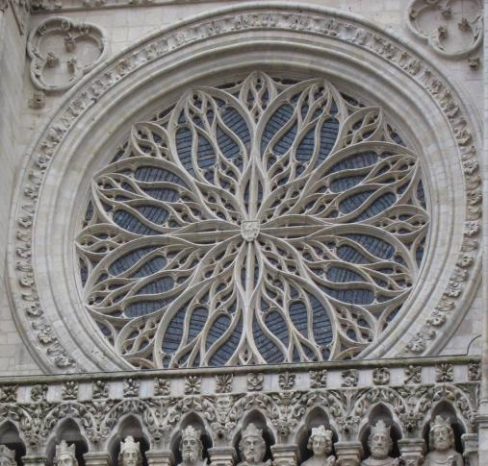
- recognition. *Neural Networks*, 41, 188–201.
123. Mohemmed, A., Schliebs, S., Matsuda, S., & Kasabov, N. (2012). SPAN: spike pattern association neuron for learning spatio-temporal sequences. *International Journal of Neural Systems*, 22(4), 1–16.
 124. Benuskova, L., Kasabov, N.: *Computational neuro-genetic modelling*, 290 pages. Springer, New York (2007)
 125. Zhdanov, V.P.: Kinetic models of gene expression including non-coding RNAs. *Phys. Rep.* 500, 1–42 (2011)
 126. Lauter, Judith L; P Herscovitch, C Formby, ME Raichle (1985). "Tonotopic organization in human auditory cortex revealed by positron emission tomography". *Hearing Research (Elsevier B.V.)* 20 (3): 199–205. doi:10.1016/0378-5955(85)90024-3. PMID 3878839
 127. Brodmann K. *Vergleichende Lokalisationslehre der Grosshirnrinde*. Leipzig: Johann Ambrosius Barth, 1909.34
 128. Ward, M., Grinstein, G., & Keim, D. (2010). *Interactive data visualization: Foundations, techniques, and applications*. Peters Ltd: USA, 56
 129. Deutsch, Diana (February 2013). "Hearing Music in Ensembles". *Physics Today*. p. 40.
 130. Cant, NB; Benson, CG (June 15, 2003). "Parallel auditory pathways: projection patterns of the different neuronal populations in the dorsal and ventral cochlear nuclei". *Brain Res Bull* 60 (5–6): 457–74. doi:10.1016/S0361-9230(03)00050-9. PMID 12787867.
 131. Bendor, D; Wang, X (2005). "The neuronal representation of pitch in primate auditory cortex". *Nature* 436 (7054): 1161–5. doi:10.1038/nature03867. PMC 1780171. PMID 16121182.
 132. Zatorre, RJ (2005). "Neuroscience: finding the missing fundamental". *Nature* 436 (7054): 1093–4. doi:10.1038/4361093a.
 133. Augusto Buchweitz I; Robert A. Mason I; Lêda M. B. Tomitch II; Marcel Adam Just I "Brain activation for reading and listening comprehension: an fMRI study of modality effects and individual differences in language comprehension". *Psychol. Neuroscience*. vol.2 no.2 Rio de Janeiro July 2009.
 134. Brattico, Elvira; Tervaniemi, Mari; Näätänen, Risto; Peretz, Isabelle (2006). "Musical scale properties are automatically processed in the human auditory cortex". *Brain Research* 1117 (1): 162–74. doi:10.1016/j.brainres.2006.08.023.
 135. Koessler, L., Maillard, L., Benhadid, A., et al. (2009). Automated cortical projection of EEG sensors: anatomical correlation via the international 10-10 system. *NeuroImage*, 46, 64–72.
 136. Arnaud Delorme, Scott Makeig, "EEGLAB: an open source toolbox for analysis of single-trial EEG dynamics including independent component analysis". *Journal of Neuroscience Methods* 134 (2004) 9–21
 137. Alex Huk. (1999) "Object and Face Recognition: Lecture Notes." p. 5.
 138. <http://sccn.ucsd.edu/wiki/SIFT>
 139. <http://www.nature.com/nano/journal/v7/n4/full/nano.2012.20.html> WT.ec_id=NANO-201204
 140. <http://www.eso.org/public/>
 141. <http://astrosuni.wordpress.com/2012/08/>
 142. http://en.wikipedia.org/wiki/Richtat_Structure
 143. [http://en.wikipedia.org/wiki/Typhoon_Muifa_\(2011\)](http://en.wikipedia.org/wiki/Typhoon_Muifa_(2011))
 144. http://en.wikipedia.org/wiki/Flower_of_Life
 145. <http://www.research.ibm.com/labs/zurich/mcs/>
 146. <http://en.wikipedia.org/wiki/Water>

147. http://en.wikipedia.org/wiki/Celtic_cross
148. http://en.wikipedia.org/wiki/Spinning_wheel
149. <http://books.google.co.nz/books>
150. <http://thewatchers.adorraeli.com/2012/04/09/ice-floes-along-the-kamchatka-coastline-seen-from-iss/>
151. <http://en.wikipedia.org/wiki/Meander>
152. http://ru.wikipedia.org/wiki/vologda_lace

Appendix A

#	A Natural Pattern	B Human Art Pattern
1		
2	<p data-bbox="411 837 507 920">H_2O</p>  <p data-bbox="419 1240 651 1317">O $1s^2 2s^2 2p^4$</p>	
3		

4		
5		
6		

7		
8		
9		
10		



- 1A** The carbon monoxide molecule, the picture is made b IBM team in Zurich. [145]
- 1B** Drawing by Leonardo da Vinci (Codex Atlanticus, fol. 307v), [144]
- 2A** A picture of H₂O molecular structure, [146]
- 2B** Vajra; it is used symbolically by the Dharma traditions of Buddhism, Jainism and Hinduism, often to represent firmness of spirit and spiritual power [14]
- 3A** LCPD images of naphthalocyanine on NaCl(2 ML)/Cu(111) measured with a CO-terminated tip.[139]
- 3B** Celtic Cross, Ireland, XII century, [147]
- 4A** Typhoon Muifa (International designation: 1109, JTWC designation: 11W, PAGASA name: Kabayan), [143]
- 4B** A decoration fragment of a spinning wheel. North of Russia, XVIII century. [148]
- 5A** The Richat Structure, also known as the Eye of the Sahara and Guelb er Richat, is a prominent circular feature in the Sahara desert of west–central Mauritania near Ouadane. [142]
- 5B** Maori Art, wood carving, fragment of canoe decoration, XVIII century,
- 6A** Moscow at night from a satellite, [141]
- 6B** Native American Mandala; Traditional Mexican Art. [149]
- 7A** Ice floes along the Kamchatka coastline seen from ISS. [150]
- 7B** Greek meander ornament. [151]
- 8A** Snow Crystals [15]
- 8B** Vologda lace. [152]
- 9A** Snow Crystals [15]
- 9B** Cathedral in France, French gothic, XIII century. [153]

10A Schematic molecule structure. [156]

10B Celtic art, Book of Kells, Dublin, Trinity College Library, MS A. I. (58) It's believed to have been created ca. 800 AD. [154]

11A The large spiral galaxy NGC 1232, as seen on 21 September 1998. NGC 1232 is located 20 degrees south of the celestial equator, in the constellation Eridanus (The River). The distance is about 100 million light-years. © ESO [140]

11B Islamic Art. Mosque in Iran, XI - XII century.